TECHNISCHE UNIVERSITÄT WIEN
Vienna University of Technology

DIPLOMARBEIT

Electrochemically Switchable Adhesion of a Catechol Functionalized Monolayer

zur Erlangung des akademischen Grades
Diplom-Ingenieur

im Rahmen des Studiums
Masterstudium Technische Physik

ausgeführt am Institut für Angewandte Physik
der Technischen Universität Wien

unter der Anleitung von
Univ.Prof. Dipl.-Ing. Dr.techn. Markus Valtiner
und
Univ.Ass. Dr.rer.nat. Hsiu-Wei Cheng

durch

Alexander Michael Imre, BSc

Rechte Bachgasse 79
7400 Oberwart
Österreich

Ort, Datum (Unterschrift Verfasser) (Unterschrift Betreuer)

Die approbierte gedruckte Originalversion dieser Diplomarbeit ist an der TU Wien Bibliothek verfügbar
The approved original version of this thesis is available in print at TU Wien Bibliothek.
TU Bibliothek Your knowledge hub WIEN

Die approbierte gedruckte Originalversion dieser Diplomarbeit ist an der TU Wien Bibliothek verfügbar
The approved original version of this thesis is available in print at TU Wien Bibliothek.

Abstract

The adhesion of marine mussels has peaked the interest of many in the scientific community because of their ability to firmly attach to a wide range of substrates in wet and saline conditions. Such environments are generally unfavorable for conventional synthetic adhesives. With the hope of developing better, potentially biocompatible adhesives a lot of work has gone into studying the mechanisms involved in mussel adhesion. The catechol functional group has been found to be crucial in the attachment process and a large number of studies using the surface force apparatus have looked into catechol mediated adhesion. In addition, the catechol group is also able to undergo a redox reaction and has been well studied using electrochemistry. Yet, so far, these two aspects of catechol chemistry have remained largely disconnected.

This work aims to demonstrate a way to connect these two approaches. A catechol functionalized self assembled monolayer was produced and then characterized using cyclic voltammetry. It was then put up against different surfaces in the electrochemical surface force apparatus where a potential dependent, switchable adhesion was measured against mica. Furthermore, adhesion was strongly dependent on the ionic strength of the environment. This observation may help understand which mechanisms mussels use in nature to form adhesive bonds.

Altogether, the combination of a functionalized monolayer and the electrochemical surface force apparatus provides a promising sample system for future study of the interfacial behavior of catechols and other electrochemically active functionalities.

As a side product of this work, a new design for a thin film electrode was developed and improvements were made to an electrochemical cell setup, which will potentially benefit future work in catechol electrochemistry and other research areas.

Die approbierte gedruckte Originalversion dieser Diplomarbeit ist an der TU Wien Bibliothek verfügbar
The approved original version of this thesis is available in print at TU Wien Bibliothek.
TU Bibliothek Your knowledge hub WIEN

Die approbierte gedruckte Originalversion dieser Diplomarbeit ist an der TU Wien Bibliothek verfügbar
The approved original version of this thesis is available in print at TU Wien Bibliothek.

Zusammenfassung

Die Adhäsion von Meeresmuscheln hat das Interesse vieler in der wissenschaftlichen Gemeinschaft geweckt, da sie in der Lage sind, sich fest an einer großen Vielfalt von Substraten festzusetzen, selbst in nasser und salziger Umgebung, die generell ungünstig für konventionelle, synthetische Klebstoffe ist. Mit der Hoffnung auf die Entwicklung besserer, potentiell biokompatibler Klebstoffe, sind große Anstrengungen in die Untersuchung der involvierten Adhesionsmechanismen geflossen. Die funktionelle Gruppe der Catechole hat sich als entscheidend für den Adhäsionsprozess herausgestellt, weshalb sich eine große Anzahl wissenschaftlicher Studien mit der Catechol-basierten Haftung im Oberflächenkraftapparat befasst hat. Abgesehen davon, ist die Catechol-Gruppe aber zu einer Redox-Reaktion fähig, die mittels elektrochemischer Verfahren gut untersucht ist. Bis jetzt sind diese beiden Aspekte aber großteils getrennt voneinander betrachtet worden.

Diese Arbeit soll eine Möglichkeit aufzeigen, diese beiden Ansätze zu vereinen. Eine Catechol-funktionalisierte, selbstorganisierte Monoschicht wurde produziert und mittels zyklischer Voltammetrie untersucht und charakterisiert. Sie wurde dann im elektrochemischen Oberflächenkraftapparat gegen verschiedene Oberflächen untersucht, wobei eine Potential-abhängige, schaltbare Adhäsion gegen Mica gemessen wurde. Zusätzlich wurde eine starke Abhängigkeit der Adhäsion von der Ionenstärke beobachtet. Dies könnte helfen zu verstehen, wie sich Meeresmuscheln in der Natur an Oberflächen anhaften.

Die Kombination aus einer funktionalisierten Monolage und dem Oberflächenkraftapparat bietet ein vielversprechendes Testsystem für die zukünftige Untersuchung des Verhaltens von Catecholen und anderer elektrochemisch aktiver Funktionalitäten an Grenzflächen.

Im Laufe dieser Arbeit wurde außerdem ein neues Design für eine Dünnschicht-Elektrode entworfen, und es wurde eine existierende elektrochemische Zelle verbessert, was eventuell zukünftigen Arbeiten an der Catechol Elektrochemie und in anderen Bereichen zugute kommen wird.

Die approbierte gedruckte Originalversion dieser Diplomarbeit ist an der TU Wien Bibliothek verfügbar
The approved original version of this thesis is available in print at TU Wien Bibliothek.
TU Bibliothek Your knowledge hub WIEN

Die approbierte gedruckte Originalversion dieser Diplomarbeit ist an der TU Wien Bibliothek verfügbar
The approved original version of this thesis is available in print at TU Wien Bibliothek.

Acknowledgments

First and foremost, I would like to extend my sincere gratitude to Markus Valtiner for enthusiastically inviting me to join this research group first as a project student and later as a Master student and the many very educational scientific discussions. Likewise, I would like to thank my supervisor and friend Hsiu-Wei Cheng – William – for providing me the much needed ongoing support, both academic and personal. Without you I would not have been able to do this!

A special thanks also goes out to all the members of our research group for Applied Interface Physics. Even in these challenging times, it was a great pleasure to work with you and become friends in the process. In particular, I would like to thank Dominik Dworschak for always helping me and everyone else in the lab, even though he had no obligation to do so. Furthermore, I would like to express my gratitude to Valentina Wieser and Hui Yuan for helping me with the SFA whenever I was struggling. Thank you so much, Carina Brunnhofer and Marina Bishara for being the best office-mates I could have hoped for and keeping my spirits up even when frustration was running high.

I would like to offer my special thanks to my great friends Anne Satzinger and Sonja Tögl for helping me take my mind off things every once in a while and always being there when I needed them.

A big thank you also goes out to all my former teachers who encouraged me to go into science and set me on this path.

Finally, I would like to thank my parents who gave me my roots but allowed me to grow my own wings.

Die approbierte gedruckte Originalversion dieser Diplomarbeit ist an der TU Wien Bibliothek verfügbar
The approved original version of this thesis is available in print at TU Wien Bibliothek.
TU Bibliothek Your knowledge hub WIEN

Die approbierte gedruckte Originalversion dieser Diplomarbeit ist an der TU Wien Bibliothek verfügbar
The approved original version of this thesis is available in print at TU Wien Bibliothek.

Abbreviations and Symbols

Abbreviations	Description
AFM	Atomic Force Microscopy
CCD	Charge-coupled Device
CE	Counter Electrode
CV	Cyclic Voltammetry; Cyclic Voltammogram
DHCA	Dihydrocaffeic Acid
DMT	Derjaguin-Muller-Toporov Model
EC-SFA	Electrochemical Surface Force Apparatus
EDC	1-Ethyl-3-(3-dimethyl-aminopropyl)carbodiimide
EDL	Electric Double Layer
FECO	Fringes of Equal Chromatic Order
JKR	Johnson-Kandall-Roberts Model
L-DOPA	L-3,4-dihydroxyphenylalanine
ME	2-Mercaptoethanol
MFP	Mussel Foot Protein
NHS	N-hydroxysuccinimide
OPC	Open Circuit Potential
PVD	Physical Vapour Deposition
RE	Reference Electrode
SFA	Surface Force Apparatus
SHE	Standard Hydrogen Electrode
WE	Working Electrode

Die approbierte gedruckte Originalversion dieser Diplomarbeit ist an der TU Wien Bibliothek verfügbar
The approved original version of this thesis is available in print at TU Wien Bibliothek.
TU Bibliothek Your knowledge hub WIEN

Symbols	Description [SI Unit]
$a_{O/R}$	Activity coefficient [1]
F_{adh}	Adhesion Rupture Force [N]
N_A	Avogadro constant $[\frac{1}{mol}]$
Q	Charge [C]
$\mu/\tilde{\mu}$	Chemical Potential/Electrochemical Potential [J]
i/i_p	Current/Peak Current [A]
R	Radius [m]
E	Electrical Potential [V]
e	Elementary Charge [C]
H	Enthalpy $[\frac{J}{mol}]$
S	Entropy $[\frac{J}{molK}]$
F	Faraday Constant $[\frac{C}{mol}]$
$G/\tilde{G}$	Gibbs Free Energy/with External Field $[\frac{J}{mol}]$
q	Heat Energy $[\frac{J}{mol}]$
N	Number of Particles in Statistical Physics [1]
n	Number of Transferred Electrons [1]
p	Pressure [Pa]
$E^{0'}$	Reaction Formal Potential [V]
E^0	Reaction Standard Potential [V]
ν	Scan Rate in CV $[\frac{mV}{s}]$
A	Surface area [m^2]
Γ^*	Surface Coverage $[\frac{mol}{cm^2}]$
T	Temperature [K]
t	Time [s]
R	Universal Gas constant $[\frac{J}{mol \times K}]$
V	Volume [m^3]
$\Delta\gamma$	Work of Adhesion $[\frac{J}{m^2}]$

Die approbierte gedruckte Originalversion dieser Diplomarbeit ist an der TU Wien Bibliothek verfügbar
The approved original version of this thesis is available in print at TU Wien Bibliothek.
TU Bibliothek Your knowledge hub WIEN

Contents

Abstract I

German Abstract III

Acknowlegements V

Abbreviations and Symbols VII

Contents IX

1. Introduction 1
- 1.1. Motivation . . . 1
- 1.2. Literature review . . . 2
  - 1.2.1. From Mussel to Catechol . . . 2
  - 1.2.2. Catechols and Catecholamines . . . 5
  - 1.2.3. Catechol electrochemistry . . . 6
  - 1.2.4. Self Assembled Monolayers . . . 7
  - 1.2.5. Catechol Functionalized Self Assembled Monolayers . . . 8
- 1.3. Aims and Objectives of this Thesis . . . 9

2. Methodology 11
- 2.1. Self assembled monolayers . . . 11
- 2.2. Electrochemistry . . . 12
  - 2.2.1. Fundamentals relevant to this work . . . 13
  - 2.2.2. Three electrode system . . . 15
  - 2.2.3. Cyclic Voltammetry . . . 15
- 2.3. Surface Force Apparatus . . . 18
  - 2.3.1. Electrochemical Surface Force Apparatus . . . 21

3. Materials and Instrumentation 23
- 3.1. Chemicals and Surfaces . . . 23
- 3.2. SAM preparation . . . 24
- 3.3. Cyclic voltammetry . . . 25
  - 3.3.1. Electrochemical cell . . . 25

Die approbierte gedruckte Originalversion dieser Diplomarbeit ist an der TU Wien Bibliothek verfügbar
The approved original version of this thesis is available in print at TU Wien Bibliothek.
TU Bibliothek Your knowledge hub WIEN

3.3.2. Electrode Design 26
3.3.3. Data analysis 29
3.4. Surface force apparatus 30
3.4.1. Setup 30
3.4.2. Disc Preparation and Measurement 31
3.4.3. Data analysis 31

4. Results and Discussion **33**
4.1. Cyclic voltammetry 33
4.1.1. Characterization of the SAM 33
4.1.2. Calculation of the Surface Coverage 35
4.2. Electrochemical Surface Force Apparatus 39
4.2.1. Measurements against back-silvered Mica 39
4.2.2. Measurements against OH and Ti coated surfaces 43
4.3. Summary, Conclusion and Outlook 46

Bibliography **i**

A. Copyright Clearances **xi**

B. Technical Drawings **xv**

C. Data Analysis Source Code **xxiii**
C.1. Cyclic Voltammetry xxiii
C.2. Electrochemical Surface Force Apparatus xxxi

Die approbierte gedruckte Originalversion dieser Diplomarbeit ist an der TU Wien Bibliothek verfügbar
The approved original version of this thesis is available in print at TU Wien Bibliothek.

1. Introduction

1.1. Motivation

Over hundreds of millions of years, marine mussels and other maritime organisms have evolved the ability to adhere strongly to a wide range of underwater surfaces [1]. They remain tethered in a suitable habitat and are not swept away by ocean currents and tides while they perform essential biologic functions [2, 3]. This provides such a major evolutionary advantage for these creatures that they devote a significant part of their entire metabolic budget to the production and maintenance of their complex biological adhesion system [4, 5].

It turns out that this sticky peculiarity of maritime biology has a considerable societal impact in a number of areas. In the form of biofouling, the adhesive properties of maritime organisms have a massive economic and ecological effect in the naval sector due to increased fuel consumption and hull maintenance costs [6]. These problems also extend to other industries that use seawater or structures submerged in it such as industrial water cooling systems [7, 8]. A growing multi-billion dollar anti-fouling coating industry as emerged to combat these issues [9]. Yet, a more thorough study of the adhesion mechanisms is required for future advances in this area.

More recently, the adhesive abilities of mussels and other species have peaked the interest of many in industry and in the scientific community from a biomimetic perspective – exactly because of the firm attachment underwater. Given their origin and purpose, these marine adhesives are perfectly suited and made for usage and durability underwater. In stark contrast, most modern synthetic polymeric adhesives, e.g. many epoxide-based ones [10], are negatively affected by the presence of water. It is often necessary to go to great lengths to avoid any residual moisture on the parts that should be stuck together before the adhesive is applied. Even when cured, exposure to water can weaken and eventually fully degrade synthetic adhesive polymers leading to joint failure [11].

An area of potential application for glues based on the adhesives used by marine organisms is as medical tissue adhesives as a replacement for the classic surgical suture. Glues used for closing wounds or even inside the body need to be non-toxic, work well in a wet environment and be generally bio-compatible. Ideally, the adhesive would be fast and easy to apply and be degraded by the body when

Die approbierte gedruckte Originalversion dieser Diplomarbeit ist an der TU Wien Bibliothek verfügbar
The approved original version of this thesis is available in print at TU Wien Bibliothek.
TU Bibliothek Your knowledge hub WIEN

no longer needed without producing harmful waste products [12]. Mussel-adhesive based polymers may have advantages in these areas over existing medical glues like various cyanoacrylates that can have cytotoxic effects [13]. There have already been a number of promising attempts at developing biocompatible mussel-based adhesives on an elastin [14] or hydrogel basis [15–17] and the field continues to make rapid progress [18–20].

Future progress in all of these and many more applications will require a more fundamental understanding of the adhesion mechanisms employed by organisms such as marine mussels. As will be discussed in section 1.2.1, the catechol functional group is thought to play a key role in crosslinking the adhesive and forming bonds with a range of surfaces. It therefore makes sense to study the chemical and interfacial properties of catechol with the ultimate goal of understanding the bonds formed with various substrates and the energy landscape associated with these processes.

1.2. Literature review

1.2.1. From Mussel to Catechol

The most common examples of maritime organisms studied for their adhesion mechanism are the mussel species of the *Mytilus* genus, in particular *Mytilus californianus*, *Mytilus galloprovincialis* and *Mytilus edulis*. They all share an elaborate attachment system via the so-called byssus produced by the mussel foot. The byssus consists of threads that connect the base of the mussel foot inside the shell and the surface the mussel is attached to. At the distal end of each thread the attachment plaque forms the adhesive connection to the substrate [4]. An image of a mussel of the species *Mytilus californianus* with parts of the mussel foot and the byssus labeled in a schematic is shown in figure 1.1.

Study of the adhesive plaque has shown that it consists of a number of "mussel foot proteins" (mfp)[1], which take over a number of specialized functions [21]. Mfp-1 is thought to act as a protective coating while mfp-2 and mfp-4 predominantly make up the matrix and connection to the thread [22, 23]. Most notably, mfp-3 and mfp-5 are mainly found at the plaque-substrate interface and are responsible for forming bonds with the substrate and providing adhesion [3, 24]. Mfp-6 is found alongside mfp-3 and mfp-5 and has been determined to support the adhesion mechanism by creating a reducing environment [25]. Fig. 1.3 shows a schematic of the adhesive plaque in which the proposed functions of a number of mfps are indicated.

[1] Also found abbreviated in the literature as fp or m**c**fp/m**g**fp/m**e**fp where **c**, **g** or **e** stands for the species Mytilus californianus, Mytilus galloprovincialis or Mytilus edulis respectively.

Die approbierte gedruckte Originalversion dieser Diplomarbeit ist an der TU Wien Bibliothek verfügbar
The approved original version of this thesis is available in print at TU Wien Bibliothek.
TU Bibliothek Your knowledge hub WIEN

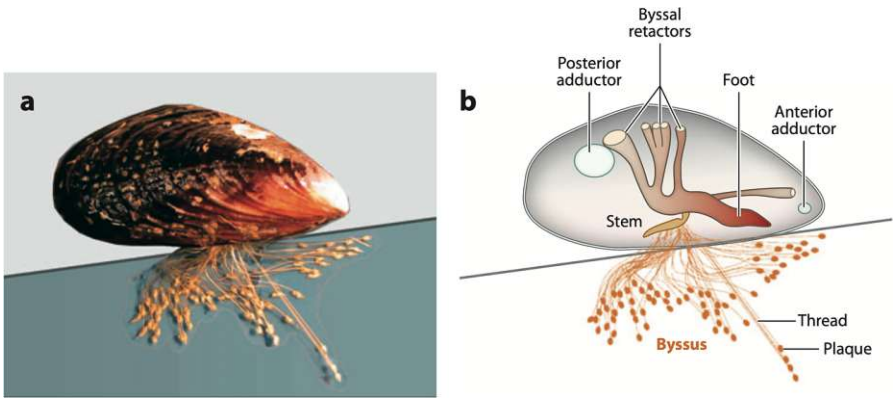

Figure 1.1.: Bio-adhesion of a mussel of the species *mytilus californianus*. a) Image of the mussel adhering to a piece of mica substrate clearly showing the byssus threads and adhesive plaques. b) Labeled drawing showing the internals of the mussel biology. Reproduced with permission form ANNUAL REVIEWS [4]. See appendix A for copyright clearance.

The process of the mussel plaque formation has been extensively studied using a variety of techniques. Initially, the mussel foot contacts the surface and creates a negative pressure environment akin to a suction cup. It then adjusts pH, ionic strength and the redox environment using various secretions before injecting the adhesive proteins. This ensures that the initial steps of the adhesion process happen under conditions very different from typical sea water conditions (pH $\sim$ 8 in an oxidizing environment). [1, 26]

Chemical analysis of the mfps has shown that they share an unusually high abundance of the catecholic amino acid 3,4-dihydroxyphenylalanine (L-DOPA, structure is shown in figure 1.4a) [27]. L-DOPA is produced after protein synthesis through hydroxylation of the proteinogenic amino acid tyrosine via tyrosine hydroxylase [28, 29]. Over the last two decades the knowledge about their key role in the adhesion mechanism has lead to the intensive study of catecholamines and catechols, which is the focus of the present work as well.

The adhesive mfp-3 and mfp-5 in particular have been found to contain the highest amount of L-DOPA with concentrations of around 20 and 30 mol % respectively. This abundance suggests that L-DOPA and consequently the catechol group are crucial for mussel glue adhesion. Indeed, it has been found that catechols enable a wide range of bonding mechanisms usable for adhesion and polymer crosslinking (see fig. (1.2) [1, 3, 30].

For adhesion to the substrate, the catechol group is thought to rely on hydrogen bonds (1.2 b), coordination bonds (1.2 c), hydrophobic interactions (1.2 d) and potentially π-π interactions (1.2 e). Crosslinking is theorized to be achieved using

Die approbierte gedruckte Originalversion dieser Diplomarbeit ist an der TU Wien Bibliothek verfügbar
The approved original version of this thesis is available in print at TU Wien Bibliothek.
TU Bibliothek Your knowledge hub WIEN

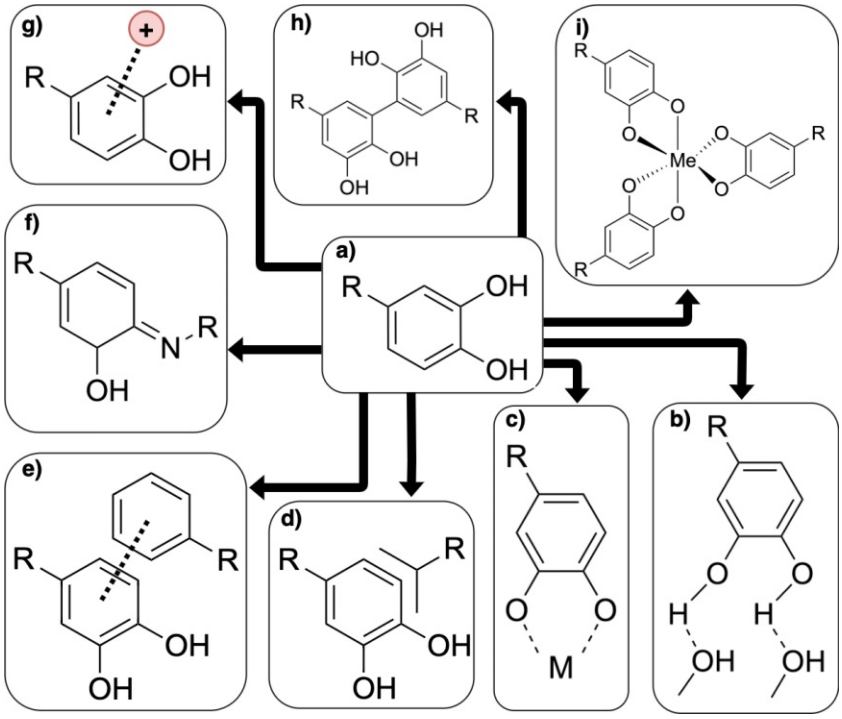

Figure 1.2.: Catechol functional group and proposed adhesion/interaction mechanisms. **a)** The catechol group. **b)** Hydrogen bonds with surface hydroxyl groups. **c)** Interaction via metal complexation. **d)** Hydrophobic interaction. **e)** π-π interaction. **f)** Covalent bonding (Schiff base reaction) **g)** cation-π interaction. **h)** One possible version of dimerization/polymerization via formation of covalent bonds. **i)** Chelation of metal ions by multiple catechol groups.

the same mechanisms in between functional groups in addition to the formation of covalent bonds via e.g. Schiff base reaction or Michael type addition (1.2 f and h) [31], chelation of metal ions by multiple catechol groups (1.2 i) and cation-π interactions (1.2 g). Other reactions of mfps for adhesion and cohesion are possible, e.g. in the form of electrostatic interactions and disulfide bonds but are generally less studied in the context of mussel based adhesion [32].

Out of these pathways, hydrogen bonds and coordination bonds have generally been considered to be the main mechanisms responsible for adhesion in catechol rich proteins but more recent work by Gebbie et al. has shown that the situation may not be as simple and that in fact cation-π interactions could play a more important role than previously thought [34]. Similarly, Bilotto et al. have shown that tyrosine is able to mediate adhesion comparable to that of catechol in the right conditions [35]. Furthermore, Shin et al. have found that the presence or absence

Die approbierte gedruckte Originalversion dieser Diplomarbeit ist an der TU Wien Bibliothek verfügbar
The approved original version of this thesis is available in print at TU Wien Bibliothek.
TU Bibliothek Your knowledge hub WIEN

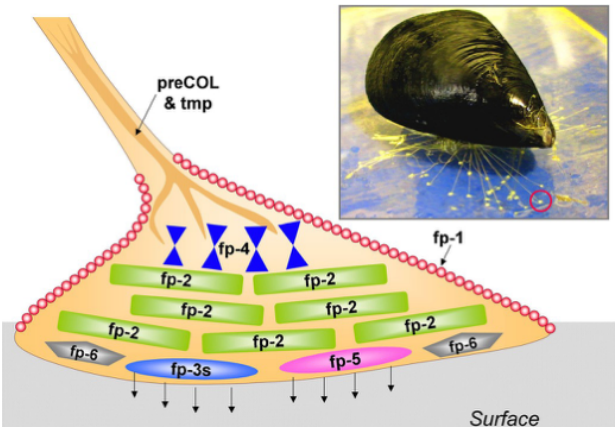

Figure 1.3.: Schematic of an adhesive plaque used in mussel adhesion indicating the primary location and function of the various mfps. The inset shows a mussel of the species *mytilus galloprovincialis* attached to a mica sheet. Reproduced with permission form THE JOURNAL OF BIOLOGICAL CHEMISTRY [33]. See appendix A for copyright clearance.

of other functionalities (in particular amine groups from the amino-acid lysine) in the vicinity of the catechol group can affect adhesion and cohesion strength [36]. Together, these results indicate that catechol chemistry alone may not be sufficient to explain marine mussel adhesion.

1.2.2. Catechols and Catecholamines

(a) L-DOPA (b) Dopamine

Figure 1.4.: Structural formula of L-DOPA and Dopamine, two biologically important catechol-amines also commonly used as the basis of mussel-inspired bio-mimetic adhesives.

Catechols are a class of compounds derived from catechol – a simple molecule with a benze ring and two ortho hydroxyl groups (see fig. 1.2 a where R is hydrogen). Members of the catecholamines additionally have an amine group and many

Die approbierte gedruckte Originalversion dieser Diplomarbeit ist an der TU Wien Bibliothek verfügbar
The approved original version of this thesis is available in print at TU Wien Bibliothek.
TU Bibliothek Your knowledge hub WIEN

of them are important to human biology as hormones and neurotransmitters.

Apart from the various mfps, L-DOPA is the most commonly studied system for mussel biomimetic adhesion and a number of studies have looked into synthetic adhesive polymers enhanced by L-DOPA [37, 38]. Many of these polymers share the same mechanisms for adhesion and cohesion as the mfps but their properties can be adjusted by changing the polymeric back bone.

Dopamine (3,4-dihydroxyphenethylamine, structure is shown in fig. 1.4b) is another catecholamine which shares the structure of L-DOPA but lacks the carboxylic acid group. It is well known for its role as a neurotransmitter in the human central nervous system where it plays a crucial role in cellular signaling. In fact, over- or underproduction of dopamine are related to illnesses such as Parkinson's disease and schizophrenia [39]. Like L-DOPA, dopamine has been commonly used to produce catechol containing polymers [40].

A common theme in polymers based on L-DOPA, dopamine and other catecholamines is the crucial influence of the amine group. It is either used for binding to a polymeric backbone or participates in covalent crosslinking. In fact these catecholamines are able to form polymers without any additives at all. The self-polymerization of L-DOPA and dopamine are well known and intensively studied, though the structure and polymerization pathways of dopamine in particular have been a much debated issue [41]. In basic or oxidizing conditions, L-DOPA and dopamine will auto-polymerize turning a solution of the compounds brown over time if exposed to environmental oxygen [42].

Poly-L-DOPA and poly-dopamine have become materials of interest in material science for use as multi purpose surface coatings [43]. Apart from increasing adhesion, potential applications range all the ways from enhancing biocompatibiliy of implant surfaces to improving CO_2 capture efficiency in membrane-separation systems [44–46]. For these purposes, polymerization can be triggered in a number of ways, including alkaline pH, exposure to UV light and through electrochemistry [42]. Natural polymerization products of L-DOPA and dopamine also play an important role in the animal kingdom (including humans) where they, among other things, are the basis for melanin pigmentation and UV-protection [47].

1.2.3. Catechol electrochemistry

A distinguishing feature of catecholic compounds is their electrochemical activity. Catechol and its derivatives can undergo a reversible oxidation reaction to an ortho-benzoquinone. In this reaction, the two hydroxyl groups are oxidized to ketones and give off one proton (H^+) and one electron (e^-) each. As may thus be expected by application of Le Chatelier's principle, the catechol form is generally more stable under acidic and reducing conditions while the oxidized quinone form is favored at higher pH and in oxidizing conditions [1]. Importantly, the quinone

Die approbierte gedruckte Originalversion dieser Diplomarbeit ist an der TU Wien Bibliothek verfügbar
The approved original version of this thesis is available in print at TU Wien Bibliothek.
TU Bibliothek Your knowledge hub WIEN

form has different chemical properties and in particular it is considered not to share the majority of the interaction mechanisms that lead to catechol adhesion [48, 49]. Instead, the oxidizdized form of L-DOPA (DOPA-quinone) is believed to contribute to cohesion through protein cross-linking [50]. Generally though, it appears that the mussel biology favors the catechol form (L-DOPA) as it invests significant amounts of its energy in providing and maintaining a reducing environment during the adhesion process through use of mfp-6 and other methods [1, 50].

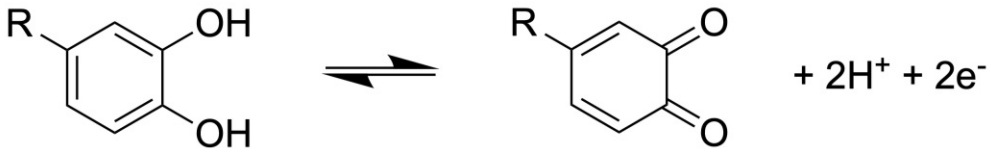

Figure 1.5.: Reversible redox reaction of catechol and ortho-benzoquinone. Two protons and two electrons are given off during oxidation.

The redox behavior of catechol and various derivatives has been thoroughly characterized in the past. Generally, an oxidation of the catechol group is observed at pH dependent standard potentials (explained by the Nernst equation; see section 2.2) unless the quinone group undergoes an irreversible follow-up reaction [51, 52]. This is reported to happen preferentially at a pH > 9 via a 1,4-Michael addition reaction [53]. The presence of an amine group in the molecule (such as in L-DOPA and in dopamine) opens up further follow-up pathways such as polymerization reactions to the oxidized species and therefore contributes greatly to electrochemical irreversibly of the system [42].

This means amine-triggered reactions can be a hindrance for researching the properties of the catechol group itself, especially in the case of studying the quasi-reversible catechol oxidation and characterization of the two distinct states. For these types of investigations, our group has therefore transitioned to working with amine-free catechol derivatives, most notably dihydrocaffeic acid (DHCA, see figure 1.6 for the structure). This compound shares the structure of L-DOPA though without the amine group, can be acquired commercially and is easy to handle [54].

1.2.4. Self Assembled Monolayers

Self assembled monolayers (SAMs) are a well known type of organic supra-molecular structures that form spontaneously out of a solution on a suitable substrate first reported by Bigelow, Pickett and Zisman in 1946 [55, 56]. They are prepared from a solution of a linear organic compounds with a head group that strongly and specifically adsorbes to a substrate incubated in the solution. As a general requirement, the enthalpy gain associated with the adsorption must be big enough

Die approbierte gedruckte Originalversion dieser Diplomarbeit ist an der TU Wien Bibliothek verfügbar
The approved original version of this thesis is available in print at TU Wien Bibliothek.
TU Bibliothek Your knowledge hub WIEN

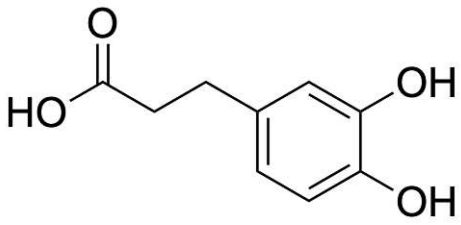

Figure 1.6.: Structural formula of DHCA, a catechol-containing compound closely related to L-DOPA but with out an amine group.

to compensate for the entropic penalty of moving the molecules from the solution into an organized 2D surface-confided structure [57]. The length of the hydrocarbon chain is a parameter that determines many of the monolayer properties where longer chain-lengths generally result in a more densely packed and both mechanically and chemically durable surface structure [58]. The other end of the organic compound (referred to as tail or end group) points away from the substrate and is at the newly formed SAM interface. A wide range of chemical functionalities are available for the end group offering a broad spectrum of surface modifications.

SAMs find application in many areas that require and use thin films and surface functionalization such as improving bio-compatibly [59], biosensing [60], microelectronics [61], production of functionalized nanoparticles [62] and corrosion inhibition [63]. Typical substrate-head group combinations are metal oxide with carboxyls, Si or SiO_2 with silanes or carboxlys and gold with sulfides or thiols [58].

1.2.5. Catechol Functionalized Self Assembled Monolayers

One area of particular relevance to this work are SAMs with an electrochemically active catechol functionalization. SAMs can be prepared on a number of substrates and with a variety of compounds. One typical combination, thiol-bound SAMs on gold, has the advantage of a conductive substrate that allows electrochemical control of the SAM end group (see section 3.2). A number of works have focused on preparing and characterizing such SAMs where this end group is comprised of a catechol group. SAMs produced from custom synthesized catechol-thiol compounds have been shown to exhibit the expected adhesive [64] and electrochemical properties [65, 66]. The SAM used in the present work is based on the one described by Salmanipour and Taher who used a cysteamine SAM that was subsequently functionalized with a catechol end group (see section 3.2) [67]. This procedure was chosen as a basis partially for its speed (compared to alternatives such as preparation of a lipid bilayer) and partially for its ease of use as it can easily be prepared in our lab which is not equipped for the organic synthesis of catechol-thiol compounds.

Die approbierte gedruckte Originalversion dieser Diplomarbeit ist an der TU Wien Bibliothek verfügbar
The approved original version of this thesis is available in print at TU Wien Bibliothek.
TU Bibliothek Your knowledge hub WIEN

1.3. Aims and Objectives of this Thesis

The surface force apparatus (SFA) has been a primary tool in the investigation of mussel adhesion in the past. A number of studies have looked at adhesion between different mfps [24], mfps and substrates (most commonly mica and TiO_2) [23, 48, 49] and variations of these systems with varying pH and additives [33, 68]. While these studies allow for a qualitative and comparative analysis of which systems behave more or less adhesive under given conditions, they come with the inherent disadvantage that it is unclear, which proportion of the present catechol groups actually participate in the measured adhesion.

These shortcomings can partially be addressed using atomic force microscopy (AFM) with single-molecule force spectroscopy as demonstrated by Utzig et al. [69]. This approach allowed for measurement of the interaction free energy of catechol with functionalized AFM tips from rupture force measurements using Jarzynski's equality [70, 71]. Nonetheless, even this approach had the disadvantage that the oxidation state is only controlled via pH.

On the other side stands electrochemistry, which allows for accurate quantitative measurements and would be sensitive to trace amounts of catechol, yet has so far been difficult to relate to adhesion. In short, so far most works have focused either on catechol adhesion or catechol electrochemistry but rarely have the two sides of the field come together. Yet, this combination may be exactly what is needed to move forward. A recently published study by Bhuiyan et al. demonstrated that electrochemical in-situ control of a catechol-containing glue is possible, even though on a macroscopic scale [72].

This thesis aims to highlight a potential new sample system and methodology for investigation of catechol based adhesion. The starting point is the working hypothesis that catechol adhesion is strictly dependent on the catechol oxidation state and can be switched electrochemically. Based on this, an experimental setup is designed in which adhesion can be measured under control of the oxidation state by combining a catechol terminated SAM with the electrochemical surface force apparatus (EC-SFA).

Using a short chain SAM creates a system in which the location and orientation of the active group is well defined and uniform because the catechol group is confined to the surface. Together with electrochemical control of the oxidation state via polarization of the surface, this gives precisely the kind of advantages needed to quantitatively measure the difference in adhesion between catechol and quinone forms. This combination will thereby help to understand the energy landscape of catechol and quinone surface interactions and elucidate their precise role in mussel adhesion.

Altogether this should help to answer some of the following research questions:

Die approbierte gedruckte Originalversion dieser Diplomarbeit ist an der TU Wien Bibliothek verfügbar
The approved original version of this thesis is available in print at TU Wien Bibliothek.
TU Bibliothek Your knowledge hub WIEN

- Does a catechol functionalized SAM exhibit similar electrochemical and adhesive properties as dissolved catechols and mfps?
- Is a catechol functionalized SAM a suitable sample system for study in the EC-SFA?
- Is it possible to measure a potential dependent adhesion in this system?
- If so, does the reduced form of catechol show a stronger adhesion then the oxidized form as is commonly assumed?

Die approbierte gedruckte Originalversion dieser Diplomarbeit ist an der TU Wien Bibliothek verfügbar
The approved original version of this thesis is available in print at TU Wien Bibliothek.
TU Bibliothek Your knowledge hub WIEN

2. Methodology

2.1. Self assembled monolayers

Gold-thiolate SAMs are one of the most commonly used type of thin films, due to the ease of use and adaptability. Molecularly smooth gold films, perfectly suited as substrate, can be produced quickly and cheaply using mica template-stripping techniques. Thiol based SAMs on such gold substrates are ubiquitously used in the field of interface physics including in our group.

Moreover, all sample systems employed for the experiments shown in this work are based on two SAMs grown from two short chain thiols, cysteamine (2-aminoethanethiol) and β-mercaptoethanol (2-mercaptoethanol, ME) whose chemical structures are shown by themselves in figure 2.1 and as a SAM in figure 2.3 a) and b).

Once a surface has been incubated and the SAM has grown, the end group may be further modified to study more complex system like bio-molecules. For this, the toolbox of synthetic organic chemistry offers a great number of options, depending on the identity of the end group [62]. One well established technique for this purpose is the usage of carbodiimde crosslinking agents such as 1-ethyl-3-(3-dimethylaminopropyl)carbodiimide (3-(ethyliminomethyleneamino)-N,N-dimethylpropan--1-amine, EDC) and N-hydroxysuccinimide (1-hydroxy-2,5-pyrrolidinedione, NHS). EDC and NHS (structures shown in figure 2.2) prompt the formation of peptide bonds between amino acids, peptides and proteins but can also be used to link surface-confined amine groups with carboxylic acids in solution or vice versa. This is a commonly used reaction employed in a broad range of fields. A breakdown of the mechanism is given e.g. by the article by ThermoFisher on carbodiimide crosslinker chemistry [73].

In the present work, EDC/NHS crosslinking was used to functionalize a SAM of

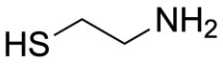

(a) Cysteamine

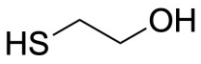

(b) 2-Mercaptoethanol (ME)

Figure 2.1.: Structural formula of cysteamine and ME, the two short chain thiols used in the gold-thiolate SAMs studied in the present work.

Die approbierte gedruckte Originalversion dieser Diplomarbeit ist an der TU Wien Bibliothek verfügbar
The approved original version of this thesis is available in print at TU Wien Bibliothek.
TU Bibliothek Your knowledge hub WIEN

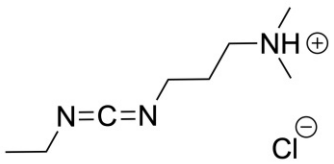

(a) 1-ethyl-3-(3-dimethylamino-propyl)carbodiimide (EDC)

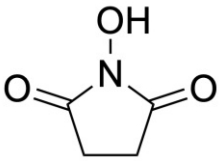

(b) N-hydroxysuccinimide (NHS)

Figure 2.2.: Structural formula of EDC and NHS, the carbodiimide crosslinking agents used in this work for modifying a cysteamine SAM.

cysteamine on a gold substrate. A catechol functionalized electrode was produced by linking the amine-terminated SAM with the carboxylic acid group of DHCA with EDC/NHS as indicated in figure 2.3 c).

2.2. Electrochemistry

Many chemical reactions involve the transfer of charge in the form of electrons (e^-) from one species (which is thereby oxidized) to another (which is reduced). These kinds of reactions, called reduction-oxidation or "redox" reactions, are some of the fundamental reaction types and are essential to all branches of chemistry. It

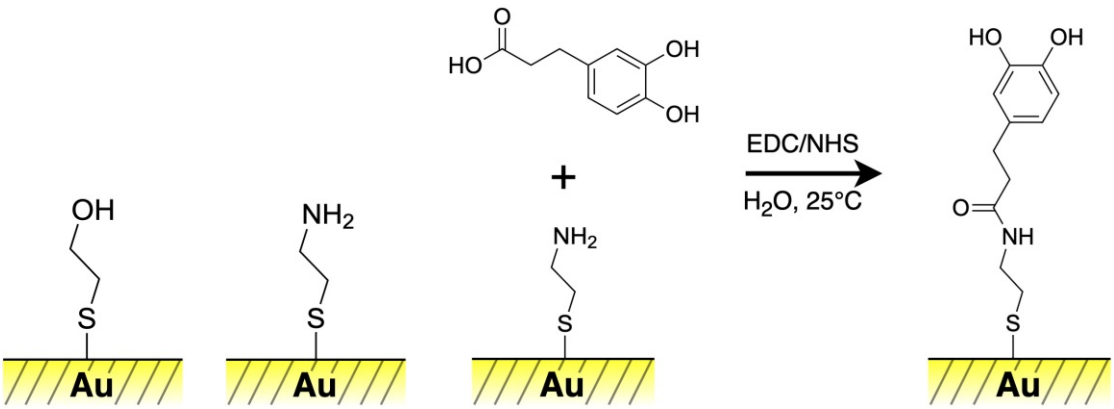

(a) (b) (c)

Figure 2.3.: Chemical structures of the used SAMs. **a)** ME SAM on gold substrate. **b)** cysteamine SAM on gold substrate. **c)** Subsequent modification of the cysteamine SAM with crosslinking chemistry through EDC/NHS. The electrochemically active catechol-terminated monolayer is produced by forming a peptide bond with DHCA.

Die approbierte gedruckte Originalversion dieser Diplomarbeit ist an der TU Wien Bibliothek verfügbar
The approved original version of this thesis is available in print at TU Wien Bibliothek.
TU Bibliothek Your knowledge hub WIEN

is further possible to split the reaction into two half reactions, in which oxidation and reduction do not necessarily need to happen in the same place.

In a liquid electrolyte with two submerged electrodes for example, it is possible to spatially separate the two reactions by allowing (e.g. in a battery) or forcing (e.g. in electrolysis) electrons to move from one electrode to the other through an external electrical connection. Electrochemistry is the branch of chemistry that studies the relation between chemical reactions and electricity. The goal is to relate fundamental and measurable quantities like the electrical potential (E), current (i), transferred charge (Q) etc. with the progress of chemical reactions and understand the thermodynamic and kinetics involved. This includes among other things electrolysis, corrosion and, more generally electrode processes.

2.2.1. Fundamentals relevant to this work

Thermodynamics allows to predict whether a process can occur spontaneously or not. For conditions of constant pressure p and temperature T the thermodynamic potential minimized is the Gibbs free energy G. This means for a reaction to proceed, a change in Gibbs free energy $\Delta G = \Delta H - T\Delta S < 0$ is required where H is enthalpy and S is entropy.

Whereas for most chemical reactions energy can only be transferred in the form of mechanical work ($\int pdV$) or heat (q) and thus $\Delta H = q$, in electrochemical systems electrical work needs to be taken into account as well. Indeed, if all work is of electrical nature, one easily arrives at equation 2.1.

$$\Delta G^0 = -nFE^0 \tag{2.1}$$

This relates the reaction Gibbs free energy with the standard potential E^0, which is a characteristic of any given electrochemical reaction. F is the Faraday constant and n corresponds to the number of transferred electrons. [74]

It is worth emphasizing that reaction standard potentials are a relative quantity. Even though every electrochemical reaction has an associated standard potential, it is only ever possible to measure differences in these potential, as a half-cell can never be measured alone. Therefore, a common reference half-cell, the so-called standard hydrogen electrode (SHE), has been established and assigned a standard potential of 0.00 V. Be that as it may, using the SHE is rather impractical for most experiments. Thus, for convenience, a number of other half-cells with a stable potential vs. the SHE are usually used for everyday measurements. One such system, that was employed for the present work, is the silver|silver chloride (Ag|AgCl) electrode in 3 M KCl which has a potential of 0.21 V vs. the SHE. [75]

The standard potential of a reaction is defined and measured in standard conditions, that is 1 M concentration of all involved species in solution (including H^+).

Die approbierte gedruckte Originalversion dieser Diplomarbeit ist an der TU Wien Bibliothek verfügbar
The approved original version of this thesis is available in print at TU Wien Bibliothek.
TU Bibliothek Your knowledge hub WIEN

Under different conditions (temperature or concentrations) the cell potential can be calculated using the Nernst equation (equation 2.2).

$$E = E^0 + \frac{RT}{nF} \ln(\frac{a_O}{a_R}) \tag{2.2}$$

Therein, R is the universal gas constant. If a potential is applied externally the Nernst equation can predict how concentrations of reduced and oxidized species will change in response. More accurately, rather than concentrations, the Nernst equation contains the activity coefficients of the oxidized and reduced species, a_O and a_R, respectively, which are a type of effective concentrations. In practice, at least in dilute solutions, the activity coefficients can be approximated as the concentrations.

For practical purposes, the standard potential E^0 is commonly replaced with the formal potential $E^{0'}$ which is more accessible experimentally. If the described redox reaction involves release or capture of H^+ the potential will therefore also be pH dependent.[1] It is important to realize that when a potential is applied the Nernst equation will initially only be fulfilled locally at the electrode (see also section 2.2.3). Over time diffusion will lead to an equilibrium in the bulk solution as well. In the case of a surface confined analyte, e.g. an electrochemically active SAM, this will be significantly sped up. [76]

From a fundamental thermodynamic perspective, the driving force for chemical change of any given species (as well as phase transitions) can be found in the chemical potential μ defined by equation 2.3. [76]

$$\mu = \frac{\partial G}{\partial N} \tag{2.3}$$

If an external electric field is present, the energy of charged species is affected which can be written as $\tilde{G} = G + nFE$ where $\tilde{G}$ is the Gibbs free energy including the external field. Inserting $\tilde{G}$ in equation 2.3 yields the electrochemical potential $\tilde{\mu}$ which can be used to describe the behavior of all participants in (electro)chemical reactions (equation 2.4). A gradient in $\tilde{\mu}$ is also the driving force behind diffusion (concentration gradient) and electro-migration (potential gradient for charged species). This quantity is thus of crucial importance for considerations of processes in electrolytes and interfaces.[2] [75, 76]

$$\tilde{\mu} = \frac{\partial \tilde{G}}{\partial N} = \frac{\partial (G + NnFE)}{\partial N} = \mu + nFE \tag{2.4}$$

[1] This is the case for catechol oxidation/reduction.

[2] It is also commonly used in solid state physics to describe electron energy.

Die approbierte gedruckte Originalversion dieser Diplomarbeit ist an der TU Wien Bibliothek verfügbar
The approved original version of this thesis is available in print at TU Wien Bibliothek.
TU Bibliothek Your knowledge hub WIEN

When an electrode is immersed in an electrolyte a difference in $\tilde{\mu}$ will cause ions to either dissolve out of the electrode material or adsorb out of the electrolyte solution. In either case this causes a charge separation between the surface and the electrolyte and thus a potential difference with an associated electric field. Charged ions in the solution are attracted to the reversely charged electrode and will accumulate in its proximity forming the so called electric double layer (EDL). The EDL plays a crucial role in all solid-liquid interface considerations. A variety of models have been developed to describe the EDL, starting from Herman von Helmholtz in 1853 [77].

2.2.2. Three electrode system

In electrochemistry research, in most cases, it would be desirable to study processes at a single electrode. However, this is a fundamental problem, as two electrodes are required to allow current flow through the electrolyte. Furthermore, current flow through a reference electrode (RE) would change the measured reference potential through concentration change and a resistive potential drop according to Ohm's law. Therefore, most electrochemical measurements, including all measurements presented in this work, use a three electrode system consisting of working electrode (WE), reference electrode and counter electrode (CE). There, the WE is the electrode of interest for the experiment. The RE has a stable, known standard potential while the CE is generally made of an inert material, commonly Pt, and designed to have a surface area much larger than the WE. This avoids diffusion limitation on that side of the cell and ensures enough current can be supplied without reaching a large overpotential at which e.g. hydrogen is produced.

In a three electrode system, the potential E is measured between the WE and the RE, but the current i flows and is measured between WE and CE. A potentiostat controls E as required by applying a current between WE and CE until the potential between WE and RE reaches the set value. Figure 2.4 shows a schematic of a three electrode system and a potentiostat in its simplest form with a simplified circuit diagram.

2.2.3. Cyclic Voltammetry

Generally, voltammetric measurements record the current i as a function of the applied electric potential E. In cyclic voltammetry (CV) the applied potential is varied linearly over time back and forth between two set potentials as shown in the bottom half of figure 2.5. Important experimental parameters of a CV[3] are the potential range, i.e. the minimum and maximum potentials, the scan rate ν

[3]Here CV also stands for cyclic voltammogram.

Die approbierte gedruckte Originalversion dieser Diplomarbeit ist an der TU Wien Bibliothek verfügbar
The approved original version of this thesis is available in print at TU Wien Bibliothek.
TU Bibliothek Your knowledge hub WIEN

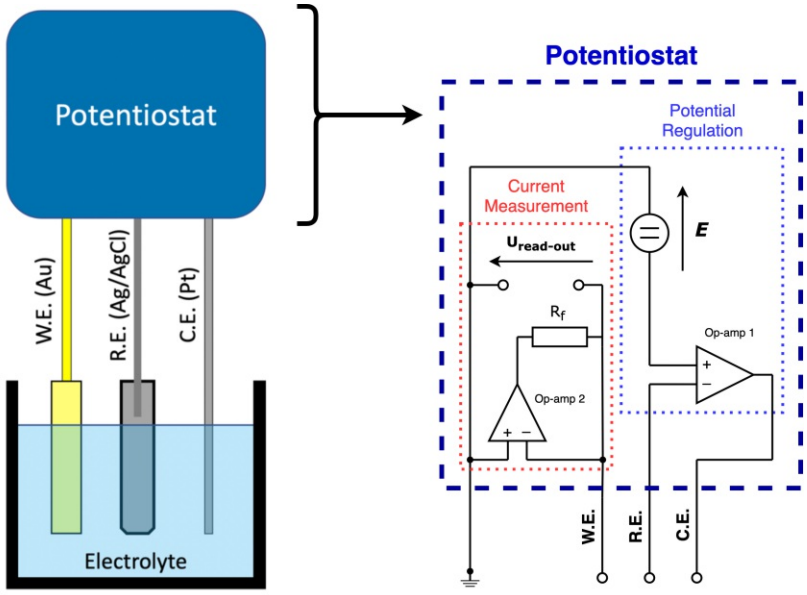

Figure 2.4.: Diagram of a three electrode system with WE, RE and CE connected to the potentiostat. On the right side a simplified circuit diagram of a potentiostat is given. In this setup the potential E is applied between the WE and RE using an ideal voltage source. An operational amplifier (Op-amp 1) provides as much current as needed to the CE while no current flows through the RE. The current is measured using a loss-free current sensor in which another operational amplifier (Op-amp 2) electrically separates WE and ground and the current is calculated using the voltage drop ($U_{read-out}$) over a know resistor (R_f). The circuit is based on drawings by ALS Co. and Custom Sensor Solutions Inc. [78, 79]

.

which is the measure of how quickly the potential is changed (given in mV/s) and the sequence number of the recorded cycle.

The measured current response (see top half of figure 2.5) is the sum of two parts: capacitive background current and faradaic current from the analyte. The capacitive current is the result of charging the surface and the EDL like in a capacitor and is present in any CV measurement irrespective of the analyte. The faradaic current stems from the electrochemical reactions happening at the electrode. Crucially for the interpretation, the presence of an electrochemically active species in solution or on the electrode surface results in a peak recorded in the current during oxidation and/or reduction if the formal potential $E^{0'}$ falls within the potential scan range. This peak is produced by two competing effects. On

Die approbierte gedruckte Originalversion dieser Diplomarbeit ist an der TU Wien Bibliothek verfügbar
The approved original version of this thesis is available in print at TU Wien Bibliothek.
TU Bibliothek Your knowledge hub WIEN

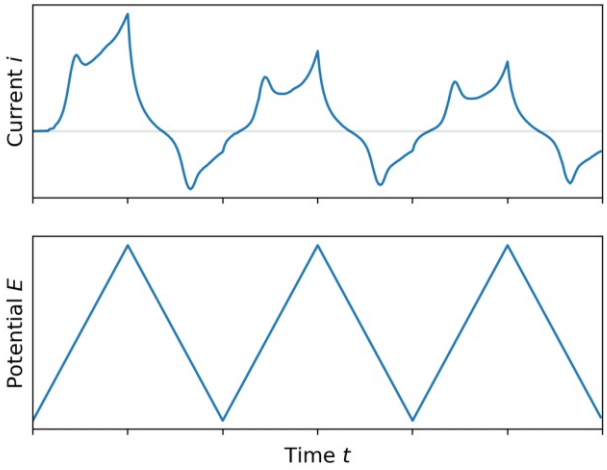

Figure 2.5.: Schematic of potential E (bottom) and current i (top) as a function of time t during a CV measurement of sample data from a quasi-reversible reaction in a bulk solution of DHCA.

the one hand, the local concentrations of oxidation and reduced species change according to the Nernst equation (equation 2.2) with the applied potential E. The concentration change, which requires oxidation or reduction and thus current flow happens faster as E gets closer to $E^{0'}$. On the other hand, the oxidation/reduction rate is limited by mass transport to and from the electrode because only the molecules present directly at the interface can give off or receive electrons. Thus, the current eventually becomes limited by diffusion as the deciding factor is transporting electrochemically active species between electrode and bulk solution. This results in a current decrease with time and thus in CV with potential too. In their usual depiction, CVs are shown as current vs. potential curves, e.g. the current shown in figure 2.5 is folded in on itself yielding a characteristic "duck"-like shape (compare e.g. figure 4.1b a). [75, 80]

CV is a commonly used analytical technique in electrochemistry as it is simple to perform but can be very sensitive to small amounts of analyte. It allows a qualitative analysis through the position of the peak currents and gives a quick assay to the presence of electrochemically active compounds. A quantitative analysis is also possible though it can be challenging, especially if more than one species contributes to the measured current.

A commonly employed analysis method is the Randles-Sevcik equation, which relates the peak current i_p with the scan rate and a number of other parameters.

Die approbierte gedruckte Originalversion dieser Diplomarbeit ist an der TU Wien Bibliothek verfügbar
The approved original version of this thesis is available in print at TU Wien Bibliothek.
TU Bibliothek Your knowledge hub WIEN

For an analyte in bulk solution the relation $i_p \propto \sqrt{\nu}$ is observed in which the proportionality factor includes the bulk concentration, the electrode surface area (A) and the diffusion coefficient. In the case of a strongly surface-adsorbed analyte (e.g. an electrochemically active SAM as proposed in this work) a *linear* relationship between i_p and ν is observed instead.[4] The peak current can then be described as shown in equation 2.5 based on the surface area and the active surface coverage Γ^* measured in molecules per surface area. The latter quantity is of particular interest as a crucial characteristic of a SAM that is is generally difficult to determine using methods other than CV. [76, 80]

$$i_p = \frac{n^2 F^2}{4RT} \nu A \Gamma^* \tag{2.5}$$

An alternative method of estimating the surface coverage is to numerically integrate the peak area of the CV and thereby calculate the amount of charge transferred in the reaction. Both approaches are employed in section 4.1.2 where they are shown to produce comparable results.

2.3. Surface Force Apparatus

The surface force apparatus is a device used to very precisely measure forces between two opposing surfaces. It can be used for the study of interactions such as electrostatic forces, van der Waals forces, capillary forces, hydration forces, hydrophobic interactions, specific protein binding and, as used in this work, adhesion forces [81, 82]. This is achieved by accurately measuring the distance and force between the two surfaces while their relative movement is controlled with using piezo-actuator. Experiments using lateral movement for the study of friction and lubrication or measuring changes of the contact area while in contact are possible, though in the most common application, the surfaces are simply brought into contact and then retracted. This approach, usually termed a force-run, is used in the present work as well. While SFA experiments in air or vacuum are possible, most experiments are performed in some solution in a liquid cell to probe the solid-liquid interface.

At this point it is necessary to discuss the force-distance profile observed for such an experiment and how adhesion can be measured from the data. Figure 2.6

[4] This assumes no desorption of the electrochemically active species which is reasonable for the case of a strongly adsorbed SAM. Since there is no dissolved species involved in the this electrochemical reaction, the current does not depend on a diffusion coefficient. In fact, here the adsorbed species acts as a form of pseudo-capacitance. A comprehensive derivation can be found in the book on electrochemical methods by Bard and Faulkner [76].

Die approbierte gedruckte Originalversion dieser Diplomarbeit ist an der TU Wien Bibliothek verfügbar
The approved original version of this thesis is available in print at TU Wien Bibliothek.
TU Bibliothek Your knowledge hub WIEN

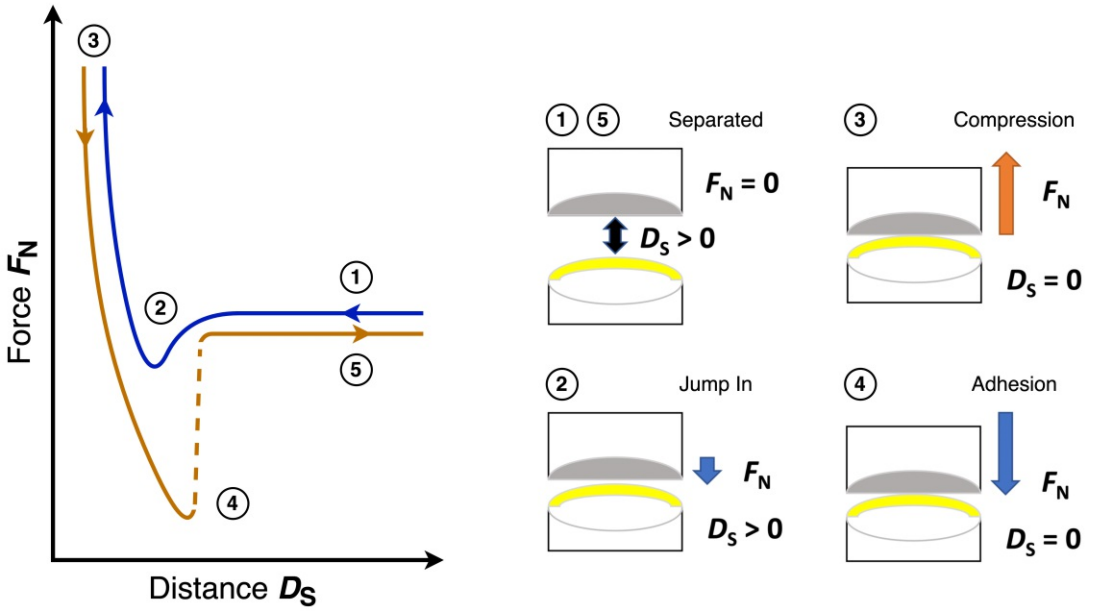

Figure 2.6.: Schematic diagram showing a typical force-distance profile measured in the SFA. Normal force (F_N) and separation distance (D_S) are pointed out for five points of interest. **(1)** and **(5)**: At large separation no force is measured. **(2)**: In the last section of the approach an attractive jump in can be observed. **(3)**: When in contact ($D_S = 0$), the discs can not move any further but a compression force is recorded. **(4)**: During retraction, an adhesion force may hold the surfaces together until the adhesion ruptures and the surfaces jump apart.

shows a schematic of the normal force F_N and the separation distance D_S for a typical force run and highlight 5 steps of interest (**(1)** through **(5)**).

At the start of the force-run, while the two surfaces are still macroscopically separated **(1)**, no interaction force is expected between the two. A small force may still be measured at this point related to mechanical or thermal drift, which can be compensated for during data analysis. As the surfaces approach, at very small D_S, a negative force may be observed over the last few nanometers of the approach **(2)**. At this point, attractive forces (commonly van der Waals forces) pull the surfaces together resulting in a fast "jump in". Once the surfaces are in contact, further movement of the piezo actuator gives no more separation distance change (except for a little deformation of the contact) but results in a compression with a linear force increase. In the force-distance plot, this is seen as a hard wall compression **(3)** with a diverging force at (close to) zero distance D_S.

At this point, the piezo movement is reversed, and the compression force de-

Die approbierte gedruckte Originalversion dieser Diplomarbeit ist an der TU Wien Bibliothek verfügbar
The approved original version of this thesis is available in print at TU Wien Bibliothek.
TU Bibliothek Your knowledge hub WIEN

creases linearly to zero. However, in an adhesive system the surfaces cannot be simply pulled apart. The adhesive interaction holds the surfaces in contact even as the piezo actuator tries to pull them apart. This results in a negative adhesion force that increases until, at some point, the work of adhesion γ_{adh} is overcome **(4)**.[5] After the adhesion rupture and the resulting "jump out", the surfaces are separated again and no force (except for a potential mechanical or thermal drift) is observed **(5)**. The highest (negative) adhesion force before rupture F_{adh} can be used for estimating the work of adhesion in further analysis. [81, 83]

The choice of surfaces lies at the heart of the SFA principle. For each experiment, suitable surfaces are customarily prepared by modifying hardened, cylindricaly cut glass discs with optical glue, mica, thin metal layers and organic functionalizations. Typical SFA configurations use molecularly smooth, template-stripped layers of gold (potentially further functionalized) and freshly cleaved mica substrates. The experimental realization of the SFA uses multiple beam interferometry to measure the distance between the two surfaces. This imposes two fundamental requirements on the surfaces: First, they need to be semi-transparent[6] so that light can pass from the white light source through the setup into the spectrometer and detector. Secondly, the surfaces need to form an optical cavity that creates the interference pattern and allows calculation of the separation distance. In practice, this means both surfaces need to have a thin, very flat metal film at or close to the interface. This is usually achieved by using thin mica sheets with 40-50 nm metal films on both sides. With this setup, either mica-mica or mica-metal configurations could traditionally be measured. However, as recently demonstrated by our group in the publication by Wieser et al., metal-metal configuration can also be achieved using a third metal layer [82].

In all SFA experiments, the two modified quartz discs are put in a cross-cylindrical, configuration i.e. rotated 90° from each other. The cross-cylindrical surface interaction is geometrically equivalent to a sphere-plane interaction which is essential for the further interpretation. When brought into close contact, light bounces back and forth between the reflective surfaces in multiple beam interferometry. The constructive and destructive interference creates Newton rings, which can be seen using a microscope aimed at the contact and can be used for positioning the contact spot and objective. The transmitted light, which consists of sets of discrete wavelengths, is then directed into an imaging spectrometer with a 2D CCD camera where this interferometric pattern appears as so called fringes

[5] Note that the "work of adhesion" is an interfacial energy (also referred to as surface tension) with the dimension of energy per area, thus in SI units $\frac{J}{m^2}$.

[6] Unless one works in reflection mode, where the light source and spectrometer are on the same side and one of the surfaces is reflective. All experiments shown in this work were performed in the usual transmission mode.

Die approbierte gedruckte Originalversion dieser Diplomarbeit ist an der TU Wien Bibliothek verfügbar
The approved original version of this thesis is available in print at TU Wien Bibliothek.
TU Bibliothek Your knowledge hub WIEN

of equal chromatic order (FECO). Changes in the absolute separation distance between the surfaces are mirrored in a wavelength shift of the FECOs which is how D_S is calculated. [81, 84]

The force in SFA was traditionally determined by monitoring the displacement of a flexible spring and Hooks law. More recently, our group has transitioned to using semiconductor strain gauges as force sensors, which are placed in between the piezo actuator and the surface holder. This gives a similarly good force resolution but decouples the two measurements and also allows for measurement of lateral forces enabling e.g. friction experiments (see again Wieser et al. [82]).

In a strain gauge, applied strain translates to a change in electrical resistance which can be measured. Its output signal, which is measured in mV/V (output/input from a Wheastone bridge) can be translated into a force, if the force is sufficiently small to be in a linear regime. This uses a calibration with a known reference force like the gravitational force from known weights. A series of small weights in the mg range was used for calibration for the experiments presented in the present thesis.

2.3.1. Electrochemical Surface Force Apparatus

The SFA can be combined with electrochemical measurements resulting in the electrochemical surface force apparatus (EC-SFA) [85]. In this mode of operation, typically one surface will function as the WE on which the potential is controlled by the potentiostat. In the setup used in this work, the RE and CE used in the SFA liquid cell are a miniature Ag|AgCl electrode and a ring made of Pt wire as implied in figure 2.7. Apart from controlling the surface polarization, this expanded SFA concept also enables study of changes in surface roughness, electrochemical thin film growth and the EDL under potential control [85].

Figure 2.7 shows a diagram of the electrochemical SFA with the important components and sensors highlighted. It also shows which parts are contained within the liquid cell and in which order the sensors are arranged.

Die approbierte gedruckte Originalversion dieser Diplomarbeit ist an der TU Wien Bibliothek verfügbar
The approved original version of this thesis is available in print at TU Wien Bibliothek.
TU Bibliothek Your knowledge hub WIEN

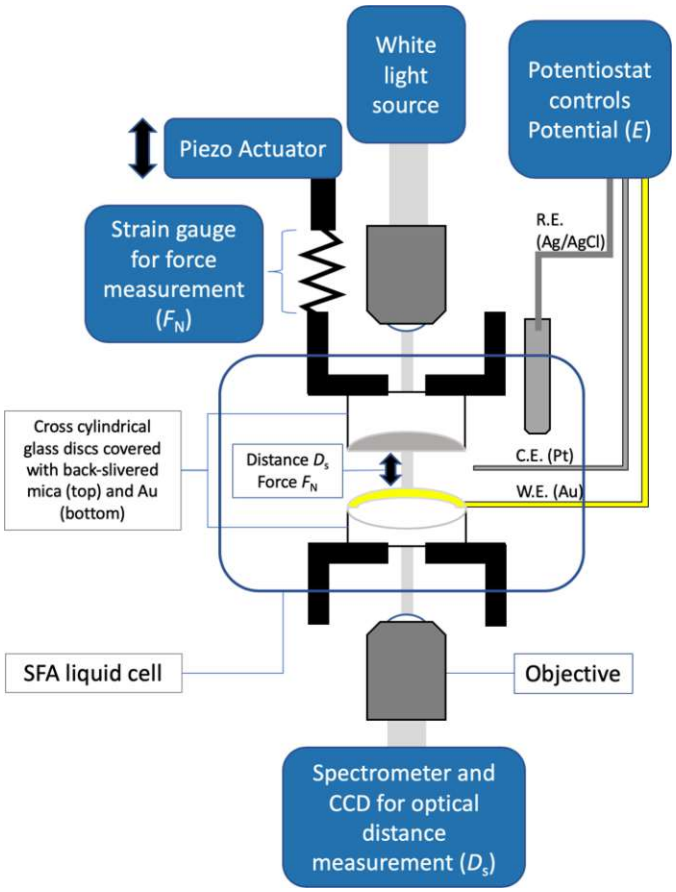

Figure 2.7.: Diagram showing the principal components of the (EC-)SFA. The setup is centered on the two cross-cylindrical discs contained in the liquid cell together with the CE, RE and WE (which is connected to a conductive surface). A piezo actuator controls the relative movement of the discs while a strain gauge is used to measure the normal force F_N. The separation distance (D_S) is determined from FECOs produced by multiple beam interferometry and measured in a imaging spectrometer.

Die approbierte gedruckte Originalversion dieser Diplomarbeit ist an der TU Wien Bibliothek verfügbar
The approved original version of this thesis is available in print at TU Wien Bibliothek.

3. Materials and Instrumentation

This thesis was typeset in LaTeXusing the online Overleaf editor. The layout is based on the template available on GitHub by Jörg Herzinger [86].

3.1. Chemicals and Surfaces

All measurements in water are performed in and all solutions are prepared with MilliQ water from a Merck-Millipore filtration system with a resistivity of 18.2 MΩ/cm and 2-3 ppm total organic content. Glassware was cleaned with concentrated sulfuric acid and MilliQ water and dried with absolute ethanol before use.

Electrochemical characterization and SFA adhesion force measurements used a 100 mM solution of sodium perchlorate (Alfa Aesar, $\geq$ 98 %) as electrolyte. Where stated, the pH of the electrolyte was adjusted to 8 using sodium hydroxide. DHCA ($\geq$ 8 %), the compound used for catechol functionalization, was obtained from Sigma-Aldrich in dry form. The crosslinking agents, EDC and NHS were both purchased from Sigma-Aldrich with a purity of $\geq$ 98 %. The thiol-based compounds used for preparing the SAMs, cysteamine in the form of cysteaminium chloride ($\geq$ 97 %) and ME in the form of pure liquid ME ($\geq$ 99 %) were acquired from Sigma-Aldrich. All shown chemical structures were drawn using ChemDraw JS [87].

Thin films of gold and silver (for surface functionalization and as semi transparent mirrors for white light interferrometry in SFA) were produced using thermal evaporation of high purity metal granules the in-house physical vapor deposition (PVD) system. Titanium adhesion layers for the electrodes described in section 3.3.2 and transparent titanium layers on SFA discs used in section 4.2.2 were produced by sputtering a titanium target with an argon plasma in the same PVD system.

All used SFA discs are prepared from standard glass SFA discs with a 1 or 2 cm curvature radius (all experiments use discs with matched curvature). Mica used for surface preparation and experiments is muscovite mica (chemical formula $(KF)_2(Al_2O_3)_3(SiO_2)_6(H_2O)$) and purchased in the form of optical grade VI mica [0001] sheets (S&J Trading Inc.). Mica-templating gold thin film SFA-discs are prepared by gluing a mica substrate with a gold layer with a thickness of around 40 nm to the disc using heat cured two component epoxy glue ("EPO-TEK" by

Die approbierte gedruckte Originalversion dieser Diplomarbeit ist an der TU Wien Bibliothek verfügbar
The approved original version of this thesis is available in print at TU Wien Bibliothek.
TU Bibliothek Your knowledge hub WIEN

Epoxy Technology). Before use, the mica substrate is peeled off while immersed in ethanol, thereby exposing a fresh, atomically smooth gold surface [88, 89]. Back-silvered mica SFA discs were prepared from cleaved mica sheets coated in a thin (approximately 40 nm) silver film which are cut to size and fixed to the disc with optical adhesive ("NOA65" from Norland; cured for at least 4 hours under a long-wavelength UV lamp). Titanium coated SFA discs were produced by sputtering titanium on SFA discs with either a back-silvered mica surface or coated with a layer of optical adhesive (disc curvature matched due to surface tension). Where necessary, weights were used to hold the mica sheets in place during the curing process to insure they follow the desired curvature.

3.2. SAM preparation

SAMs can be grown out of an ethanolic solution but both water and ethanol-water mixtures can be employed for SAMs with hydrophilic end groups (as is the case for cysteamine and ME) [90]. Based on the procedure by Salmanipour and Taher [67], water was chosen as solvent in this case for the SAM solutions and subsequent functionalization using EDC and NHS.

For preparation of the SAM, 100 mM solutions of cysteamine and ME were prepared and then diluted to 10 mM for incubation. ME was measured volumetrically because in its pure form it is a volatile liquid with a noxious smell that must be handled in a fume hood. Before contact with the clean electrodes, all solutions were filtered with a syringe-filter with a pore size ≤ 200 μm. For experiments using a mixed cysteamine/ME SAMs, electrodes were incubated in a solution mixed volumetrically as specified.

For the SAM formation, the SAM solution was filled into a small vessel with the fresh electrodes and left to rest for a minimum of four hours. The vessels were covered with a lid and a layer of aluminum foil to block out dust and outside light.

Preparation of the catechol-terminated monolayer used electrodes with the cysteamine SAM and was based on the preparation by Salmanipour and Taher [67]. The electrodes were removed from the cysteamine solution and rinsed thoroughly with MilliQ water. They were then immersed in a solution containing 2.5 mM EDC, 5 mM NHS and 10 mM DHCA for at least 14 hours over night and also again rinsed thoroughly before use.

Die approbierte gedruckte Originalversion dieser Diplomarbeit ist an der TU Wien Bibliothek verfügbar
The approved original version of this thesis is available in print at TU Wien Bibliothek.
TU Bibliothek Your knowledge hub WIEN

3.3. Cyclic voltammetry

3.3.1. Electrochemical cell

All electrochemical measurements shown in this work were performed using a PalmSense4 potentiostat system and the PSTrace 5.8 software. For all CV experiments a leak-free miniature Ag|AgCl electrode was used as RE and a platinum mesh was used as CE. Two types of gold electrodes were employed as WE as discussed below.

CV measurements were performed in an electrochemical cell originally designed for use in our group by Dominik Dworschak. This cell (shown in figure 3.2 a) has a cylindrical main chamber in which the WE, RE, and CE can be placed for measurement. The main chamber is connected to three side chambers which have holes that allow a gas to be blown in from the outside during operation. By virtue of this design, gas can bubble through the electrolyte, saturate the liquid and displace any other dissolved gasses without causing turbulence in the main chamber. For the present work, inert argon gas was bubbled through the chamber.

However, this cell did not have an easy and consistent way to place the electrodes needed for the intended experiments. Since a consistent electrode placement is a necessity for reproducible and comparable electrochemical measurements (due to varying ohmic drop across WE and CE), one of the first challenges of this thesis was to design a suitable cap for the electrochemical cell.

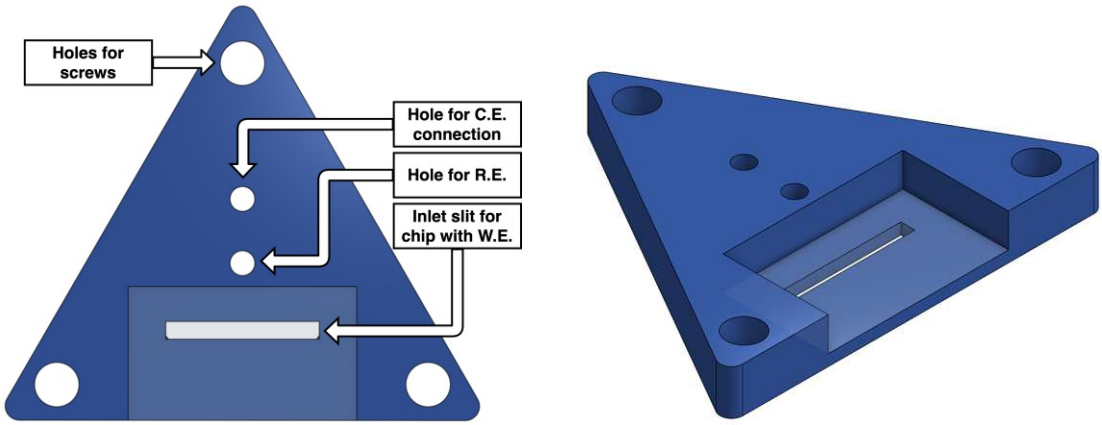

(a) (b)

Figure 3.1.: Design of the new cap for the electrochemical cell. The cap has holes for screws, the RE and a wire connecting the CE platinum mesh. It also has a slit opening to accommodate the glass chips with the working electrode. **a)** Frontal view. **b)** Isometric view.

Die approbierte gedruckte Originalversion dieser Diplomarbeit ist an der TU Wien Bibliothek verfügbar
The approved original version of this thesis is available in print at TU Wien Bibliothek.
TU Bibliothek Your knowledge hub WIEN

The final design of this cap is shown in figure 3.1. When placed on and secured with screws to the top of the cell, it provides openings for the RE and a wire connected to the platinum mesh CE. An inlet slit opening holds the glass chip with the WE (as described below) in place and allows for quick removal and exchange of the used electrode. Figure 3.2 b shows the cap installed on the cell.

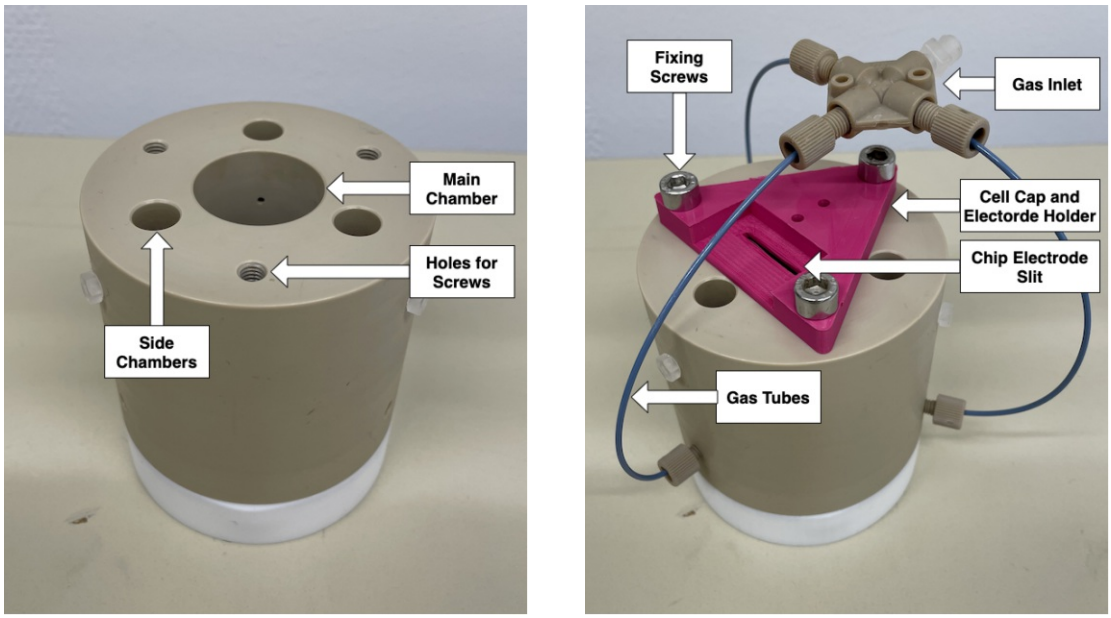

(a) (b)

Figure 3.2.: Pictures taken of the electrochemical cell used for all measurement in this work. The liquid volume of the cell is divided into a main chamber where the measurement takes place and three side chambers for gas exchange. **a)** Design of the cell without any additions. **b)** The cell setup with the gas inlet tubes and the new cell cap electrode holder installed.

3.3.2. Electrode Design

The first type of electrode was prepared by template-stripping from mica sheets with a 80-100 nm layer of gold. Glass chips with a size of around 10×26 mm^2 were cut from microscopy slides (VWR) glued to the gold side using optical adhesive. Shortly prior to use, the chips with the gold were then peeled off the mica under ethanol. To determine the geometric surface area, a close-up picture was taken of the electrodes next to a millimeter scale and the outline was traced in ImageJ.

A second type of electrode was newly designed and produced for the present

Die approbierte gedruckte Originalversion dieser Diplomarbeit ist an der TU Wien Bibliothek verfügbar
The approved original version of this thesis is available in print at TU Wien Bibliothek.
TU Bibliothek Your knowledge hub WIEN

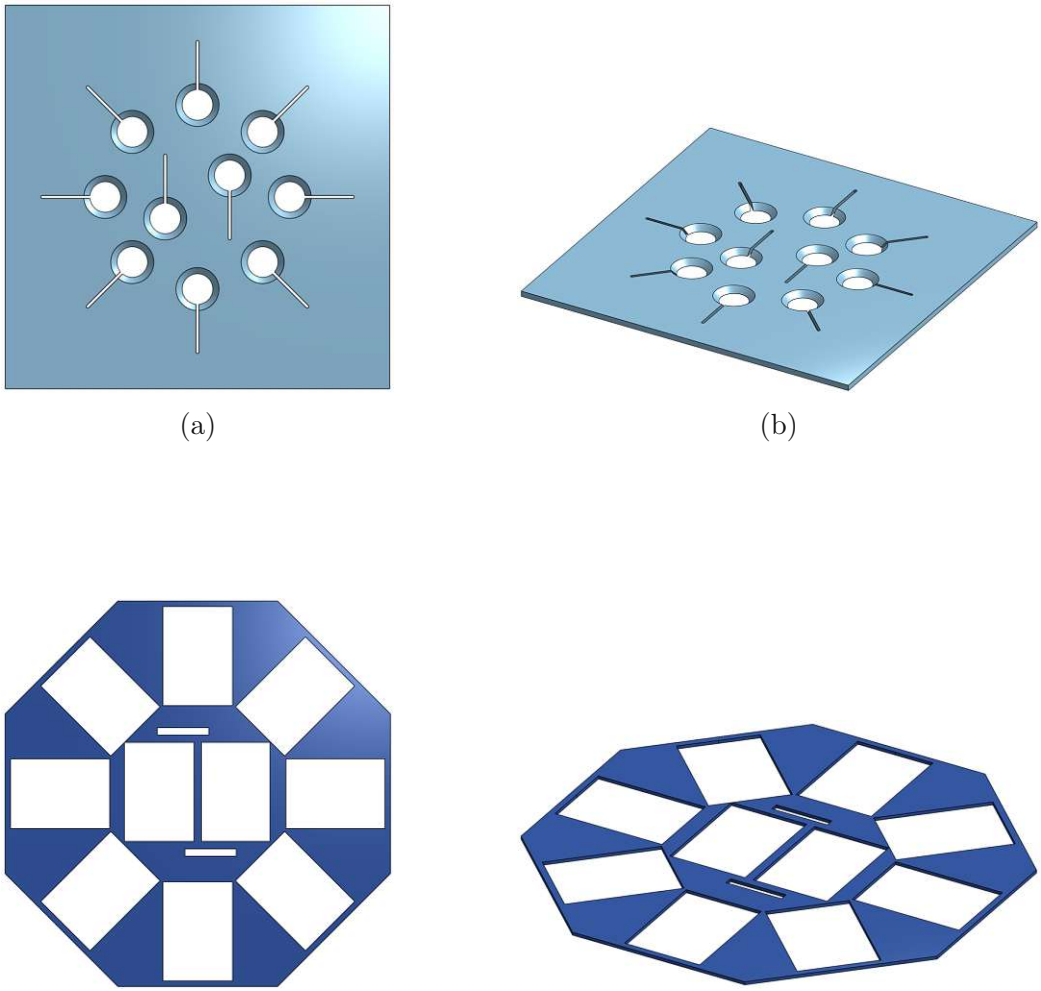

(a) (b)

(c) (d)

Figure 3.3.: Parts used for making the thin film electrodes using PVD. The glass chips placed on the evaporation mask (**a** and **b**) and aligned using the evaporation holder (**c** and **d**). The cut outs in the mask define the electrode geometry. Up to 10 electrodes can be prepared simultaneously. **a)** Frontal view of the evaporation mask. **b)** Isometric view of the evaporation mask. **c)** Frontal view of the evaporation chip holder. **d)** Isometric view of the evaporation chip holder.

work and the development process was a substantial part of this thesis. It uses direct evaporation of gold onto glass rather then template-stripping. This has the advantage of a simpler production and a higher control of real surface area per geometric surface area. An evaporation mask (see figure 3.3) was designed that

Die approbierte gedruckte Originalversion dieser Diplomarbeit ist an der TU Wien Bibliothek verfügbar
The approved original version of this thesis is available in print at TU Wien Bibliothek.
TU Bibliothek Your knowledge hub WIEN

limits the gold covered area to a defined shape and thus to a known geometric surface area.

Glass chips with a size of around 13×26 mm^2 were cut from microscopy slides (VWR) and thoroughly cleaned using ethanol in an ultrasonic bath. For the evaporation, they are placed on the backside of the evaporation mask where they are held in place using a simple, 3D printed chip holder and weighed down by a thin metal plate. Mask and chips are then placed in the PVD where they are first covered with a thin (≈ 5nm) titanium adhesion layer and then with ≈50 nm of thermally evaporated gold. After evaporation, the electrode chips are immediately ready for use.

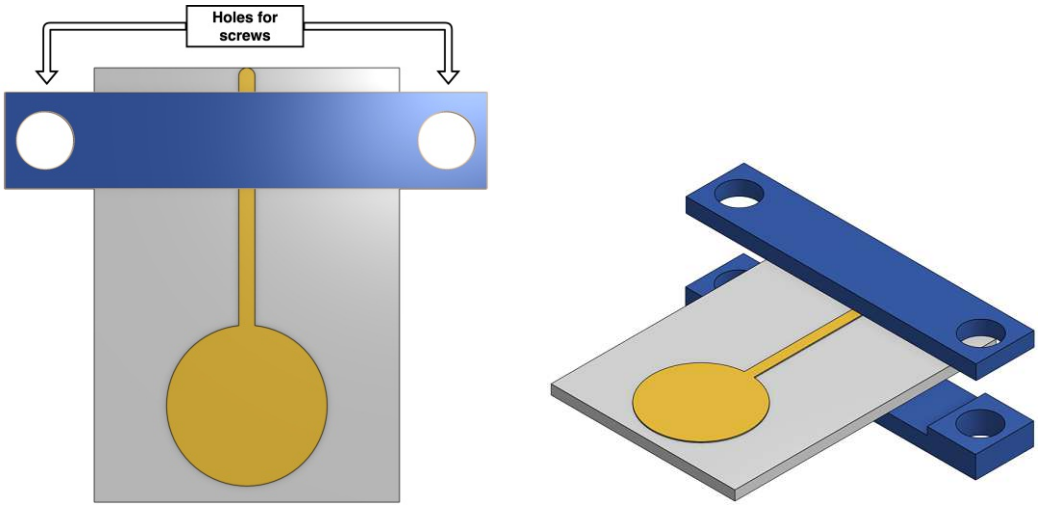

(a) (b)

Figure 3.4.: New design of thin film electrode that is evaporated directly on a glass chip with the the clamp for holding and connecting a wire. **a)** Frontal view of electrode and clamp with the holes for the screws highlighted. **b)** Exploded isometric view of the clamp and chip design for the thin film electrode.

A simple 3D-printed clamp was designed to hold the chips as shown in figure 3.4. When assembled, the clamps are held together with two 10 mm M4 size screws and fitting nuts. A piece of gold wire is placed on top of the thin evaporated extension on the glass chip during assembly which later serves as connection between electrode and potentiostat. Rectangular pieces of parafilm are placed between glass chip and clamp and are supposed to compress and deform when tightening the screws. This holds the chip and the wire tightly in place during incubation and measurement. A picture of a finished electrode of this type is shown in figure 3.5.

Technical drawings of the evaporation mask, the chip holder, the electrode clamp

Die approbierte gedruckte Originalversion dieser Diplomarbeit ist an der TU Wien Bibliothek verfügbar
The approved original version of this thesis is available in print at TU Wien Bibliothek.
TU Bibliothek Your knowledge hub WIEN

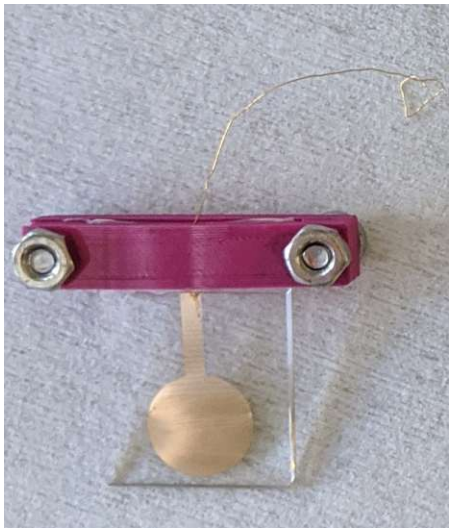

Figure 3.5.: Picture of the custom designed thin film electrode with clamp and gold wire and ready for use.

and a contraption that aides the assembly of the clamp are shown in appendix B.

3.3.3. Data analysis

Analysis of the electrochemical data was performed with custom written Python 3.8 scripts using mainly the NumPy module for calculations and the Matplotlib module for plotting [91, 92]. Here only a short overview is given of the necessary analysis steps performed on the raw data. The basic python scripts used for reading, manipulating and plotting the data are shown in appendix C.1 for reference and are also available upon request.

CV data is exported by PSTrace in a CSV table format which is read in using the pandas library and then converted into a numpy array containing the potential and current for each cycle. Apart from plotting the current vs. potential curves, two types of further data analysis were required in this work. First, integration of peak areas was needed for comparing the loss of signal over a number of subsequent cycles and to estimate the surface coverage of electrochemically active species. This was achieved using a simple numerical integration via the trapezoidal rule (built into NumPy). Second, the peak current of each cycle within a given potential range needs to be extracted and analyzed according to the Randles-Sevcik equation (compare section 2.2.3). Finding the peak current can be accomplished by taking the maximum current in the potential range (potentially with a subtracted background and filtered from fake peaks using the scipy.signals module). With a set of scan rates and the corresponding peak currents, an electrochemically active

Die approbierte gedruckte Originalversion dieser Diplomarbeit ist an der TU Wien Bibliothek verfügbar
The approved original version of this thesis is available in print at TU Wien Bibliothek.
TU Bibliothek Your knowledge hub WIEN

coverage Γ^* can then be calculated using a linear regression (see section 4.1.2).

3.4. Surface force apparatus

3.4.1. Setup

The SFA used for the measurements described in this work has been described in detail in the recently published paper by Wieser et al. [82]. Figure 3.6 shows a drawing of the liquid cell from said work. The setup uses a white LED source (400–700 nm) and driver from Thorlabs. FECO analysis uses an imaging spectrometer and a sCMOS (Zyla) camera cooled to -20 °C from Andor. A Quantalux TM 2.1 MP camera is used to view the Newton rings and position the contact. Fine disc movement is controlled by piezoelectric actuators and a loop controller by PI instruments. Manual, coarse movement is performed via xyz-translation stages by Thorlabs. The normal force is measured using a strain gauge force sensor ME-Messysteme GmbH. The SFA setup is isolated from outside vibrations by suspension from bungee cords attached to the ceiling and the liquid cell and strain gauge are surrounded by a plexiglass casing to reduce thermal fluctuations.

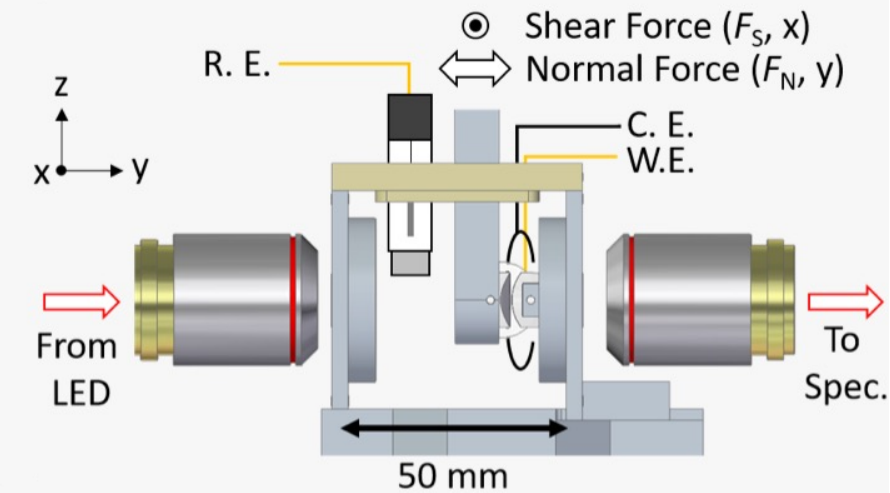

Figure 3.6.: Schematic of the EC-SFA cell. Shown are the placement of the electrodes, the force senor and the light source and objective. Reproduced with permission from AIP Publishing [82]. See appendix A for the copyright clearance.

On the software side, the imaging spectrometer and associated camera are controlled by Andor Solis. The Quantalux camera is operated by ThorCam. Piezo actuators are controlled by a LABVIEW based software and the strain gauge

Die approbierte gedruckte Originalversion dieser Diplomarbeit ist an der TU Wien Bibliothek verfügbar
The approved original version of this thesis is available in print at TU Wien Bibliothek.

signal is read out by GSVmulti (ME-Messysteme GmbH). Andor Solis saves the spectroscopic data in the form of image files which are then converted into distance datapoints by SFA Explorer developed in our group by Kai Schwenzfeier [84].

3.4.2. Disc Preparation and Measurement

Preparation of functionalized SFA discs with hydroxyl- and catechol-terminated SAMs was performed as described in section 3.2. Special care needs to be taken when handling SFA discs because SFA experiments are susceptible to contamination with microscopic "particles" (e.g. dust grains). A "particle" in close proximity of the contact spot will result in an apparent force before the surfaces are actually touching. To prevent contamination, SFA discs are always handled in a clean room and in a laminar flow hood. Additionally, they are kept in closed containers whenever they are not immediately needed. Functionalized discs were always kept under water (MilliQ) except when transferring between containers and for short unavoidable periods during assembly. Cell assembly with the functionalized discs was performed immersed in water until the cell was able to hold liquid without leaking. Only for non air-sensitive surfaces, i.e. back-silvered mica and Ti discs which are partially prepared in ambient atmosphere anyways, assembly took place in air.

Measurements of the catechol-terminated SAM vs. mica were performed first in MilliQ water and subsequently in 100 mM sodium perchlorate. Before measurement, the cell content was drained using the attached tubes, rinsed and then refilled with fresh MilliQ water.

Prior to the force-run measurements, a clean, "particle-free" contact spot is located using the translation stages, the camera and the strain gauge signal. Force-runs are then recorded as described in section 2.3. For each force-run, the piezo voltage is linearly increased up to a set threshold (at which the surfaces are in hard contract) and then decreased back in the same fashion until the surfaces are separated with or without an adhesion rupture event. The offset voltage of the piezo actuator may be changed in between force-runs if the surfaces are observed to be drifting further apart or closer together. Both data sources, spectrometer and strain gauge, are set to the same sampling rate, usually 10 Hz, so that matching data points can be collected and later used to generate a force-distance curve.

3.4.3. Data analysis

The two data sets collected for a typical SFA measurement are the distance between the surfaces as determined from white light interferometry and force data collected by a strain gauge. Out of this raw data, one can extract force-distance curves and values for the maximum recorded adhesion force.

Die approbierte gedruckte Originalversion dieser Diplomarbeit ist an der TU Wien Bibliothek verfügbar
The approved original version of this thesis is available in print at TU Wien Bibliothek.
TU Bibliothek Your knowledge hub WIEN

While these appear to be relatively simple measures to extract, there are a few issues that need to be addressed first.

The strain gauge signal, for example, is prone to a permanent linear drift. Therefore, it is necessary to subtract a linear background from the force data in a first step. This requires a number of data points to be recorded at large D_S where no force[1] is acting between the surfaces. Furthermore, since the devices cannot be assumed to have started measuring at the exact same time as the strain gauge signal and the spectrometer readout are processed separately, a slight time offset must be corrected for. Using a region of suitable data points, e.g. the "jump in" or adhesion rupture, where sudden jumps happen in both force and distance, the two complementary data arrays are aligned in time. Finally, the strain gauge data (recorded in mV/V) needs to be translated into a force per radius using the calibration factor (see section 2.3) and the disc curvature.

To calculate the adhesion force the background-corrected force sensor data is split into an in- and and out-run. F_{adh} is estimated as the minimum value of the out-run, while the minimum of the in-run is the "jump in" (though this is not always observed above the strain gauge noise).

For processing this data, interactive Jupyter notebooks and a number of helper modules were implemented using python 3.8 as part of this thesis [93]. The notebooks, modules and supporting scripts mainly make use of the NumPy, pandas and Matplotlib modules [91, 92, 94]. A short overview of this notebook and parts of the source code for the most important modules is shown in appendix C.2.

[1] except for Stokes' drag and gravity

Die approbierte gedruckte Originalversion dieser Diplomarbeit ist an der TU Wien Bibliothek verfügbar
The approved original version of this thesis is available in print at TU Wien Bibliothek.
TU Bibliothek Your knowledge hub WIEN

4. Results and Discussion

A series of experiments was executed to study the electrochemical and adhesive properties of the catechol terminated SAM introduced in section 2.3. Below the most important results are presented and their implications for the understanding of catechol based adhesion are discussed.

4.1. Cyclic voltammetry

4.1.1. Characterization of the SAM

Prior to any further investigation of the catechol terminated SAM, it is first necessary to confirm whether the catechol group is indeed present on the SAM and to understand how this system reacts to a change of potential. Both questions can be answered using CV by looking for and studying the characteristic redox peak pair produced by the electrochemically active catechol.

For this a set of template stripped gold electrodes was produced and functionalized according to the protocol explained in section 3.2. CVs were recorded for the functionalized electrodes and a non-functionalized template stripped gold electrode that was similarly prepared and stored in Milli-Q water. Figure 4.1b a shows CV cycles for functionalized (blue) and non-functionalized (green) electrodes compared to a measurement of 1 mM DHCA solution (orange) obtained in a simplified electrochemistry cell. The bulk solution reference data was recorded by the author for a related project thesis that preceded the current work. The current in figure 4.1b a has been normalized and is given in arbitrary units to account for the different cell geometries and current ranges.

The presence of the redox peaks for the incubated surface clearly shows that the catechol-functionalization of the SAM was successful but it also reveals some change in the electrochemical behavior compared to the bulk solution. In particular the standard/formal potential $E^0/E^{0'}$ which can be estimated as the average value of the potential at the oxidation and reduction peak is shifted towards lower potential. In general, more background current is measured compared to the bulk solution.

This makes sense, as only a very limited total amount of redox-active analyte is available for reaction in the SAM compared to the case of a bulk solution which

Die approbierte gedruckte Originalversion dieser Diplomarbeit ist an der TU Wien Bibliothek verfügbar
The approved original version of this thesis is available in print at TU Wien Bibliothek.
TU Bibliothek Your knowledge hub WIEN

provides a reservoir of un-reacted species. This makes the capacitive current resulting form charging of the electric double layer a bigger factor for the catechol terminated SAM.

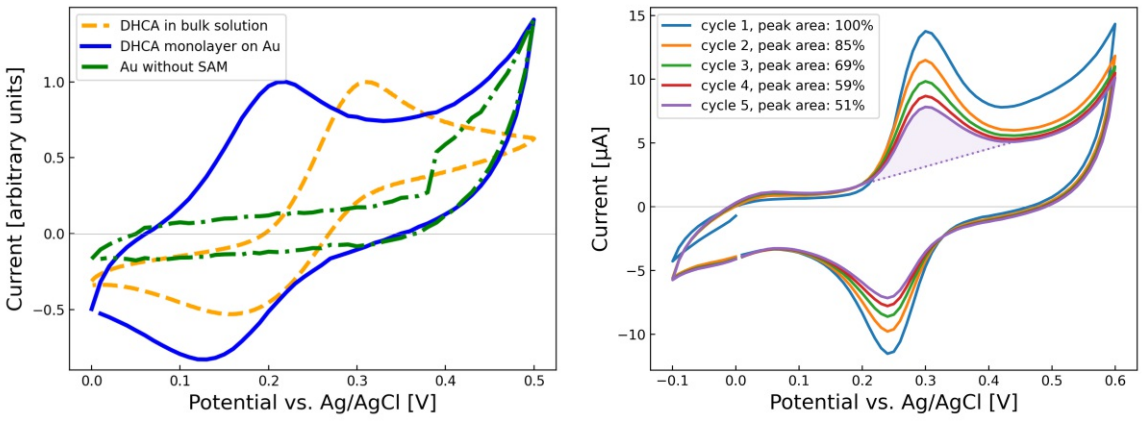

(a) (b)

Figure 4.1.: Electrochemical characterization of the catechol-terminated SAM. All measurements used 100 mM $NaClO_4$ as electrolyte. **a)** Comparison of CV curves for a 1 mM DHCA solution (orange), a non-functionalized template stripped gold electrode and a catechol-functionalized template stripped gold electrode (blue). Current in arbitrary units. **b)** Decrease of peak currents for a catechol-functionalized template stripped gold electrode over 5 CV cycles quantified using the area under the oxidation peak as indicated in cycle 5.

Another important aspect of the SAM characterization is analyzing its stability towards repeated polarization. Prior measurements of DHCA in solution[1] indicate a slow decrease in peak current over many CV cycles.

A similar trend was also observed for the catechol-terminated SAM. Figure 4.1 b shows 5 successive CV cycles recorded for a voltage range of -0.1 to 0.6 V vs. a Ag|AgCl RE. A noticeable decrease in peak current is already observed for these 5 cycles. The decrease was quantified using the area under the peak with a linear background subtracted to account for capacitive current. The region of the current (i) used to calculate the peak area is indicated for the fifth cycle. This measure is related to the charge (Q) transferred in the reaction and therefore the amount

[1] at the time of writing unpublished

Die approbierte gedruckte Originalversion dieser Diplomarbeit ist an der TU Wien Bibliothek verfügbar
The approved original version of this thesis is available in print at TU Wien Bibliothek.

of molecules participating in the reaction since the charge can be obtained by integrating the current over time (equation 4.2). During the anodic trace in CV the potential E is directly related to time t via the scan rate ν and thus the same result can also be obtained by integrating the CV curve directly (equation 4.1).

$$E(t) = E(t = 0) + \nu t \Rightarrow \mathrm{d}E = \nu \mathrm{d}t \tag{4.1}$$

$$Q = \int i \mathrm{d}t = \int \frac{1}{\nu} i \mathrm{d}E \tag{4.2}$$

Using this method a decrease of almost 50 % was observed within the first 5 cycles. In general a quicker decrease is observed for larger potential ranges which demonstrates that there exists a trade-off between the voltage range and cyclability of the system. The used potential range thus needs to be chosen carefully and specifically for each experiment.

This significant decrease also stands in direct contrast to the findings of Salmanipour and Taher who reported no change in the CVs over 100 cycles for a cysteamine SAM functionalized with protocatechuic acid, which only differs form DHCA by the length of the carbon chain [67].

The decrease of oxidation and reduction current may mean that there are some unexpected side reactions going on that make the system only semi-reversible. The exact nature of these side reactions is not clear but they might be related to the amine groups also present on the surface from un-reacted cysteamine.

4.1.2. Calculation of the Surface Coverage

As alluded to in section 1.3, the major advantage of a catechol-functionalized SAM lies in providing a consistent density of catechol groups confined to the interface which is absolutely necessary for studying the binding strength of the catechol group using the SFA. This consistency is not feasible using e.g. films of mfps, catechol containing hydrogels or catechol-polymers where an arbitrary amount of catechol groups may be participating in cohesion or be far removed from the interface.

The surface coverage Γ^* was estimated using the Randles-Sevcik equation for surface adsorbed species (equation 2.5) by finding the relationship between the catechol-oxidation peak current (i_p) and the scan rate (ν). For a set of 8 template-stripped catechol-functionalized gold electrodes CVs were recorded at 4 different scan rates (50, 100, 150 and 200 $\frac{mV}{s}$) and the peak current were determined. Between the measurements for different scan rates, no potential was applied for 15 seconds to allow for re-equilibriation of the electrolyte in the vicinity of the electrode.

Die approbierte gedruckte Originalversion dieser Diplomarbeit ist an der TU Wien Bibliothek verfügbar
The approved original version of this thesis is available in print at TU Wien Bibliothek.
TU Bibliothek Your knowledge hub WIEN

For each electrode the peak currents for the four scan rates and are shown in figure 4.2 b and are fit to the linear model: $i_p = k*\nu+d$. An intercept (d) not equal to zero is explicitly allowed in this model to account for the capacitve background current. From the used electrodes a mean value and standard deviation for the slope k are computed and then used to calculate the surface coverage Γ^* according to equation 4.3.

$$\Gamma^* = \frac{4RT}{n^2F^2}\frac{i_p}{A\nu} = \frac{4RT}{n^2F^2}k \tag{4.3}$$

Using this calculation one arrives at a value for the slope[2] k of $(1.0\pm0.4)*10^{-2}\,\frac{mAs}{cm^2V}$ which translates into a surface coverage Γ^* of $(2.7 \pm 1.0) * 10^{-12}\,\frac{mol}{cm^2}$. This value seems reasonable compared to the estimate of $4.0 \times 10^{-11}\,\frac{mol}{cm^2}$ by Salamipour and Taher who used a polished gold electrode that was electrochemically treated in sulfuric acid [67].

Numerical integration of the peak area as discussed above provides an alternative calculation of the surface coverage. The transferred charge Q is calculated from by integrating the recorded current (with the subtraction of a linear background to account for the capacitive current). It is then translated into a surface coverage via equation 4.4 using the elementary charge e, the Avogadro constant N_A, the number of transferred electrons n $(= 2)$ and the surface area A.

$$\Gamma^* = \frac{Q}{enN_AA} = \frac{\int i\mathrm{d}t}{enN_AA} = \frac{\int \frac{1}{\nu}\mathrm{d}E}{enN_AA} \tag{4.4}$$

This approach yields a surface coverage Γ^* of $(1.8 \pm 0.9) * 10^{-12}\,\frac{mol}{cm^2}$ from the same set of electrodes (only scan rates of 100, 150 and 200 $\frac{mV}{s}$ were considered) which compares well to the above estimate and thus supports the applicability of the Randles-Sevcik equation for surface adsorbed species for this system. The major drawback of the calculation via integration of the peak area lies in the choice of a suitable background to subtract. The choice of the right beginning and end potential for the linear interpolation is subject to error and can thus greatly skew the integration result, especially at lower scan rates, where the peak may be more of a "shoulder". For this reason, the Randles-Sevcik equation for surface adsorbed species is employed going forward.

The density of a pure cysteamine SAM has been reported to be in the range of $10^{-9}\,\frac{mol}{cm^2}$ on thin film electrodes produced via thermal evaporation [95]. This means

[2]The unit of k can be simplified to a capacitance per area but this does not add to the discussion.

Die approbierte gedruckte Originalversion dieser Diplomarbeit ist an der TU Wien Bibliothek verfügbar
The approved original version of this thesis is available in print at TU Wien Bibliothek.
TU Bibliothek Your knowledge hub WIEN

that less than 1 % of the SAM amine head groups were catechol-functionalized assuming a similar cysteamine coverage in this experiment[3].

It is noteable however, that significantly higher active coverages (in the range of around $4 \times 10^{-10} \frac{mol}{cm^2}$) were reported in cases where the SAM was formed using catechol-functionalized thiol compunds [65, 66]. Such a system may be a promising candidate for further research.

A similar experimental procedure was performed with a number of sets of electrodes that were incubated in a mixed cysteamine/ME SAM solution prior to catechol functionalization. The SAM mixture was prepared with a cumulative concentration of 100 mM with cysteamine and ME added by weight or volume according to the desired molar fraction (%) and diluted to 10 mM for incubation. Measurements were performed for cysteamine molar fractions of 0, 20, 40, 50, 60 and 80 % and used the thermally evaporated gold electrodes (see preparation detailed in section 3.3.2). The calculated coverages are shown in figure 4.1b in comparison to the coverage calculated for the template stripped electrode above (using a 100 % cysteamine SAM).[4]

This measurement yields a calculated coverage in the same range as the one for the template stripped electrode for cysteamine fractions of 40 % and above. For the SAM with 20 % cysteamine, a coverage of only around $1.8 * 10^{-12} \frac{mol}{cm^2}$ was calculated. In the case of the pure ME SAM a coverage of $0.7 * 10^{-12} \frac{mol}{cm^2}$ was calculated using the same algorithm, however, for this system no catechol oxidation peak was present to begin with. Here the only contribution to the current stems from the background current, which also varies linearly with the scan rate [80].

It is unexpected that the coverage for both electrode types falls in the same range even though the roughness of the gold film for the electrodes produced by thermal evaporation should be considerably higher (about 5-6 fold) than for template stripped gold electrodes and thus have an also significantly larger real surface area per geometric surface area available for functionalization [85, 89]. The exact reason for this can only be speculated upon without further research, but it may be related to a low overall efficiency in the functionalization.

[3]The exact value would depend on the conversion factor between real and geometric surface area and the efficiency of the cysteamine incubation which may vary slightly.

[4]Note that the shown values represent a single measurement each and thus no error bar can be provided. This is due to a relatively high failure rate of the electrodes, especially at lower cysteamine concentrations.

Die approbierte gedruckte Originalversion dieser Diplomarbeit ist an der TU Wien Bibliothek verfügbar
The approved original version of this thesis is available in print at TU Wien Bibliothek.
TU Bibliothek Your knowledge hub WIEN

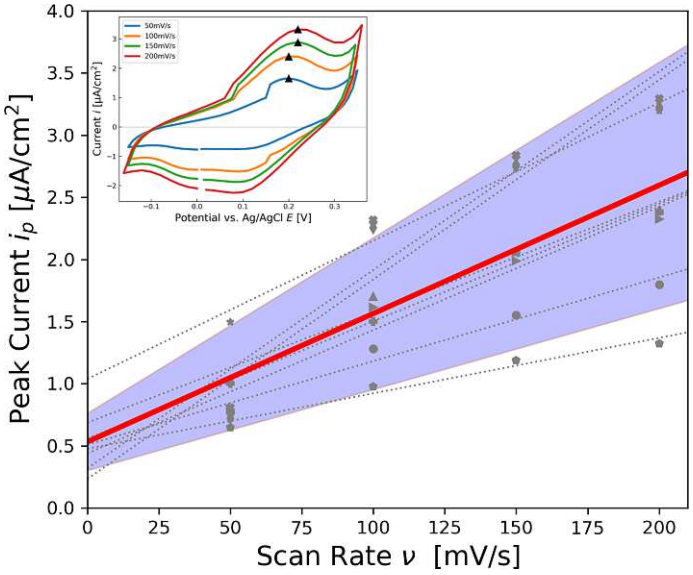

(a)

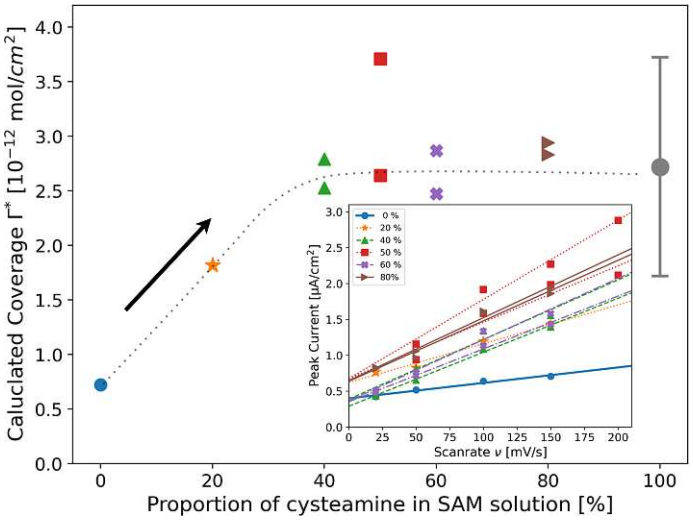

(b)

Figure 4.2.: Calculation of surface coverage of electrochemically active catechol species for the catechol-functionalized gold electrodes. **a)** Oxidation peak currents of 8 template stripped electrodes (gray) as a function of the used scan rate fit to a linear model. Mean value (red) and standard deviation (blue) of the linear regression are highlighted. The inset shows an example CV from which the peak currents are estimated. **b)** Coverages as calculated for a number of thin film electrodes incubated with a mixed cysteamine/ME SAM before catechol functionalization. The value at 100 % is calculated in a) for template stripped electrodes. The inset shows the measured peak oxidation current and the corresponding linear fits. A dashed line and arrow indicate increasing coverage below 40 % cysteamine content and a constant coverage above that value.

Die approbierte gedruckte Originalversion dieser Diplomarbeit ist an der TU Wien Bibliothek verfügbar
The approved original version of this thesis is available in print at TU Wien Bibliothek.

4.2. Electrochemical Surface Force Apparatus

Based on the information gained form the electrochemical characterization of the catechol-terminated SAM, parameters were set for probing its adhesive properties in the EC-SFA. Various measurements were performed using gold coated SFA discs that were prepared and functionalized as described in section 3.2. Unless otherwise specified, the functionalized disc was connected to the working electrode and the opposing disc, which is attached to the strain gauge and the piezo actuator, is not connected to the potentiostat, i.e. at a floating potential.

4.2.1. Measurements against back-silvered Mica

Back-silvered mica, a common substrate for testing of mussel adhesion in the SFA[5], was used as the opposing surface for assessing the effects of potential control on the adhesive properties of the functionalized surface. Force-distance curves were recorded as described in section 2.3 and values for the adhesion force were calculated from the strain gauge data using the script shown in appendix C.2.

In experiments performed in this system in MilliQ water (figure 4.3 a), two force runs were recorded without an external potential applied (OCP). This was followed by force runs at reducing and oxidizing potentials in the alternating sequence shown in figure 4.3 a. There, the x-axis shows the experimental sequence of the recorded force runs with color coding for the applied potential. The potentials for reduction and oxidation were chosen as 0.00 V and 0.35 V vs. Ag|AgCl (RE) respectively as these values were determined to be suitable for reduction and oxidation in the employed pH ranges. A matching sequence of force-distance curves was recorded for a hydroxyl-terminated SAM produced from ME and is shown as a reference measurement. The adhesion measurement was first performed in MilliQ water and then continued in the pH 8 adjusted 100 mM sodium perchlorate electrolyte solution.

A significant difference in adhesion force was observed between high and low potentials for the catechol-functionalized surface. At reducing potential, forces around 1-2 mN/m were measured compared to forces around 9-11 mN/m for the first oxidation sequence and 6-7 mN/m for the second sequence.

No such trend was observed for the ME SAM, which showed almost no change in adhesion force between oxidizing and reducing potential. Instead, it exhibited a small increase over time. This may be related to a slow drift of the piezo position which causes a slightly longer and harder compression, and thus a minor increase in maximum contact area over time. Altogether, this shows that there

[5]Compare e.g. the work by Danner et al. [24].

Die approbierte gedruckte Originalversion dieser Diplomarbeit ist an der TU Wien Bibliothek verfügbar
The approved original version of this thesis is available in print at TU Wien Bibliothek.
TU Bibliothek Your knowledge hub WIEN

is a clear potential-dependence effect of the adhesion properties for the catechol-functionalized SAM.

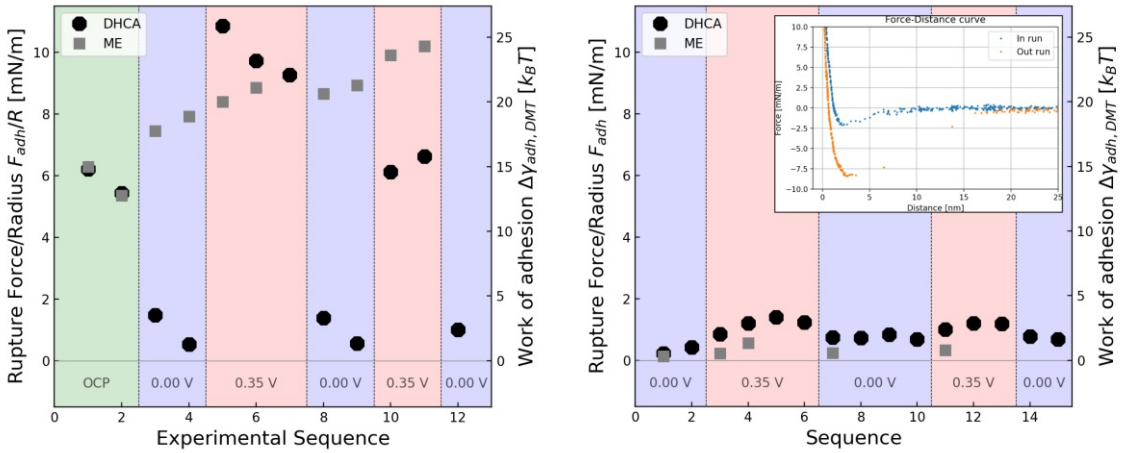

(a) MilliQ (b) 100 mM $NaClO_4$

Figure 4.3.: Potential dependent adhesion measured between the catechol functionalized SAM (black octagons) and a mica substrate in the EC-SFA in to subsequent experiments. A reference measurement of a hydroxyl-terminated SAM vs. mica is shown as grey squares. The left axis shows the measured adhesion rupture force and the right axis shows the calculated interaction free energy per catechol group calculated using the surface density estimated in the previous section. Individual measurements are shown in the recorded experimental sequence (x-axis). The applied potential is by color with blue for reducing (0.00 V), red for oxidizing (0.35 V) and green for the open circuit potential (OCP) of around 0.2 V. **a)** shows the measurement is MilliQ water. **b)** shows the same configuration in 100 mM sodium perchlorate solution with the same axis scaling. The inset shows an example of a force run recorded in MilliQ water.

A vastly different behavior presents itself when the same surfaces are measured in a different aqueous environment with high ionic strength as seen in figure 4.3 b. In this follow up experiment the surfaces were separated, the MilliQ water was removed from the chamber and replaced by the 100 mM pH 8 adjusted $NaClO_4$ electrolyte solution. With the surfaces back in close proximity, the potential dependent adhesion measurement was continued.

Again, at reducing potential adhesion forces around 1-2 mN/m are measured for the catechol-functionalized surface. However, at oxidizing potential the adhesion force no longer increases immediately but it rather creeps up to a value aorund

Die approbierte gedruckte Originalversion dieser Diplomarbeit ist an der TU Wien Bibliothek verfügbar
The approved original version of this thesis is available in print at TU Wien Bibliothek.
TU Bibliothek Your knowledge hub WIEN

only 3-4 mN/m, which is just barely more then what was measured at 0.00 V. Likewise, the disc with the hydroxyl-terminated SAM showed a significantly reduced adhesion as well. The respective adhesion forces of around 1 mN/m shown in figure 4.3b are just barely resolved above the noise recorded by the strain gauge.

Reference data on the adhesion between gold and mica in the EC-SFA measured in our group (so far unpublished) showed comparably small non-potential dependent adhesion of less than 1 mN/m in the voltage range of 0.0 V to 0.35 V which is studied here. A slightly increase in adhesion is observed in these reference measurements at higher potentials, though even at 0.7 V the measured force/radius remains below 2 mN/m.

Using a suitable theory of adhesion, the work of adhesion[6] $\Delta\gamma_{adh}$ can be calculated form the measured adhesion force F_{adh} in SFA. Two commonly used theoretical models for this purpose applicable down to microscopy length-scales, are the Derjaguin-Muller-Toporov (DMT) and the Johnson-Kandall-Roberts (JKR) theories of adhesive contacts. Both models describe the interaction of a sphere with a plane (equivalent to the cross-cylindrical geometry used in SFA) but they differ slightly in their assumptions. In the DMT model, adhesive forces act outside the contact area, while the compressed contacting area behaves repulsively. In contrast, in the JKR model both adhesive and repulsive forces are experiences in a deformed contact area. The expression relating F_{adh} with $\Delta\gamma_{adh}$ in the two models are given by equations 4.5 (DMT) and 4.6 (JKR) which only differ by a constant factor of $\frac{3}{4}$. In both cases, R is the radius of curvature of the sphere from the assumption of sphere-plane interaction. In SFA this translates into the radius of curvature of the two cross-cylindrical discs. The DMT model is used for the scale showing the work of work of adhesion scale in the figure 4.3b. [96, 97]

$$F_{adh} = 2\pi R \Delta\gamma_{adh,DMT} \tag{4.5}$$

$$F_{adh} = \frac{3}{2}\pi R \Delta\gamma_{adh,JKR} \tag{4.6}$$

While the adhesion rupture forces can be directly related to a value for $\Delta\gamma$, the quantity of most interest is the difference in the work of adhesion between the oxidizing and reduced potential. Using the average adhesion force from the first (reducing) and second (oxidizing) polarization shown in figure 4.3b, a $\Delta\gamma_{ox} - \Delta\gamma_{red} = \frac{F_{ox}-F_{red}}{2\pi R}$ of $1.4 \pm 0.1 \frac{mJ}{m^2}$ is calculated using the DMT model and a value of $1.9 \pm 0.2 \frac{mJ}{m^2}$ is arrived at using the JKR model. Combined with the surface coverage calculated above this yields a difference in adhesion energy between the

[6] This quantity is directly related to the difference in surface energy between the former and newly formed interfaces, thus the symbol uses a Δ.

Die approbierte gedruckte Originalversion dieser Diplomarbeit ist an der TU Wien Bibliothek verfügbar
The approved original version of this thesis is available in print at TU Wien Bibliothek.
TU Bibliothek Your knowledge hub WIEN

two states of $52.7 \pm 20.1 \frac{kJ}{mol}$ (DMT; $70.3 \pm 26.8 \frac{kJ}{mol}$ JKR) which corresponds to $21.3 \pm 8.1\ k_BT$ (DMT; $28.4 \pm 10.8\ k_BT$ JKR) per molecule at a temperature of 25 °C. These values are at the upper range of what was measured by Utzig et al. for the interaction between L-DOPA and various substrates with the AFM [69]. For comparison, hydrogen bonds in biomolecules typically fall in the range of 2-12 k_BT per bond [98]. Given this information, one may begin to speculate about the mechanism behind the potential dependent adhesion.

Interestingly, the Gibbs free energy of the catechol–quinone redox reaction calculated from the standard potential of the reaction[7] according to equation 2.1 gives a (pH dependent) value of around 77-97 $\frac{kJ}{mol}$. This corresponds to 31-39 k_BT per molecule, which is comparable to the estimate of the difference in the work of adhesion calculated above ($21.3 \pm 8.1\ k_BT$ DMT; $28.4 \pm 10.8\ k_BT$ JKR). It may be possible to relate these two quantities and extract a more fundamental understanding of the energy landscape. However, a more detailed study with other counter-surfaces will be necessary to tell for sure.

It is interesting and somewhat unexpected, that a higher adhesion is observed for oxidizing potential, as according to most sources, the reduced catechol form is considered to be required for most adhesion mechanisms. On a mineral substrate such as mica, the expected main mode to mediate adhesion should be through complexation of surface metal atoms. However, as recent work by Bilotto et al. has shown, catechol chemistry alone can not explain mussel adhesion [35]. In line with this Gebbie et al. have have shown that cation-π interaction may play a more important role than so far thought [34].

Furthermore, it needs to be taken into consideration, that according to the the electrochemical measurements less then 1 % of the surface cysteamine groups are catechol functionalized. This may have a two-fold contribution to the observed behavior. First, it cannot be ruled out that nearby surface amine groups could interact with the oxidized catechol groups. Follow-up reactions after catechol oxidation are well known to be a limiting factor for the catechol adhesion and electrochemical reversibility. Second, surface amines may themselves interact with the opposing substrate. The amine-mica interaction is well known and does result in an adhesive contact. There could be a so far little considered synergy and charge transfer connected with catechol oxidation, especially considering every catechol group releases two protons affecting the local pH upon oxidation.

Additionally, recent work by Shin et al. has shown a clear influence of nearby amine groups in the form of the amino acid lysine on the adhesion of catechol

[7] As measured by Lin et al., the pH dependent formal potential is in the range of about 0.15-0.25 V vs. a standard calomel electrode for a pH of 6-7. This corresponds to around 0.4-0.5 V vs. the SHE.

Die approbierte gedruckte Originalversion dieser Diplomarbeit ist an der TU Wien Bibliothek verfügbar
The approved original version of this thesis is available in print at TU Wien Bibliothek.
TU Bibliothek Your knowledge hub WIEN

containing peptides [36]. Altogether, the interaction between this catechol functionalized monolayer and the mica substrate is unquestionably more complex than one might initially assume.

4.2.2. Measurements against OH and Ti coated surfaces

A similar measurement to the one presented above was also performed with the catechol-functionalized SAM vs. a titania (TiO_2) and a hydroxyl-terminated surface. These two surfaces provide a particularly suitable sample system for testing catechol adhesion. TiO_2 has been reported as one of the substrates with the strongest catechol mediated adhesion [69]. Specifically, at a pH > 7, a bidentate adhesion with two coordination bonds occurs while in more acidic conditions a somewhat weaker monodentate coordination bond or hydrogen bonding is expected [48]. The hydroxyl-terminated surface (provided by a ME SAM on gold substrate) in contrast should provide the ideal reference system for testing out catechol adhesion via hydrogen bonding alone.

Figure 4.4 shows the adhesion values measured for these two surfaces. For the TiO_2 surface, produced from cured optical adhesive and a sputtered Ti layer as explained in section 3.1, an adhesion rupture force of around 10 mN/m was recorded irrespective of the applied surface polarization. Additional testing (not shown here) with lower and higher potentials applied to the catechol functionalized WE surface yielded the same result. Notably, adhesion forces vs. the OH-terminated ME SAM surface[8] were considerably higher and fell within a range of 45 to 60 mN/m.[9] Nonetheless, this system also showed no dependence of the adhesion force on the applied potential. Measurements for both surfaces, TiO_2 and the ME SAM, were also performed in 100 mM $NaClO_4$ solution but no significant adhesion force (> 1 mN/m) was recorded and is thus not shown.

Like the adhesion measurement against mica substrate, these experiments show some potentially unexpected results. The large difference in adhesion strength between titania and the ME SAM is remarkable, as is the fact, that the hydroxyl terminated substrate gave the largest force/radius. This is again in direct contrast to the results obtained by Utzig et al. who found that titania gave the largest interaction free energy in single molecule adhesion against L-DOPA functionalized AFM tips [69].

It is worth noting though, that the titania surface is produced via sputtering

[8] For ease of use, in this experiment, the surfaces were switched and the potential was applied to the disc with the ME SAM.

[9] Three values (shown in grey) were recorded after minimal contact due to mechanical/thermal drift of the piezo actuator and can thus not be taken into consideration. However, they serve to illustrate the strength of adhesion seen in this system, as even these imperfect measurements give significantly higher values than what is observed with any other substrate.

Die approbierte gedruckte Originalversion dieser Diplomarbeit ist an der TU Wien Bibliothek verfügbar
The approved original version of this thesis is available in print at TU Wien Bibliothek.
TU Bibliothek Your knowledge hub WIEN

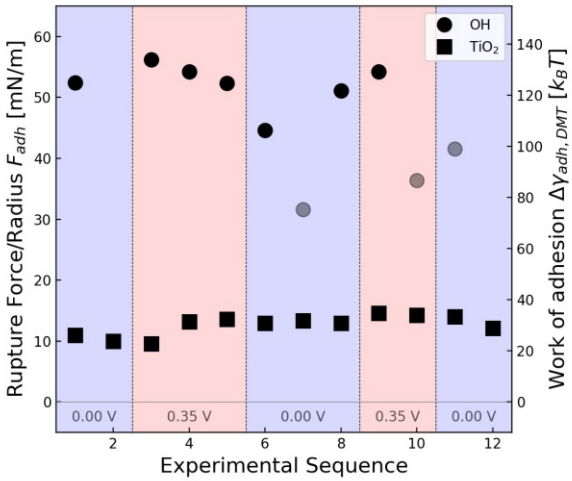

Figure 4.4.: Adhesion measured between the catechol functionalized SAM and a titania coated surface (squares) and a hydroxyl terminated SAM (circles). The left axis shows the measured adhesion rupture force and the right axis shows the calculated interaction free energy per catechol group calculated using the surface density estimated using electrochemistry (see section 4.1. Individual measurements are shown in the recorded experimental sequence (x-axis). The applied potential is by color with blue for reducing (0.00 V) and red for oxidizing (0.35 V). Unlike for the mica substrate, no change in adhesion is observed following a switch in polarization. Adhesion measurements were also performed in 100 mM water but there no adhesion was observed. In three measurements, shown in grey, a drift of the piezo actuator resulted in the surfaces only lightly touching and thus a reduced adhesion. However even in these cases, the recorded adhesion was still much larger than for any other surface configuration.

which results in a much rougher surface compared to template stripped gold and cleaved mica. The real contact area may thus be much smaller then in the other shown experiments since only the protruding parts of the TiO_2 topography may contact the opposing surface. The extent of this effect is hard to quantify as it depends on the growth mode of titanium on the glue and microscopic deformation of both glue and titania when in contact.

In these systems a contribution of the non-catechol functionalized cysteamine molecules in the SAM also cannot be ruled out. For interaction with the ME SAM, a work of adhesion of over 100 k_BT per molecule is obtained under the assumption that only the catechol groups on the surface participate to the adhesion force.

Die approbierte gedruckte Originalversion dieser Diplomarbeit ist an der TU Wien Bibliothek verfügbar
The approved original version of this thesis is available in print at TU Wien Bibliothek.
TU Bibliothek Your knowledge hub WIEN

An interaction free energy of that magnitude would indicate the formation and breaking of covalent bonds between the catechols and the opposing surface, if there is no participation of surface amine groups. Additionally, in the case of the ME SAM, the opposing surface has the ability to donate hydrogen bonds given a suitable acceptor.

Effectively, no difference in adhesion is observed between oxidizing and reducing potentials, which begs the question, what makes these two systems so different from the case of catechol vs. mica. Unfortunately, this is difficult to answer without more data. A short discussion on what may be required to address this issue is given in the outlook section below.

One notable trend, that was observed in all three studied configurations is the drastic decrease in adhesion in 100 mM sodium perchlorate solution, i.e. in a high ionic strength environment. Under these conditions, the catechol functionalized SAM vs. titania and ME SAM resulted in no measurable adhesion, while catechol functionalized SAM vs. mica gave a strongly decreased adhesion that was still potential dependent. It is thus likely, that a similar effect is in play for all systems.

A different study[10] in our group looked at the strength of amine-mica interaction in sodium chloride solutions of various concentrations using the SFA. It revealed a clear decrease in adhesion strength with increasing ionic strength, which can most likely be attributed to a layer of sodium cations (over-)adsorbed to the mica surface (inner EDL). With increasing sodium chloride concentration, this layer is more densely packed and less defect rich and becomes more effective at preventing amine groups from interacting with the surface.

It is possible that the same effect is responsible for the lowered adhesion vs. the catechol functionalized surface. If sodium ions (or another species) are present at and adsorbed to the interface in large quantities, the catechol may be hindered from interacting with the surface thus preventing or significantly reducing adhesion. For this consideration, it doesn't matter whether the catechol interacts more strongly in the reduced or oxidized form or even if other mechanisms (such as cation-π interactions as proposed by Gebbie et al. [34]) are involved. Figure 4.5 illustrates this concept for the case of a mica surface in a solution containing sodium cations.

For the case of underwater mussel adhesion this means saline conditions would always impede attachment because of the high ion concentration at the interface unless seawater is removed prior to mfp injection. Of course, water removal is exactly what happens during the attachment process, when the mussel foot acts as a form of "suction cup" just before plaque formation. Presumably, once the

[10] at the time of writing unpublished

Die approbierte gedruckte Originalversion dieser Diplomarbeit ist an der TU Wien Bibliothek verfügbar
The approved original version of this thesis is available in print at TU Wien Bibliothek.
TU Bibliothek Your knowledge hub WIEN

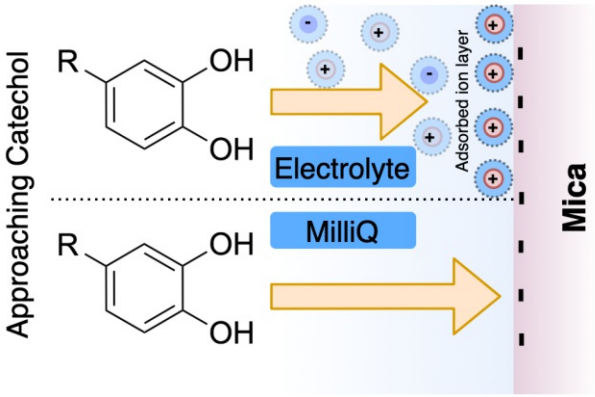

Figure 4.5.: A significantly reduced adhesion was recorded for all systems in 100 mM sodium perchlorate compared to MilliQ. A proposed explanation is adsorbed ions from the inner EDL blocking catechol groups from accessing and interacting with the mica surface as indicated here for mica substrate and adsorbed cations (sodium). This explanation agrees with findigs from another (not yet published) study performed in our group.

adhesive bonds have been formed and the plaque and byssus polymers are cross-linked, a hydration of the interface would be energetically unfavorable. Thus, even if ions can later diffuse back into the structure, seawater components could no longer break these bonds.

4.3. Summary, Conclusion and Outlook

In summary, CV was used to characterize the catechol functionalized SAM introduced in section 1.3. It confirmed the presence of electrochemically active catechol species after functionalization and gave an insight into their stability. Furthermore, it was possible to estimate a surface coverage of active catechol groups that could then be used for relating results of the EC-SFA experiments to single molecules. Two methods, analysis via the Randles-Sevcik equation for surface adsorbed species and integration of the transferred charge, were used for this estimation which produced compatible results. Both methods gave similar results and in either case, the surface coverage was surprisingly low; less then 1 % of amine groups of the underlying cysteamine SAM appear to have been converted into electrochemically active catechol groups. While this number should be sufficient to study the effects of catechol oxidation and reduction on adhesion, the presence

Die approbierte gedruckte Originalversion dieser Diplomarbeit ist an der TU Wien Bibliothek verfügbar
The approved original version of this thesis is available in print at TU Wien Bibliothek.
TU Bibliothek Your knowledge hub WIEN

of amines and other functional groups needs to be taken into consideration in any interpretation.

Following electrochemical characterization, adhesion measurements under potential control were performed with the catechol functionalized SAM in the EC-SFA. In a configuration of monolayer vs. mica a reversible, potential dependent adhesion was observed in MilliQ water that was significantly reduced in sodium perchlorate solution. Interestingly, stronger adhesion was observed at oxidizing potential, even though the reduced catechol form is usually associated with adhesion. This supports the idea that there may be more to mussel adhesion than just catechol chemistry as suggested by the works of Gebbie et al. and Bilotto et al. [34, 35].

Experiments that put a titania surface and a hydroxyl terminated SAM up against the catechol functionalized monolayer showed a significant adhesion, that was not potential dependent. Furthermore, these sample systems showed little to no adhesion once the high ionic strength electrolyte was introduced.

This last observation, which all studied sample systems had in common, may be explained by adsorbed electrolyte ions blocking interaction sites on the substrate as highlighted in figure 4.5. If the catechol groups are unable to reach the surface they consequently cannot participate in any adhesion either.

It is worth reiterating here that in nature, mussels use a sophisticated "suction cup" like mechanism to keep seawater (which has a high salt concentration) away from the interface during initial steps of the plaque formation. This behavior makes perfect sense from a biologic perspective if the presence of ions at the interface interferes with catechol mediated adhesion.

The sample systems presented in this work provide a good basis for further study of electrochemically switchable catechol adhesion, but as always, further research will be necessary. Follow-up investigations may go in a number of potentially interesting directions and make improvements based on what was learned so far.

Problems with the catechol functionalized SAM used in this work are the functionalization efficiency (and thus low surface coverage) and potential of interaction with amine groups from the base cysteamine layer. Both of these issues could be addressed by using a SAM grown from a solution of a catechol-thiol compound as demonstrated by Simmons et al. [65]. To the author's knowledge, suitable compounds are not commercially available and thus will need to be custom synthesized, but in return such a system may give a much denser catechol coverage and a more sensitive adhesion measurement.

Future EC-SFA experiments could further look at a range of other opposing surfaces with various functionalizations. Interesting options for this would include amine groups to study covalent bonding as a follow up to oxidation and even a

Die approbierte gedruckte Originalversion dieser Diplomarbeit ist an der TU Wien Bibliothek verfügbar
The approved original version of this thesis is available in print at TU Wien Bibliothek.
TU Bibliothek Your knowledge hub WIEN

catechol vs. catechol configuration to elucidate crosslinking mechanisms. Furthermore, the used electrolyte offers another parameter to play with. Using varying concentrations and salt species could allow a better understanding of the kinetic of how adsorbed ions block catechol access and limit adhesion. Finally, one can consider adding small quantities of additives to the electrolyte solution to study e.g. the interaction in the presence of dissolved Fe^{3+} or boronates which are well know to form complexes with catechols [68, 99].

Altogether, the work presented in this thesis shows a promising new way of studying catechol adhesion under electrochemical control. It also largely answered the research questions asked at the beginning, though naturally new questions have arisen that will need to be answered by future works. Some of these include:

- To what extent is mussel adhesion dependent on catechol chemistry?
- What other mechanisms play a central or supporting role?
- What is the impact on adhesion of different ion species present at the interface?

Nonetheless, the use of a functionalized SAM provides a simple, yet consistent sample system with a knowable surface coverage of catechols. Combining this with the EC-SFA opens up new possibilities for the future study of catechol adhesion with a much greater control of the oxidation state at the surface. Going forward, this concept could even be extended to study the interfacial properties of other electrochemically active species. This approach can enable a more comprehensive study of the catechol bond energy landscape and thereby provide the basis for the development of novel biomimetic adhesives.

Die approbierte gedruckte Originalversion dieser Diplomarbeit ist an der TU Wien Bibliothek verfügbar
The approved original version of this thesis is available in print at TU Wien Bibliothek.
TU Bibliothek Your knowledge hub WIEN

Bibliography

[1] J. H. Waite, "Mussel adhesion – essential footwork", Journal of Experimental Biology **220**, 517–530 (2017).

[2] C. M. Yonge, "On The Primitive Significance of the Byssus in the Bivalvia and its Effects in Evolution", Journal of the Marine Biological Association of the United Kingdom **42**, 113–125 (1962).

[3] J. Saiz-Poseu, J. Mancebo-Aracil, F. Nador, F. Busqué, and D. Ruiz-Molina, "The Chemistry behind Catechol-Based Adhesion", Angewandte Chemie International Edition **58**, 696–714 (2019).

[4] B. P. Lee, P. Messersmith, J. Israelachvili, and J. Waite, "Mussel-Inspired Adhesives and Coatings", Annual Review of Materials Research **41**, 99–132 (2011).

[5] A. Hawkins and B. Bayne, "Seasonal variation in the relative utilization of carbon and nitrogen by the mussel Mytilus edulis: budgets, conversion efficiencies and maintenance requirements", Marine Ecology Progress Series **25**, 181–188 (1985).

[6] M. P. Schultz, J. A. Bendick, E. R. Holm, and W. M. Hertel, "Economic impact of biofouling on a naval surface ship", Biofouling **27**, 87–98 (2011).

[7] S. Rajagopal, H. A. Jenner, and V. P. Venugopalan, *Operational and Environmental Consequences of Large Industrial Cooling Water Systems* (Springer Science & Business Media, Jan. 7, 2012), 491 pp.

[8] H. Polman, F. Verhaart, and M. Bruijs, "Impact of biofouling in intake pipes on the hydraulics and efficiency of pumping capacity", Desalination and Water Treatment **51**, 997–1003 (2013).

[9] R. Tripathi, *Advances In Antifouling Coatings Technology*, Coatings World, (10-10-16) `https://www.coatingsworld.com/issues/2016-10-01/view_features/advances-in-antifouling-coatings-technology/` (visited on 02/05/2021).

[10] J. Zhou, Y. Wan, N. Liu, H. Yin, B. Li, D. Sun, and Q. Ran, "Epoxy adhesive with high underwater adhesion and stability based on low viscosity modified Mannich bases", Journal of Applied Polymer Science **135**, 45688 (2018).

[11] I. A. Ashcroft and J. Comyn, "Effect of Water and Mechanical Stress on Durability", in *Handbook of Adhesion Technology*, edited by L. F. M. da Silva, A. Öchsner, and R. D. Adams (Springer, Berlin, Heidelberg, 2011), pp. 787–822.

Die approbierte gedruckte Originalversion dieser Diplomarbeit ist an der TU Wien Bibliothek verfügbar
The approved original version of this thesis is available in print at TU Wien Bibliothek.
TU Bibliothek Your knowledge hub WIEN

[12]R. A. Chivers, "Adhesion in Medicine", in *Handbook of Adhesion Technology*, edited by L. F. M. da Silva, A. Öchsner, and R. D. Adams (Springer International Publishing, Cham, 2018), pp. 1729–1749.

[13]D. J. Wilson, D. H. Chenery, H. K. Bowring, K. Wilson, R. Turner, J. Maughan, P. J. West, and C. W. G. Ansell, "Physical and biological properties of a novel siloxane adhesive for soft tissue applications", Journal of Biomaterials Science, Polymer Edition **16**, 449–472 (2005).

[14]M. J. Brennan, B. F. Kilbride, J. J. Wilker, and J. C. Liu, "A bioinspired elastin-based protein for a cytocompatible underwater adhesive", Biomaterials **124**, 116–125 (2017).

[15]Y. Liang, X. Zhao, T. Hu, Y. Han, and B. Guo, "Mussel-inspired, antibacterial, conductive, antioxidant, injectable composite hydrogel wound dressing to promote the regeneration of infected skin", Journal of Colloid and Interface Science **556**, 514–528 (2019).

[16]M. Rahimnejad and W. Zhong, "Mussel-inspired hydrogel tissue adhesives for wound closure", RSC Advances **7**, 47380–47396 (2017).

[17]N. Hiraishi, D. Kaneko, S. Taira, S. Wang, M. Otsuki, and J. Tagami, "Mussel-mimetic, bioadhesive polymers from plant-derived materials", Journal of Investigative and Clinical Dentistry **6**, 59–62 (2015).

[18]Q. Guo, J. Chen, J. Wang, H. Zeng, and J. Yu, "Recent progress in synthesis and application of mussel-inspired adhesives", Nanoscale **12**, 1307–1324 (2020).

[19]N. K. Kaushik, N. Kaushik, S. Pardeshi, J. G. Sharma, S. H. Lee, and E. H. Choi, "Biomedical and Clinical Importance of Mussel-Inspired Polymers and Materials", Marine Drugs **13**, 6792–6817 (2015).

[20]N. Patil, C. Jérôme, and C. Detrembleur, "Recent advances in the synthesis of catechol-derived (bio)polymers for applications in energy storage and environment", Progress in Polymer Science **82**, 34–91 (2018).

[21]H. Zhao, N. B. Robertson, S. A. Jewhurst, and J. H. Waite, "Probing the Adhesive Footprints of Mytilus californianus Byssus", Journal of Biological Chemistry **281**, 11090–11096 (2006).

[22]D. G. DeMartini, J. M. Errico, S. Sjoestroem, A. Fenster, and J. H. Waite, "A cohort of new adhesive proteins identified from transcriptomic analysis of mussel foot glands", Journal of The Royal Society Interface **14**, 20170151 (2017).

[23]Q. Lin, D. Gourdon, C. Sun, N. Holten-Andersen, T. H. Anderson, J. H. Waite, and J. N. Israelachvili, "Adhesion mechanisms of the mussel foot proteins mfp-1 and mfp-3", Proceedings of the National Academy of Sciences **104**, 3782–3786 (2007).

Die approbierte gedruckte Originalversion dieser Diplomarbeit ist an der TU Wien Bibliothek verfügbar
The approved original version of this thesis is available in print at TU Wien Bibliothek.
TU Bibliothek Your knowledge hub WIEN

[24]E. W. Danner, Y. Kan, M. U. Hammer, J. N. Israelachvili, and J. H. Waite, "Adhesion of Mussel Foot Protein Mefp-5 to Mica: An Underwater Superglue", Biochemistry **51**, 6511–6518 (2012).

[25]S. C. T. Nicklisch, S. Das, N. R. Martinez Rodriguez, J. H. Waite, and J. N. Israelachvili, "Antioxidant efficacy and adhesion rescue by a recombinant mussel foot protein-6", Biotechnology Progress **29**, 1587–1593 (2013 Nov-Dec).

[26]N. R. Martinez Rodriguez, S. Das, Y. Kaufman, J. N. Israelachvili, and J. H. Waite, "Interfacial pH during mussel adhesive plaque formation", Biofouling **31**, 221–227 (2015).

[27]J. H. Waite, "Adhesion à la Moule1", Integrative and Comparative Biology **42**, 1172–1180 (2002).

[28]H. G. Silverman and F. F. Roberto, "Understanding Marine Mussel Adhesion", Marine Biotechnology (New York, N.y.) **9**, 661–681 (2007).

[29]S. C. Daubner, T. Le, and S. Wang, "Tyrosine hydroxylase and regulation of dopamine synthesis", Archives of Biochemistry and Biophysics **508**, 1–12 (2011).

[30]L. Li and H. Zeng, "Marine mussel adhesion and bio-inspired wet adhesives", Biotribology **5**, 44–51 (2016).

[31]J. Yang, V. Saggiomo, A. H. Velders, M. A. C. Stuart, and M. Kamperman, "Reaction Pathways in Catechol/Primary Amine Mixtures: A Window on Crosslinking Chemistry", PLOS ONE **11**, e0166490 (2016).

[32]A. H. Hofman, I. A. van Hees, J. Yang, and M. Kamperman, "Bioinspired Underwater Adhesives by Using the Supramolecular Toolbox", Advanced Materials **30**, 1704640 (2018).

[33]D. S. Hwang, H. Zeng, A. Masic, M. J. Harrington, J. N. Israelachvili, and J. H. Waite, "Protein- and Metal-dependent Interactions of a Prominent Protein in Mussel Adhesive Plaques *", Journal of Biological Chemistry **285**, 25850–25858 (2010).

[34]M. A. Gebbie, W. Wei, A. M. Schrader, T. R. Cristiani, H. A. Dobbs, M. Idso, B. F. Chmelka, J. H. Waite, and J. N. Israelachvili, "Tuning underwater adhesion with cation– π interactions", Nature Chemistry **9**, 473–479 (2017).

[35]P. Bilotto, C. Labate, M. P. De Santo, K. Deepankumar, A. Miserez, and B. Zappone, "Adhesive Properties of Adsorbed Layers of Two Recombinant Mussel Foot Proteins with Different Levels of DOPA and Tyrosine", Langmuir **35**, 15481–15490 (2019).

Die approbierte gedruckte Originalversion dieser Diplomarbeit ist an der TU Wien Bibliothek verfügbar
The approved original version of this thesis is available in print at TU Wien Bibliothek.
TU Bibliothek Your knowledge hub WIEN

[36]M. Shin, J. Y. Shin, K. Kim, B. Yang, J. W. Han, N.-K. Kim, and H. J. Cha, "The position of lysine controls the catechol-mediated surface adhesion and cohesion in underwater mussel adhesion", Journal of Colloid and Interface Science **563**, 168–176 (2020).

[37]S. Moulay, "Dopa/Catechol-Tethered Polymers: Bioadhesives and Biomimetic Adhesive Materials", Polymer Reviews **54**, 436–513 (2014).

[38]X. Zhang, H. Liu, L. Yue, Y. Bai, and J. He, "Mussel-mimetic polymer underwater adhesives with l -Dopa functionality: influencing adhesion properties and simplified operation procedures", Journal of Materials Science **55**, 7981–7997 (2020).

[39]S. D. Iversen and L. L. Iversen, "Dopamine: 50 years in perspective", Trends in Neurosciences, Fifty Years of Dopamine Research **30**, 188–193 (2007).

[40]X. Xiong, Y. Liu, F. Shi, G. Zhang, J. Weng, and S. Qu, "Enhanced Adhesion of Mussel-inspired Adhesive through Manipulating Contents of Dopamine Methacrylamide and Molecular Weight of Polymer", Journal of Bionic Engineering **15**, 461–470 (2018).

[41]J. Liebscher, R. Mrówczyński, H. A. Scheidt, C. Filip, N. D. Hădade, R. Turcu, A. Bende, and S. Beck, "Structure of Polydopamine: A Never-Ending Story?", Langmuir **29**, 10539–10548 (2013).

[42]S. Schindler and T. Bechtold, "Mechanistic insights into the electrochemical oxidation of dopamine by cyclic voltammetry", Journal of Electroanalytical Chemistry **836**, 94–101 (2019).

[43]H. A. Lee, E. Park, and H. Lee, "Polydopamine and Its Derivative Surface Chemistry in Material Science: A Focused Review for Studies at KAIST", Advanced Materials **32**, 1907505 (2020).

[44]G. Fredi, F. Simon, D. Sychev, I. Melnyk, A. Janke, C. Scheffler, and C. Zimmerer, "Bioinspired Polydopamine Coating as an Adhesion Enhancer Between Paraffin Microcapsules and an Epoxy Matrix", ACS Omega **5**, 19639–19653 (2020).

[45]H. Wang, C. Lin, X. Zhang, K. Lin, X. Wang, and S. G. Shen, "Mussel-Inspired Polydopamine Coating: A General Strategy To Enhance Osteogenic Differentiation and Osseointegration for Diverse Implants", ACS Applied Materials & Interfaces **11**, 7615–7625 (2019).

[46]L. Dong, M. Chen, X. Wu, D. Shi, W. Dong, H. Zhang, and C. Zhang, "Multifunctional polydopamine coating: simultaneous enhancement of interfacial adhesion and CO2 separation performance of mixed matrix membranes", New Journal of Chemistry **40**, 9148–9159 (2016).

Die approbierte gedruckte Originalversion dieser Diplomarbeit ist an der TU Wien Bibliothek verfügbar
The approved original version of this thesis is available in print at TU Wien Bibliothek.
TU Bibliothek Your knowledge hub WIEN

[47]S. Mondal, A. Thampi, and M. Puranik, "Kinetics of Melanin Polymerization during Enzymatic and Nonenzymatic Oxidation", The Journal of Physical Chemistry B **122**, 2047–2063 (2018).

[48]J. Yu, W. Wei, M. S. Menyo, A. Masic, J. H. Waite, and J. N. Israelachvili, "Adhesion of Mussel Foot Protein-3 to TiO2 Surfaces: the Effect of pH", Biomacromolecules **14**, 1072–1077 (2013).

[49]J. Yu, W. Wei, E. Danner, J. N. Israelachvili, and J. H. Waite, "Effects of Interfacial Redox in Mussel Adhesive Protein Films on Mica", Advanced Materials **23**, 2362–2366 (2011).

[50]J. Yu, W. Wei, E. Danner, R. K. Ashley, J. N. Israelachvili, and J. H. Waite, "Mussel protein adhesion depends on interprotein thiol-mediated redox modulation", Nature Chemical Biology **7**, 588–590 (2011).

[51]Q. Lin, Q. Li, C. Batchelor-McAuley, and R. G. Compton, "Two-Electron, Two-Proton Oxidation of Catechol: Kinetics and Apparent Catalysis", The Journal of Physical Chemistry C **119**, 1489–1495 (2015).

[52]C. Giacomelli, K. Ckless, D. Galato, F. S. Miranda, and A. Spinelli, "Electrochemistry of Caffeic Acid Aqueous Solutions with pH 2.0 to 8.5", Journal of the Brazilian Chemical Society **13**, 332–338 (2002).

[53]A. Kiani, J.-B. Raoof, D. Nematollahi, and R. Ojani, "Electrochemical Study of Catechol in the Presence of Dibuthylamine and Diethylamine in Aqueous Media: Part 1. Electrochemical Investigation", Electroanalysis **17**, 1755–1760 (2005).

[54]PubChem, *Dihydrocaffeic acid*, `https://pubchem.ncbi.nlm.nih.gov/compound/348154` (visited on 03/05/2021).

[55]W. C. Bigelow, D. L. Pickett, and W. A. Zisman, "Oleophobic monolayers: I. Films adsorbed from solution in non-polar liquids", Journal of Colloid Science **1**, 513–538 (1946).

[56]J. E. Greene, "Tracing the 4000 year history of organic thin films: From monolayers on liquids to multilayers on solids", Applied Physics Reviews **2**, 011101 (2015).

[57]H. M. Schessler, D. S. Karpovich, and G. J. Blanchard, "Quantitating the Balance between Enthalpic and Entropic Forces in Alkanethiol/Gold Monolayer Self Assembly", Journal of the American Chemical Society **118**, 9645–9651 (1996).

[58]B. Bhushan, "Self-Assembled Monolayers (SAMs) for Controlling Adhesion, Friction, and Wear", in *Springer Handbook of Nanotechnology*, edited by B. Bhushan, Springer Handbooks (Springer, Berlin, Heidelberg, 2007), pp. 1379–1416.

Die approbierte gedruckte Originalversion dieser Diplomarbeit ist an der TU Wien Bibliothek verfügbar
The approved original version of this thesis is available in print at TU Wien Bibliothek.
TU Bibliothek Your knowledge hub WIEN

[59]A. Hasan and L. M. Pandey, "6 - Self-assembled monolayers in biomaterials", in *Nanobiomaterials*, edited by R. Narayan (Woodhead Publishing, Jan. 1, 2018), pp. 137–178.

[60]N. K. Chaki and K. Vijayamohanan, "Self-assembled monolayers as a tunable platform for biosensor applications", Biosensors and Bioelectronics **17**, 1–12 (2002).

[61]M. Singh, N. Kaur, and E. Comini, "The role of self-assembled monolayers in electronic devices", Journal of Materials Chemistry C **8**, 3938–3955 (2020).

[62]J. C. Love, L. A. Estroff, J. K. Kriebel, R. G. Nuzzo, and G. M. Whitesides, "Self-Assembled Monolayers of Thiolates on Metals as a Form of Nanotechnology", Chemical Reviews **105**, 1103–1170 (2005).

[63]F. P. Zamborini and R. M. Crooks, "Corrosion Passivation of Gold by n-Alkanethiol Self-Assembled Monolayers:.1667em Effect of Chain Length and End Group", Langmuir **14**, 3279–3286 (1998).

[64]M. Guardingo, E. Bellido, R. Miralles-Llumà, J. Faraudo, J. Sedó, S. Tatay, A. Verdaguer, F. Busqué, and D. Ruiz-Molina, "Bioinspired Catechol-Terminated Self-Assembled Monolayers with Enhanced Adhesion Properties", Small **10**, 1594–1602 (2014).

[65]N. J. Simmons, K. O. A. Chin, J. A. Harnisch, B. Vaidya, W. S. Trahanovsky, M. D. Porter*, and R. J. Angelici*, "Synthesis and characterization of a catechol-terminated alkanethiolate monolayer adsorbed on gold", Journal of Electroanalytical Chemistry **482**, 178–187 (2000).

[66]K. Nakano, K. Ohkubo, H. Taira, M. Takagi, and T. Imato, "Electrocatalytic oxidation of dihydronicotineamide adenine dinucleotide on gold electrode modified with catechol-terminated alkanethiol self-assembly", Analytica Chimica Acta, Papers Presented at the 9th Asian Conference on Analytical Chemistry (Asianalysis IX) **619**, 30–36 (2008).

[67]A. Salmanipour and M. A. Taher, "A catechol-terminated self-assembled monolayer at the surface of a gold electrode and its application for the electrocatalytic determination of dopamine", Analyst **136**, 545–549 (2011).

[68]Y. Kan, E. W. Danner, J. N. Israelachvili, Y. Chen, and J. H. Waite, "Boronate Complex Formation with Dopa Containing Mussel Adhesive Protein Retards pH-Induced Oxidation and Enables Adhesion to Mica", PLOS ONE **9**, e108869 (2014).

[69]T. Utzig, P. Stock, and M. Valtiner, "Resolving Non-Specific and Specific Adhesive Interactions of Catechols at Solid/Liquid Interfaces at the Molecular Scale", Angewandte Chemie International Edition **55**, 9524–9528 (2016).

Die approbierte gedruckte Originalversion dieser Diplomarbeit ist an der TU Wien Bibliothek verfügbar
The approved original version of this thesis is available in print at TU Wien Bibliothek.
TU Bibliothek Your knowledge hub WIEN

[70]C. Jarzynski, "Work Fluctuation Theorems and Single-Molecule Biophysics", Progress of Theoretical Physics Supplement **165**, 1–17 (2006).

[71]S. Raman, T. Utzig, T. Baimpos, B. Ratna Shrestha, and M. Valtiner, "Deciphering the scaling of single-molecule interactions using Jarzynski's equality", Nature Communications **5**, 5539 (2014).

[72]M. S. Akram Bhuiyan, J. D. Roland, B. Liu, M. Reaume, Z. Zhang, J. D. Kelley, and B. P. Lee, "In Situ Deactivation of Catechol-Containing Adhesive Using Electrochemistry", Journal of the American Chemical Society **142**, 4631–4638 (2020).

[73]*Carbodiimide Crosslinker Chemistry - AT*, `//www.thermofisher.com/uk/en/home/life-science/protein-biology/protein-biology-learning-center/protein-biology-resource-library/pierce-protein-methods/carbodiimide-crosslinker-chemistry.html` (visited on 07/16/2020).

[74]P. Atkins, J. de Paula, and J. Keeler, *Atkins' Physical Chemistry*, Eleventh Edition (Oxford University Press, Oxford, New York, Dec. 28, 2017), 944 pp.

[75]R. G. Compton and C. E. Banks, *Understanding Voltammetry*, 2nd edition (ICP, London, Nov. 15, 2010), 444 pp.

[76]A. J. Bard and L. R. Faulkner, *Electrochemical Methods: Fundamentals and Applications*, 2nd edition (Wiley, New York, Dec. 18, 2000), 864 pp.

[77]H. Helmholtz, "Ueber einige Gesetze der Vertheilung elektrischer Ströme in körperlichen Leitern mit Anwendung auf die thierisch-elektrischen Versuche", `10.1002/andp.18531650603` (1853).

[78]*support/potentiostat*, `https://www.als-japan.com/1790.html` (visited on 01/20/2021).

[79]*Custom Sensor Solutions, Inc. - Potentiostat Operation Simplified*, `http://www.customsensorsolutions.com/ap-pstat.html` (visited on 03/09/2021).

[80]N. Elgrishi, K. J. Rountree, B. D. McCarthy, E. S. Rountree, T. T. Eisenhart, and J. L. Dempsey, "A Practical Beginner's Guide to Cyclic Voltammetry", Journal of Chemical Education **95**, 197–206 (2018).

[81]J. Israelachvili, Y. Min, M. Akbulut, A. Alig, G. Carver, W. Greene, K. Kristiansen, E. Meyer, N. Pesika, K. Rosenberg, and H. Zeng, "Recent advances in the surface forces apparatus (SFA) technique", Reports on Progress in Physics **73**, 036601 (2010).

[82]V. Wieser, P. Bilotto, U. Ramach, H. Yuan, K. Schwenzfeier, H.-W. Cheng, and M. Valtiner, "Novel in situ sensing surface forces apparatus for measuring gold versus gold, hydrophobic, and biophysical interactions", Journal of Vacuum Science & Technology A **39**, 023201 (2021).

Die approbierte gedruckte Originalversion dieser Diplomarbeit ist an der TU Wien Bibliothek verfügbar
The approved original version of this thesis is available in print at TU Wien Bibliothek.
TU Bibliothek Your knowledge hub WIEN

[83] J. N. Israelachvili, *Intermolecular and Surface Forces* (Academic Press, May 29, 2015), 706 pp.

[84] K. A. Schwenzfeier, A. Erbe, P. Bilotto, M. Lengauer, C. Merola, H.-W. Cheng, L. L. E. Mears, and M. Valtiner, "Optimizing multiple beam interferometry in the surface forces apparatus: Novel optics, reflection mode modeling, metal layer thicknesses, birefringence, and rotation of anisotropic layers", Review of Scientific Instruments **90**, 043908 (2019).

[85] M. Valtiner, X. Banquy, K. Kristiansen, G. W. Greene, and J. N. Israelachvili, "The Electrochemical Surface Forces Apparatus: The Effect of Surface Roughness, Electrostatic Surface Potentials, and Anodic Oxide Growth on Interaction Forces, and Friction between Dissimilar Surfaces in Aqueous Solutions", Langmuir **28**, 13080–13093 (2012).

[86] J. Herzinger, *Joerg/abschlussarbeit-tuwien-physik*, Nov. 26, 2020.

[87] *ChemDraw JS Sample Page*, `https://chemdrawdirect.perkinelmer.cloud/js/sample/index.html#` (visited on 01/21/2021).

[88] M. Valtiner, K. Kristiansen, G. W. Greene, and J. N. Israelachvili, "Effect of Surface Roughness and Electrostatic Surface Potentials on Forces Between Dissimilar Surfaces in Aqueous Solution", Advanced Materials **23**, 2294–2299 (2011).

[89] L. Chai and J. Klein, "Large Area, Molecularly Smooth (0.2 nm rms) Gold Films for Surface Forces and Other Studies", Langmuir **23**, 7777–7783 (2007).

[90] A. Kowalczyk and C. Yu, "Ethanol vs. water: influence of the terminal functional group of the alkyl chain and environment of the self-assembly process on electron transport through the thiol layer", RSC Advances **10**, 21582–21592 (2020).

[91] C. R. Harris, K. J. Millman, S. J. van der Walt, R. Gommers, P. Virtanen, D. Cournapeau, E. Wieser, J. Taylor, S. Berg, N. J. Smith, R. Kern, M. Picus, S. Hoyer, M. H. van Kerkwijk, M. Brett, A. Haldane, J. F. del Río, M. Wiebe, P. Peterson, P. Gérard-Marchant, K. Sheppard, T. Reddy, W. Weckesser, H. Abbasi, C. Gohlke, and T. E. Oliphant, "Array programming with NumPy", Nature **585**, 357–362 (2020).

[92] J. D. Hunter, "Matplotlib: A 2D Graphics Environment", Computing in Science Engineering **9**, 90–95 (2007).

[93] T. Kluyver, B. Ragan-Kelley, F. Pérez, B. Granger, M. Bussonnier, J. Frederic, K. Kelley, J. B. Hamrick, J. Grout, S. Corlay, P. Ivanov, D. Avila, S. Abdalla, C. Willing, and J. D. Team, "Jupyter Notebooks - a publishing format for reproducible computational workflows", in ELPUB (2016).

Die approbierte gedruckte Originalversion dieser Diplomarbeit ist an der TU Wien Bibliothek verfügbar
The approved original version of this thesis is available in print at TU Wien Bibliothek.
TU Bibliothek Your knowledge hub WIEN

[94]J. Reback, W. McKinney, jbrockmendel, J. V. den Bossche, T. Augspurger, P. Cloud, gfyoung, Sinhrks, A. Klein, M. Roeschke, S. Hawkins, J. Tratner, C. She, W. Ayd, T. Petersen, M. Garcia, J. Schendel, A. Hayden, MomIsBestFriend, V. Jancauskas, P. Battiston, S. Seabold, chris-b1, h-vetinari, S. Hoyer, W. Overmeire, alimcmaster1, K. Dong, C. Whelan, and M. Mehyar, *Pandas-dev/pandas: Pandas 1.0.3*, Zenodo, Mar. 18, 2020.

[95]M. Wirde, U. Gelius, and L. Nyholm, "Self-Assembled Monolayers of Cystamine and Cysteamine on Gold Studied by XPS and Voltammetry", Langmuir **15**, 6370–6378 (1999).

[96]X. Shi and Y.-P. Zhao, "Comparison of various adhesion contact theories and the influence of dimensionless load parameter", Journal of Adhesion Science and Technology **18**, 55–68 (2004).

[97]M. Ciavarella, J. Joe, A. Papangelo, and J. R. Barber, "The role of adhesion in contact mechanics", Journal of The Royal Society Interface **16**, 20180738 (2019).

[98]R. Milo and R. Phillips, *Cell Biology by the Numbers*, 1st edition (Garland Science, New York, NY, Dec. 7, 2015), 400 pp.

[99]N. Holten-Andersen, M. J. Harrington, H. Birkedal, B. P. Lee, P. B. Messersmith, K. Y. C. Lee, and J. H. Waite, "pH-induced metal-ligand cross-links inspired by mussel yield self-healing polymer networks with near-covalent elastic moduli", Proceedings of the National Academy of Sciences **108**, 2651–2655 (2011).

Die approbierte gedruckte Originalversion dieser Diplomarbeit ist an der TU Wien Bibliothek verfügbar
The approved original version of this thesis is available in print at TU Wien Bibliothek.
TU Bibliothek Your knowledge hub WIEN

Die approbierte gedruckte Originalversion dieser Diplomarbeit ist an der TU Wien Bibliothek verfügbar
The approved original version of this thesis is available in print at TU Wien Bibliothek.

A. Copyright Clearances

Copyright clearances were obtained for all reproduced figures shown in this work and are provided below.

Die approbierte gedruckte Originalversion dieser Diplomarbeit ist an der TU Wien Bibliothek verfügbar
The approved original version of this thesis is available in print at TU Wien Bibliothek.
TU Bibliothek Your knowledge hub WIEN

TU WIEN Bibliothek Your knowledge hub
Die approbierte gedruckte Originalversion dieser Diplomarbeit ist an der TU Wien Bibliothek verfügbar
The approved original version of this thesis is available in print at TU Wien Bibliothek.

Copyright Clearance Center | Marketplace™

Annual Reviews, Inc. - License Terms and Conditions

This is a License Agreement between Alexander Michael Imre ("You") and Annual Reviews, Inc. ("Publisher") provided by Copyright Clearance Center ("CCC"). The license consists of your order details, the terms and conditions provided by Annual Reviews, Inc., and the CCC terms and conditions.

All payments must be made in full to CCC.

Order Date	22-Jan-2021	Type of Use	Republish in a thesis/dissertation
Order license ID	1092291-1	Publisher	ANNUAL REVIEWS
ISSN	1545-4118	Portion	Chart/graph/table/figure

LICENSED CONTENT

Publication Title	Annual review of materials research	Rightsholder	Annual Reviews, Inc.
Date	01/01/2001	Publication Type	e-Journal
Language	English	URL	http://arjournals.annualreviews.org/loi/matsci
Country	United States of America		

REQUEST DETAILS

Portion Type	Chart/graph/table/figure	Distribution	Worldwide
Number of charts / graphs / tables / figures requested	1	Translation	Original language of publication
Format (select all that apply)	Print, Electronic	Copies for the disabled?	No
Who will republish the content?	Academic institution	Minor editing privileges?	Yes
Duration of Use	Life of current and all future editions	Incidental promotional use?	No
Lifetime Unit Quantity	Up to 499	Currency	EUR
Rights Requested	Main product		

NEW WORK DETAILS

Title	MSc Thesis Alexander Michael Imre	Institution name	TU Vienna, Institute of Applied Physics
Instructor name	Prof. Markus Valtiner	Expected presentation date	2021-06-01

ADDITIONAL DETAILS

Order reference number	N/A	The requesting person / organization to appear on the license	Alexander Michael Imre

REUSE CONTENT DETAILS

Title, description or numeric reference of the portion(s)	Figure 2 Adhesion in the marine mussel Mytilus californianus.	Title of the article/chapter the portion is from	Mussel-Inspired Adhesives and Coatings
Editor of portion(s)	N/A	Author of portion(s)	Bruce P. Lee, P.B. Messersmith, J.N. Israelachvili, and J.H. Waite
Volume of serial or monograph	41		
Page or page range of portion	pp 99-132	Issue, if republishing an article from a serial	N/A
		Publication date of portion	2011-08-01

CCC Republication Terms and Conditions

1. Description of Service; Defined Terms. This Republication License enables the User to obtain licenses for republication of one or more copyrighted works as described in detail on the relevant Order Confirmation (the "Work(s)"). Copyright Clearance Center, Inc. ("CCC") grants licenses through the Service on behalf of the rightsholder identified on the Order Confirmation (the "Rightsholder"). "Republication", as used herein, generally means the inclusion of a Work, in whole or in part, in a new work or works, also as described on the Order Confirmation. "User", as used herein, means the person or entity making such republication.

2. The terms set forth in the relevant Order Confirmation, and any terms set by the Rightsholder with respect to a particular Work, govern the terms of use of Works in connection with the Service. By using the Service, the person transacting for a republication license on behalf of the User represents and warrants that he/she/it (a) has been duly authorized by the User to accept, and hereby does accept, all such terms and conditions on behalf of User, and (b) shall inform User of all such terms and conditions. In the event such person is a "freelancer" or other third party independent of User and CCC, such party shall be deemed jointly a "User" for purposes of these terms and conditions. In any event, User shall be deemed to have accepted and agreed to all such terms and conditions if User republishes the Work in any fashion.

3. Scope of License; Limitations and Obligations.

   3.1. All Works and all rights therein, including copyright rights, remain the sole and exclusive property of the Rightsholder. The license created by the exchange of an Order Confirmation (and/or any invoice) and payment by User of the full amount set forth on that document includes only those rights expressly set forth in the Order Confirmation and in these terms and conditions, and conveys no other rights in the Work(s) to User. All rights not expressly granted are hereby reserved.

   3.2. General Payment Terms: You may pay by credit card or through an account with us payable at the end of the month. If you and we agree that you may establish a standing account with CCC, then the following terms apply: Remit Payment to: Copyright Clearance Center, 29118 Network Place, Chicago, IL 60673-1291. Payments Due: Invoices are payable upon their delivery to you (or upon our notice to you that they are available to you for downloading). After 30 days, outstanding amounts will be subject to a service charge of 1-1/2% per month or, if less, the maximum rate allowed by applicable law. Unless otherwise specifically set forth in the Order Confirmation or in a separate written agreement signed by CCC, invoices are due and payable on "net 30" terms. While User may exercise the rights licensed immediately upon issuance of the Order Confirmation, the license is automatically revoked and is null and void, as if it had never been issued, if complete payment for the license is not received on a timely basis either from User directly or through a payment agent, such as a credit card company.

   3.3. Unless otherwise provided in the Order Confirmation, any grant of rights to User (i) is "one-time" (including the editions and product family specified in the license), (ii) is non-exclusive and non-transferable and (iii) is subject to any and all limitations and restrictions (such as, but not limited to, limitations on duration of use or circulation) included in the Order Confirmation or invoice and/or in these terms and conditions. Upon completion of the licensed use, User shall either secure a new permission for further use of the Work(s) or immediately cease any new use of the Work(s) and shall render inaccessible (such as by deleting or by removing or severing links or other locators) any further copies of the Work (except for copies printed on paper in accordance with this license and still in User's stock at the end of such period).

   3.4. In the event that the material for which a republication license is sought includes third party materials (such as photographs, illustrations, graphs, inserts and similar materials) which are identified in such material as having been used by permission, User is responsible for identifying, and seeking separate licenses (under this Service or otherwise) for, any of such third party materials; without a separate license, such third party materials may not be used.

   3.5. Use of proper copyright notice for a Work is required as a condition of any license granted under the Service. Unless otherwise provided in the Order Confirmation, a proper copyright notice will read substantially as follows: "Republished with permission of [Rightsholder's name], from [Work's title, author, volume, edition number and year of copyright]; permission conveyed through Copyright Clearance Center, Inc." Such notice must be provided in a reasonably legible font size and must be placed either immediately adjacent to the Work as used (for example, as part of a by-line or footnote but not as a separate electronic link) or in the place where substantially all other credits or notices for the new work containing the republished Work are located. Failure to include the required notice results in loss to the Rightsholder and CCC, and the User shall be liable to pay liquidated damages for each such failure equal to twice the use fee specified in the Order Confirmation, in addition to the use fee itself and any other fees and charges specified.

   3.6. User may only make alterations to the Work if and as expressly set forth in the Order Confirmation. No Work may be used in any way that is defamatory, violates the rights of third parties (including such third parties' rights of copyright, privacy, publicity, or other tangible or intangible property), or is otherwise illegal, sexually explicit or obscene. In addition, User may not conjoin a Work with any other material that may result in damage to the reputation of the Rightsholder. User agrees to inform CCC if it becomes aware of any infringement of any rights in a Work and to cooperate with any reasonable request of CCC or the Rightsholder in connection therewith.

4. Indemnity. User hereby indemnifies and agrees to defend the Rightsholder and CCC, and their respective employees and directors, against all claims, liability, damages, costs and expenses, including legal fees and expenses, arising out of any use of a Work beyond the scope of the rights granted herein, or any use of a Work which has been altered in any unauthorized way by User, including claims of defamation or infringement of rights of copyright, publicity, privacy or other tangible or intangible property.

5. Limitation of Liability. UNDER NO CIRCUMSTANCES WILL CCC OR THE RIGHTSHOLDER BE LIABLE FOR ANY DIRECT, INDIRECT, CONSEQUENTIAL OR INCIDENTAL DAMAGES (INCLUDING WITHOUT LIMITATION DAMAGES FOR LOSS OF BUSINESS PROFITS OR INFORMATION, OR FOR BUSINESS INTERRUPTION) ARISING OUT OF THE USE OR INABILITY TO USE A WORK, EVEN IF ONE OF THEM HAS BEEN ADVISED OF THE POSSIBILITY OF SUCH DAMAGES. In any event, the total liability of the Rightsholder and CCC (including their respective employees and directors) shall not exceed the total amount actually paid by User for this license. User assumes full liability for the actions and omissions of its principals, employees, agents, affiliates, successors and assigns.

6. Limited Warranties. THE WORK(S) AND RIGHT(S) ARE PROVIDED "AS IS". CCC HAS THE RIGHT TO GRANT TO USER THE RIGHTS GRANTED IN THE ORDER CONFIRMATION DOCUMENT. CCC AND THE RIGHTSHOLDER DISCLAIM ALL OTHER WARRANTIES RELATING TO THE WORK(S) AND RIGHT(S), EITHER EXPRESS OR IMPLIED, INCLUDING WITHOUT LIMITATION IMPLIED WARRANTIES OF MERCHANTABILITY OR FITNESS FOR A PARTICULAR PURPOSE. ADDITIONAL RIGHTS MAY BE REQUIRED TO USE ILLUSTRATIONS, GRAPHS, PHOTOGRAPHS, ABSTRACTS, INSERTS OR OTHER PORTIONS OF THE WORK (AS OPPOSED TO THE ENTIRE WORK) IN A MANNER CONTEMPLATED BY USER; USER UNDERSTANDS AND AGREES THAT NEITHER CCC NOR THE RIGHTSHOLDER MAY HAVE SUCH ADDITIONAL RIGHTS TO GRANT.

7. Effect of Breach. Any failure by User to pay any amount when due, or any use by User of a Work beyond the scope of the license set forth in the Order Confirmation and/or these terms and conditions, shall be a material breach of the license created by the Order Confirmation and these terms and conditions. Any breach not cured within 30 days of written notice thereof shall result in immediate termination of such license without further notice. Any unauthorized (but licensable) use of a Work that is terminated immediately upon notice thereof may be liquidated by payment of the Rightsholder's ordinary license price therefor; any unauthorized (and unlicensable) use that is not terminated immediately for any reason (including, for example, because materials containing the Work cannot reasonably be recalled) will be subject to all remedies available at law or in equity, but in no event to a payment of less than three times the Rightsholder's ordinary license price for the most closely analogous licensable use plus Rightsholder's and/or CCC's costs and expenses incurred in collecting such payment.

8. Miscellaneous.

   8.1. User acknowledges that CCC may, from time to time, make changes or additions to the Service or to these terms and conditions, and CCC reserves the right to send notice to the User by electronic mail or otherwise for the purposes of notifying User of such changes or additions; provided that any such changes or additions shall not apply to permissions already secured and paid for.

   8.2. Use of User-related information collected through the Service is governed by CCC's privacy policy, available online here: https://marketplace.copyright.com/rs-ui-web/mp/privacy-policy

   8.3. The licensing transaction described in the Order Confirmation is personal to User. Therefore, User may not assign or transfer to any other person (whether a natural person or an organization of any kind) the license created by the Order Confirmation and these terms and conditions or any rights granted hereunder; provided, however, that User may assign such license in its entirety on written notice to CCC in the event of a transfer of all or substantially all of User's rights in the new material which includes the Work(s) licensed under this Service.

   8.4. No amendment or waiver of any terms is binding unless set forth in writing and signed by the parties. The Rightsholder and CCC hereby object to any terms contained in any writing prepared by the User or its principals, employees, agents or affiliates and purporting to govern or otherwise relate to the licensing transaction described in the Order Confirmation, which terms are in any way inconsistent with any terms set forth in the Order Confirmation and/or in these terms and conditions or CCC's standard operating procedures, whether such writing is prepared prior to, simultaneously with or subsequent to the Order Confirmation, and whether such writing appears on a copy of the Order Confirmation or in a separate instrument.

   8.5. The licensing transaction described in the Order Confirmation document shall be governed by and construed under the law of the State of New York, USA, without regard to the principles thereof of conflicts of law. Any case, controversy, suit, action, or proceeding arising out of, in connection with, or related to such licensing transaction shall be brought, at CCC's sole discretion, in any federal or state court located in the County of New York, State of New York, USA, or in any federal or state court whose geographical jurisdiction covers the location of the Rightsholder set forth in the Order Confirmation. The parties expressly submit to the personal jurisdiction and venue of each such federal or state court. If you have any comments or questions about the Service or Copyright Clearance Center, please contact us at 978-750-8400 or send an e-mail to support@copyright.com.

v 1.1

Figure A.1.: Copyright clearance for figure 1.1 originally by Lee et al. [4].

TU WIEN Bibliothek Your knowledge hub
Die approbierte gedruckte Originalversion dieser Diplomarbeit ist an der TU Wien Bibliothek verfügbar
The approved original version of this thesis is available in print at TU Wien Bibliothek.

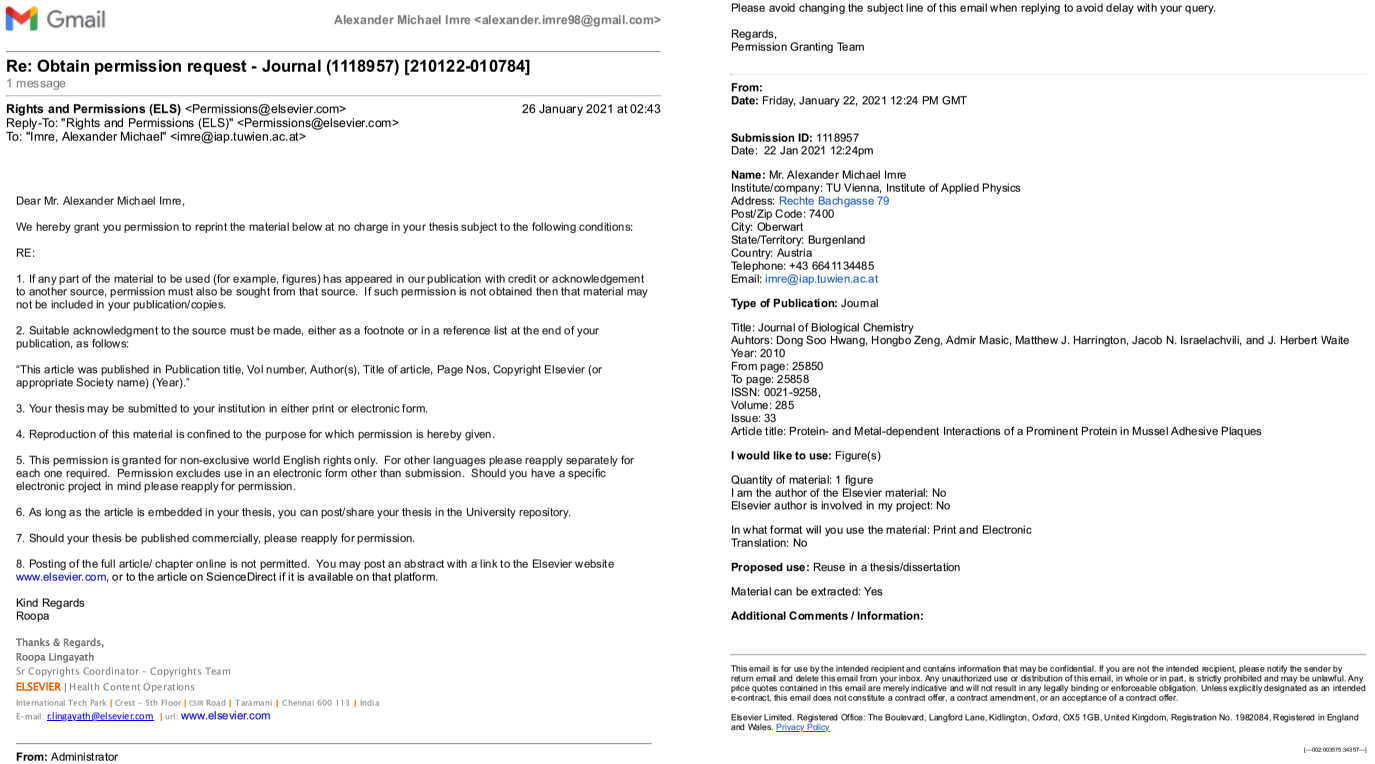

Gmail Alexander Michael Imre <alexander.imre98@gmail.com>

Re: Obtain permission request - Journal (1118957) [210122-010784]
1 message

Rights and Permissions (ELS) <Permissions@elsevier.com> 26 January 2021 at 02:43
Reply-To: "Rights and Permissions (ELS)" <Permissions@elsevier.com>
To: "Imre, Alexander Michael" <imre@iap.tuwien.ac.at>

Dear Mr. Alexander Michael Imre,

We hereby grant you permission to reprint the material below at no charge in your thesis subject to the following conditions:

RE:

1. If any part of the material to be used (for example, figures) has appeared in our publication with credit or acknowledgement to another source, permission must also be sought from that source. If such permission is not obtained then that material may not be included in your publication/copies.

2. Suitable acknowledgment to the source must be made, either as a footnote or in a reference list at the end of your publication, as follows:

"This article was published in Publication title, Vol number, Author(s), Title of article, Page Nos, Copyright Elsevier (or appropriate Society name) (Year)."

3. Your thesis may be submitted to your institution in either print or electronic form.

4. Reproduction of this material is confined to the purpose for which permission is hereby given.

5. This permission is granted for non-exclusive world English rights only. For other languages please reapply separately for each one required. Permission excludes use in an electronic form other than submission. Should you have a specific electronic project in mind please reapply for permission.

6. As long as the article is embedded in your thesis, you can post/share your thesis in the University repository.

7. Should your thesis be published commercially, please reapply for permission.

8. Posting of the full article/ chapter online is not permitted. You may post an abstract with a link to the Elsevier website www.elsevier.com, or to the article on ScienceDirect if it is available on that platform.

Kind Regards
Roopa

Thanks & Regards,
Roopa Lingayath
Sr Copyrights Coordinator – Copyrights Team
ELSEVIER | Health Content Operations
International Tech Park | Crest – 5th Floor | CSIR Road | Taramani | Chennai 600 113 | India
E-mail: rlingayath@elsevier.com | url: www.elsevier.com

From: Administrator
Date: Friday, January 22, 2021 12:24 PM GMT

Dear ,

Thank you for contacting the Permissions Granting Team.

We acknowledge the receipt of your request and we aim to respond within seven business days. Your unique reference number is 210122-010784.

Please avoid changing the subject line of this email when replying to avoid delay with your query.

Regards,
Permission Granting Team

From:
Date: Friday, January 22, 2021 12:24 PM GMT

Submission ID: 1118957
Date: 22 Jan 2021 12:24pm

Name: Mr. Alexander Michael Imre
Institute/company: TU Vienna, Institute of Applied Physics
Address: Rechte Bachgasse 79
Post/Zip Code: 7400
City: Oberwart
State/Territory: Burgenland
Country: Austria
Telephone: +43 6641134485
Email: imre@iap.tuwien.ac.at

Type of Publication: Journal

Title: Journal of Biological Chemistry
Auhtors: Dong Soo Hwang, Hongbo Zeng, Admir Masic, Matthew J. Harrington, Jacob N. Israelachvili, and J. Herbert Waite
Year: 2010
From page: 25850
To page: 25858
ISSN: 0021-9258,
Volume: 285
Issue: 33
Article title: Protein- and Metal-dependent Interactions of a Prominent Protein in Mussel Adhesive Plaques

I would like to use: Figure(s)

Quantity of material: 1 figure
I am the author of the Elsevier material: No
Elsevier author is involved in my project: No

In what format will you use the material: Print and Electronic
Translation: No

Proposed use: Reuse in a thesis/dissertation

Material can be extracted: Yes

Additional Comments / Information:

This email is for use by the intended recipient and contains information that may be confidential. If you are not the intended recipient, please notify the sender by return email and delete this email from your inbox. Any unauthorized use or distribution of this email, in whole or in part, is strictly prohibited and may be unlawful. Any price quotes contained in this email are merely indicative and will not result in any legally binding or enforceable obligation. Unless explicitly designated as an intended e-contract, this email does not constitute a contract offer, a contract amendment, or an acceptance of a contract offer.

Elsevier Limited. Registered Office: The Boulevard, Langford Lane, Kidlington, Oxford, OX5 1GB, United Kingdom, Registration No. 1982084, Registered in England and Wales. Privacy Policy

[—002.003675 34 57—]

Figure A.2.: Copyright clearance for figure 1.3 originally by Hwang et al. [33].

TU WIEN Bibliothek Your knowledge hub
Die approbierte gedruckte Originalversion dieser Diplomarbeit ist an der TU Wien Bibliothek verfügbar
The approved original version of this thesis is available in print at TU Wien Bibliothek.

Figure A.3.: Copyright clearance for figure 3.6 originally by Wieser et al. [82].

AIP PUBLISHING LICENSE TERMS AND CONDITIONS

Mar 20, 2021

This Agreement between Mr. Alexander Imre ("You") and AIP Publishing ("AIP Publishing") consists of your license details and the terms and conditions provided by AIP Publishing and Copyright Clearance Center.

License Number	4994220972908
License date	Jan 22, 2021
Licensed Content Publisher	American Vacuum Society
Licensed Content Publication	Journal of Vacuum Science & Technology A
Licensed Content Title	Novel in situ sensing surface forces apparatus for measuring gold versus gold, hydrophobic, and biophysical interactions
Licensed Content Author	Valentina Wieser, Pierluigi Bilotto, Ulrich Ramach, et al
Licensed Content Date	Mar 1, 2021
Licensed Content Volume	39
Licensed Content Issue	2
Type of Use	Thesis/Dissertation
Requestor type	Student
Format	Print and electronic
Portion	Figure/Table
Number of figures/tables	1
Title	MSc Thesis Alexander Michael Imre
Institution name	TU Vienna, Institute of Applied Physics
Expected presentation date	Jun 2021
Portions	Figure 1
Requestor Location	Mr. Alexander Imre Rechte Bachgasse 79 Oberwart, Burgenland 7400 Austria Attn: Mr. Alexander Imre
Total	**0.00 EUR**

Terms and Conditions

American Vacuum Society -- Terms and Conditions: Permissions Uses

American Vacuum Society ("AVS") hereby grants to you the non-exclusive right and license to use and/or distribute the Material according to the use specified in your order, on a one-time basis, for the specified term, with a maximum distribution equal to the number that you have ordered. Any links or other content accompanying the Material are not the subject of this license.

1. You agree to include the following copyright and permission notice with the reproduction of the Material:"Reprinted with permission from [FULL CITATION]. Copyright [PUBLICATION YEAR], American Vacuum Society." For an article, the copyright and permission notice must be printed on the first page of the article or book chapter. For photographs, covers, or tables, the copyright and permission notice may appear with the Material, in a footnote, or in the reference list.
2. If you have licensed reuse of a figure, photograph, cover, or table, it is your responsibility to ensure that the material is original to AVS and does not contain the copyright of another entity, and that the copyright notice of the figure, photograph, cover, or table does not indicate that it was reprinted by AVS, with permission, from another source. Under no circumstances does AVS, purport or intend to grant permission to reuse material to which it does not hold copyright.
3. You may not alter or modify the Material in any manner. You may translate the Material into another language only if you have licensed translation rights. You may not use the Material for promotional purposes. AVS reserves all rights not specifically granted herein.
4. The foregoing license shall not take effect unless and until AVS or its agent, Copyright Clearance Center, receives the Payment in accordance with Copyright Clearance Center Billing and Payment Terms and Conditions, which are incorporated herein by reference.
5. AVS or the Copyright Clearance Center may, within two business days of granting this license, revoke the license for any reason whatsoever, with a full refund payable to you. Should you violate the terms of this license at any time, AVS, American Vacuum Society, or Copyright Clearance Center may revoke the license with no refund to you. Notice of such revocation will be made using the contact information provided by you. Failure to receive such notice will not nullify the revocation.
6. AVS makes no representations or warranties with respect to the Material. You agree to indemnify and hold harmless AVS, American Vacuum Society, and their officers, directors, employees or agents from and against any and all claims arising out of your use of the Material other than as specifically authorized herein.
7. The permission granted herein is personal to you and is not transferable or assignable without the prior written permission of AVS. This license may not be amended except in a writing signed by the party to be charged.
8. If purchase orders, acknowledgments or check endorsements are issued on any forms containing terms and conditions which are inconsistent with these provisions, such inconsistent terms and conditions shall be of no force and effect. This document, including the CCC Billing and Payment Terms and Conditions, shall be the entire agreement between the parties relating to the subject matter hereof.

This Agreement shall be governed by and construed in accordance with the laws of the State of New York. Both parties hereby submit to the jurisdiction of the courts of New York County for purposes of resolving any disputes that may arise hereunder.

Questions? customercare@copyright.com or +1-855-239-3415 (toll free in the US) or +1-978-646-2777.

B. Technical Drawings

Below technical drawings of some devices and parts developed over the course of this thesis are shown. All of these items are related to the manufacture and measurement of thin film electrodes on glass chips as described in section 3.3.2. The items in the order as shown are:

- the electrochemical cell cap and electrode holder
- the evaporation mask for producing thin film electrodes on 12 × 26 mm^2 glass chips
- a template to position and hold the glass chips in place on the evaporation mask
- a two part clamp to hold the electrode and the connecting gold wire
- an aid to assemble the clamps that prevents the thin film from touching any surfaces

The drawings are supposed to be printed on A4 size paper and measures on the drawings are in millimeters, thus sizes as seen in the printed version of this thesis are not to scale despite the label "1:1" scale label. All drawings, as well as 3D CAD files can be obtained from the author upon reasonable request.

Die approbierte gedruckte Originalversion dieser Diplomarbeit ist an der TU Wien Bibliothek verfügbar
The approved original version of this thesis is available in print at TU Wien Bibliothek.
TU Bibliothek Your knowledge hub WIEN

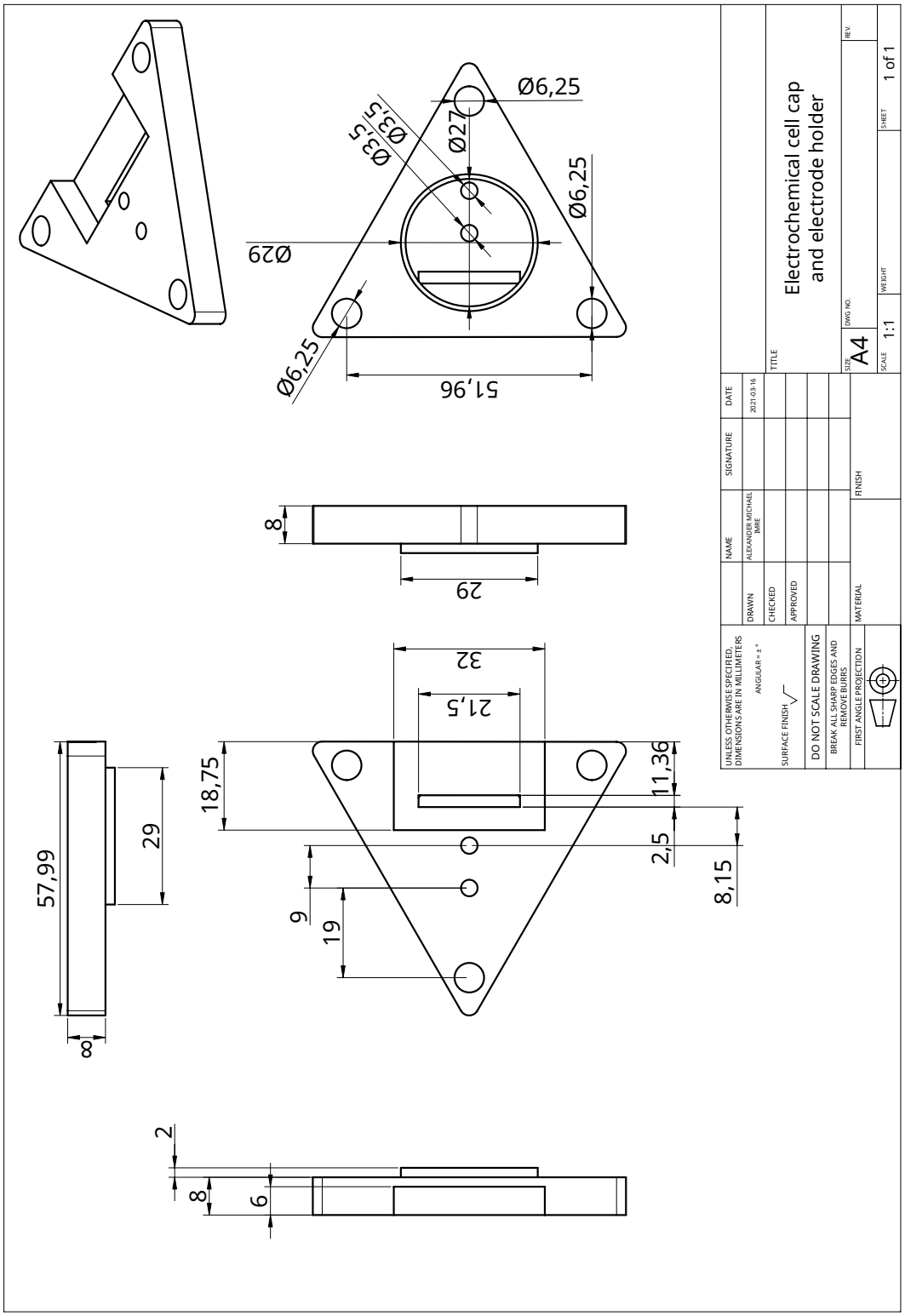

Figure B.1.: Cap and electrode holder for the existing electrochemical cell.

TU Bibliothek Your knowledge hub WIEN
Die approbierte gedruckte Originalversion dieser Diplomarbeit ist an der TU Wien Bibliothek verfügbar
The approved original version of this thesis is available in print at TU Wien Bibliothek.

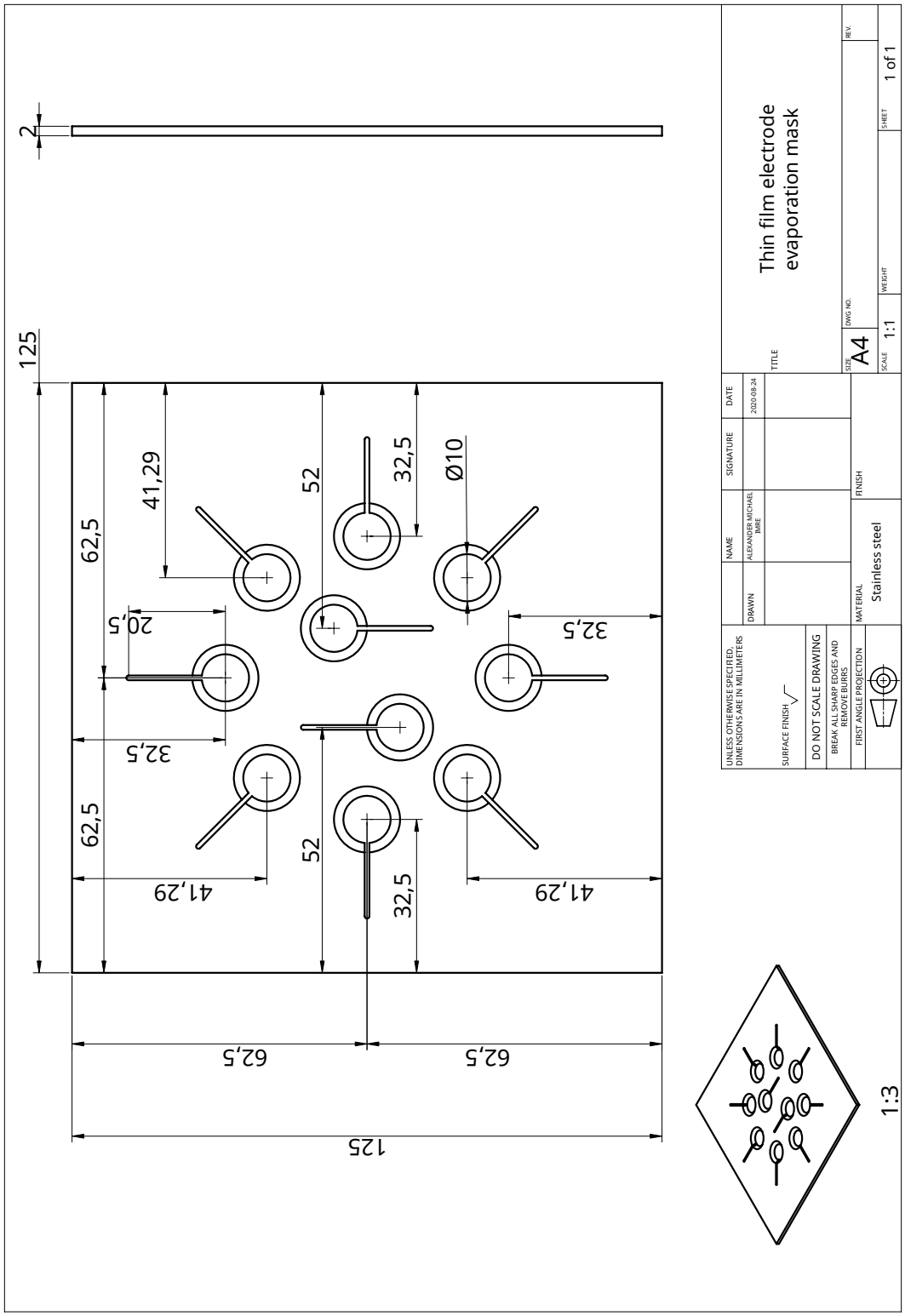

Figure B.2.: Evaporation mask for production of thin film electrodes on glass chips.

Die approbierte gedruckte Originalversion dieser Diplomarbeit ist an der TU Wien Bibliothek verfügbar
The approved original version of this thesis is available in print at TU Wien Bibliothek.

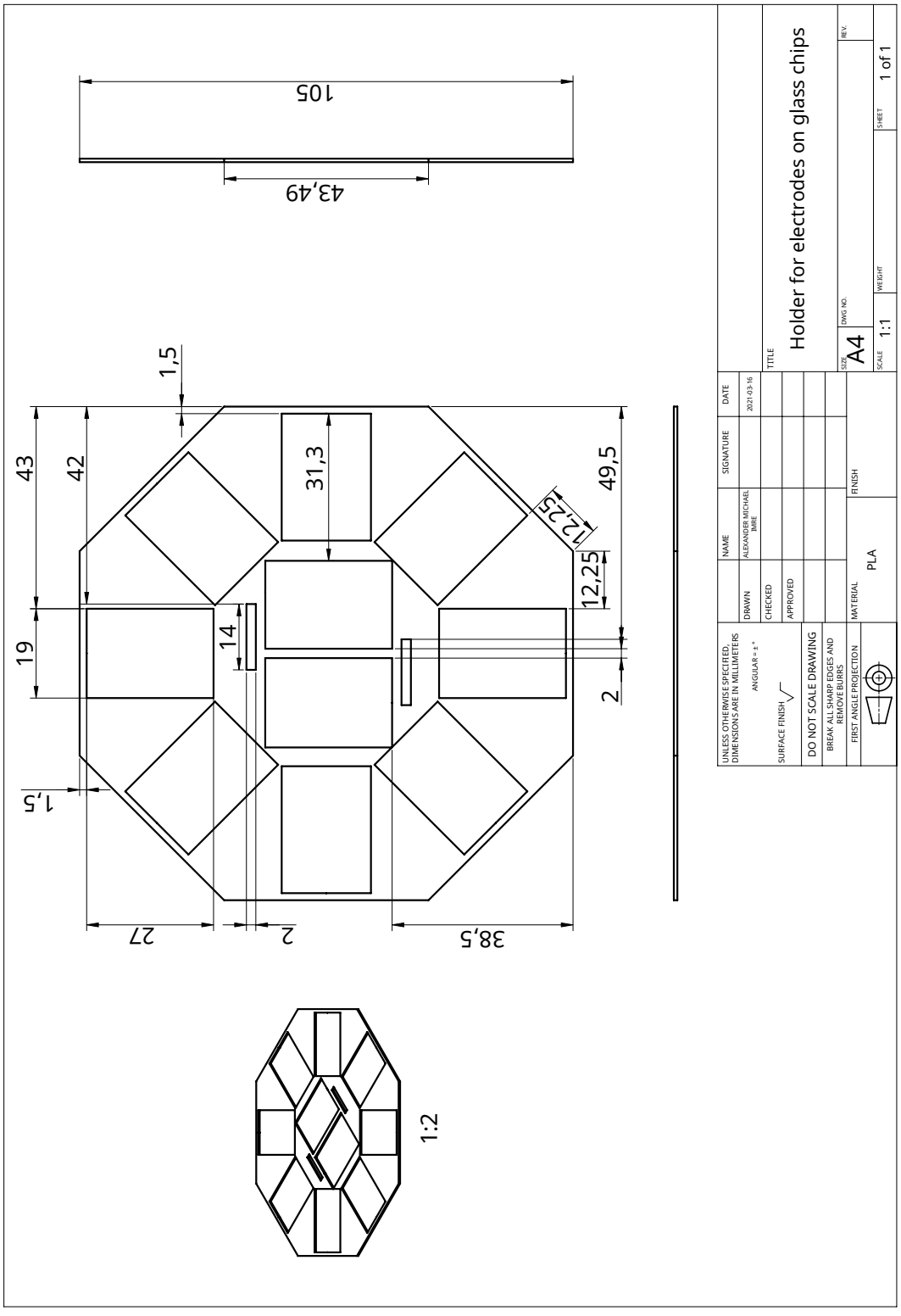

Figure B.3.: Template to position and hold glass on the evaporation mask.

Die approbierte gedruckte Originalversion dieser Diplomarbeit ist an der TU Wien Bibliothek verfügbar
The approved original version of this thesis is available in print at TU Wien Bibliothek.

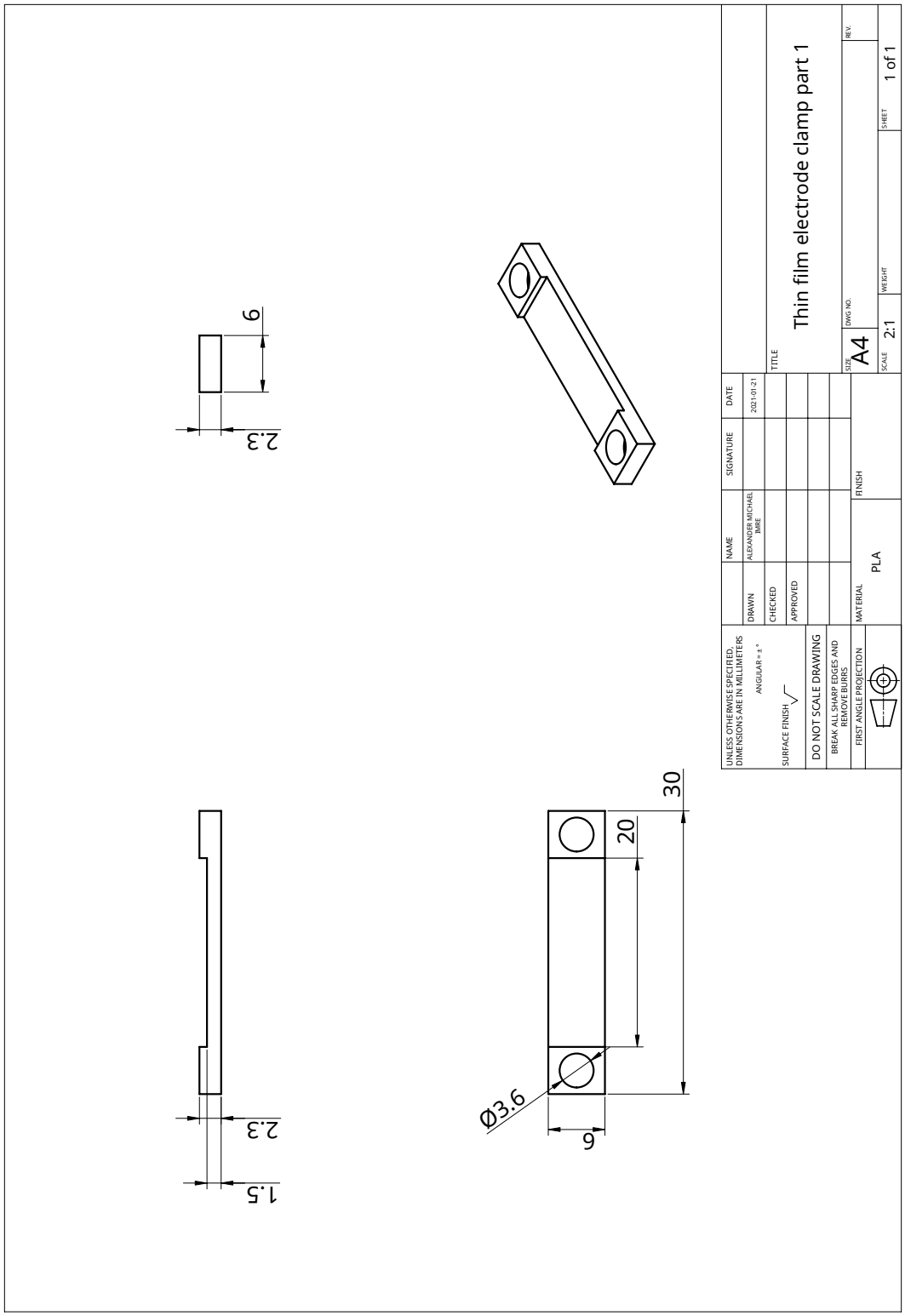

Figure B.4.: Part 1 of the clamp used to hold the chip with the thin film electrode and the connecting wire. When assembled, the clamp is held together by two M6 screws.

Die approbierte gedruckte Originalversion dieser Diplomarbeit ist an der TU Wien Bibliothek verfügbar
The approved original version of this thesis is available in print at TU Wien Bibliothek.

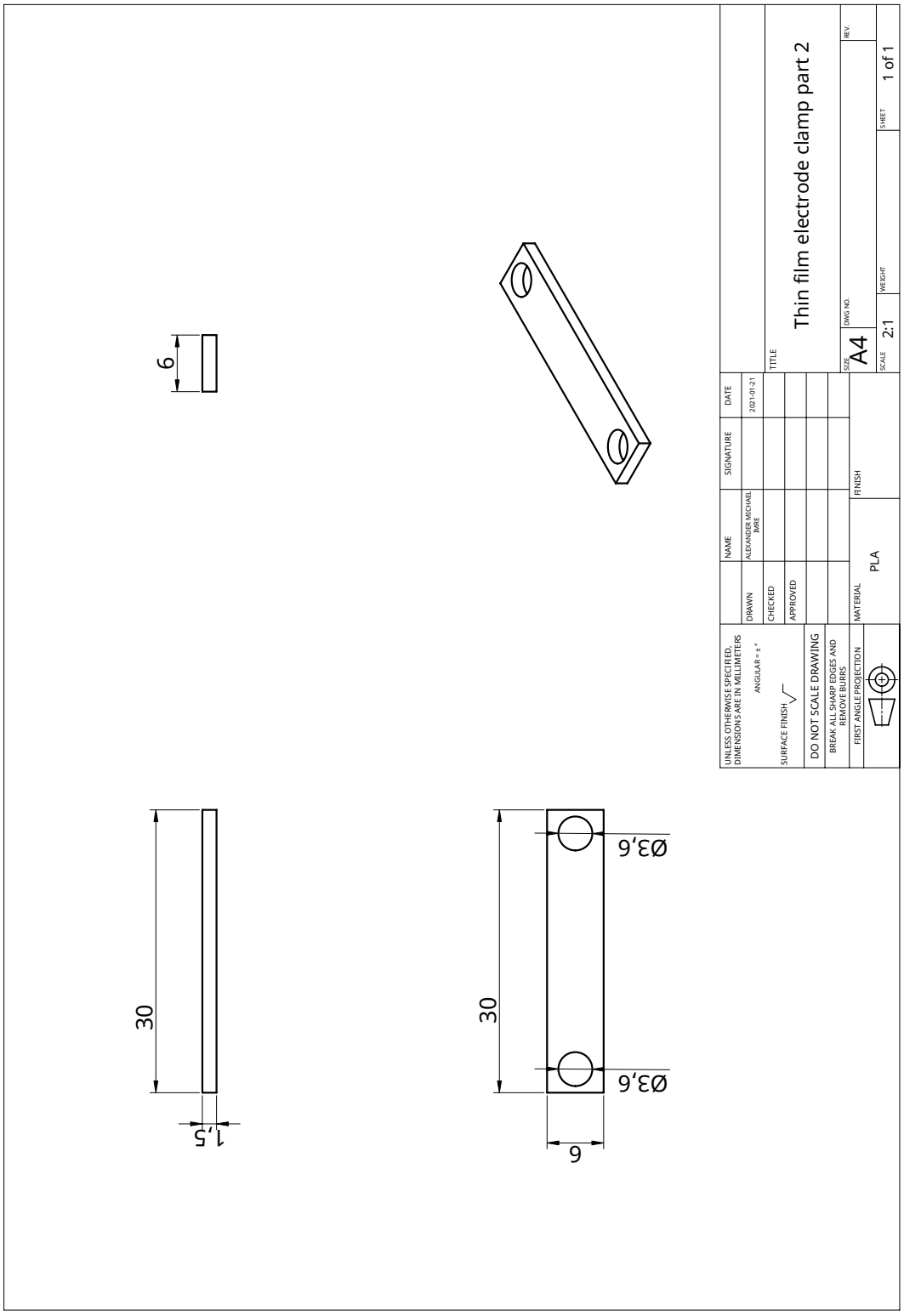

Figure B.5.: Part 2 of the clamp used to hold the chip with the thin film electrode and the connecting wire. When assembled, the clamp is held together by two M6 screws.

Die approbierte gedruckte Originalversion dieser Diplomarbeit ist an der TU Wien Bibliothek verfügbar
The approved original version of this thesis is available in print at TU Wien Bibliothek.

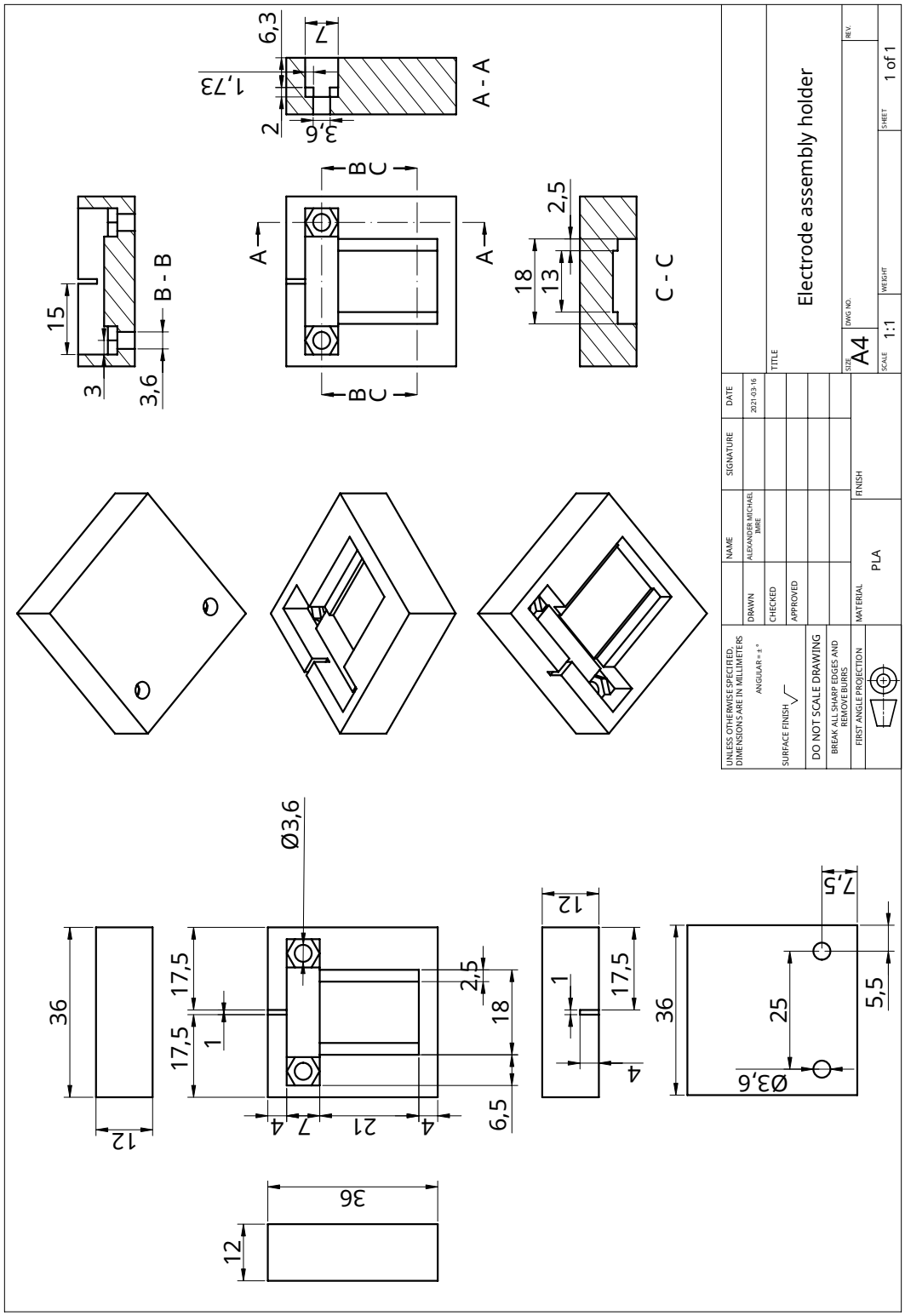

Figure B.6.: An aid that can be used to put assemble the clamps and with the thin film electrode and the connecting wire while preventing the thin metal film to scrape against any surfaces.

TU Bibliothek Your knowledge hub WIEN
Die approbierte gedruckte Originalversion dieser Diplomarbeit ist an der TU Wien Bibliothek verfügbar
The approved original version of this thesis is available in print at TU Wien Bibliothek.

Die approbierte gedruckte Originalversion dieser Diplomarbeit ist an der TU Wien Bibliothek verfügbar
The approved original version of this thesis is available in print at TU Wien Bibliothek.

C. Data Analysis Source Code

Below, some samples of custom written python code is shown that was used for data analysis in this thesis. The development of this code was an important part of the present work and is the basis for all data interpretation. All analysis code was written in a functional way rather than an object-oriented approach. The shown pieces of source code have been shortened for readability and only parts relevant to the fundamental analysis are shown. The sections used to produce various plots in this thesis are not shown because they are only suitable for that particular set of experiment and set of data and are of no general use. However, all source code is available upon reasonable request to the author.

C.1. Cyclic Voltammetry

The data analysis of CV data was performed in the PyCharm integrated development environment using python 3.7. A schematic directory tree of the used files is shown below:

```
CV library
    analyze_CV.py
    plot_CV.py
    read_CV.py
data
    Exp_XX
        data_file_1.csv
        ...
Exp_XX
    analysis_script.py
    ...
```

A set of shared modules (`analyze_CV.py`, `plot_CV.py`, `read_CV.py`) is used for reading in, manipulating and plotting data. The contents of these files and a short template (`analysis_script.py`) for reading in and displaying CVs from a file (`data_file_1.py`) is shown below. Any further analysis can then be "pieced together" using loops, conditional statements, etc. and functions from `analyze_CV.py` as required by the user.

Die approbierte gedruckte Originalversion dieser Diplomarbeit ist an der TU Wien Bibliothek verfügbar
The approved original version of this thesis is available in print at TU Wien Bibliothek.
TU Bibliothek Your knowledge hub WIEN

```python
from analyse_CV import *
import pandas as pd

'''
Dataframes are specific to the used potentiostat (as they may record and save different
things). The arrays used for plotting and numerical analysis are of the same structure
in both cases. This code is for use with data recorded in PSTrace.
'''

# convert dataframe to numpy array
def PSTrace_to_np(directory, filename):
    raw_data = pd.read_csv(directory + filename, encoding="utf-16",
                           skip_blank_lines = True, header=[4])
    # first 4 lines contain date etc.
    # If a comment was added in PSTrace this may raise an error

    raw_data = raw_data.apply(pd.to_numeric, errors='coerce') # forces number or NaN
    raw_data = raw_data.dropna(axis='rows', how='all') # removes all rows with NaN
    raw_data = raw_data.dropna(axis='columns', how='any') # removes any incomplete cycles

    # This is not the best great solution because it will discard non complete datasets.
    # It will also discard cycles if they don't have the same number of datapoints!

    '''
    This gives a pandas dataframe with 2*n coloums for n cycles – coloums contain
    alternatingly voltage and current i.e.: E_1,i_1, E_2, i_2, ...

    Now this is turned into a numpy array with (index 0 = cycle Nr.; index 1 = 0 for
    voltage, 1 for current; index 2 = datapoint).
    It's a bit complicated to get it right because you need to be really careful with the
    indices.
    '''

    temp = raw_data.to_numpy()
    CV_data = []
    for i in range(int(temp.shape[1] / 2)):
        cycle = temp[:, 2 * i:2 * i + 2]
        CV_data.append(cycle)
    return CV_data
```

Figure C.1.: File `read_CV.py`.

Die approbierte gedruckte Originalversion dieser Diplomarbeit ist an der TU Wien Bibliothek verfügbar
The approved original version of this thesis is available in print at TU Wien Bibliothek.
TU Bibliothek Your knowledge hub WIEN

```python
import numpy as np
from scipy.signal import find_peaks

# This file contains functions for ANALYSIS of CVs

# new version, for only one cycle but more powerful
def find_cycle_peaks(data,  width = None, height = None,
                     subtract_background_first = False, low_E = None, high_E = None,
                     decimals = 2, debug_plot= False):
    data = data.copy()  # deep copy is important here!
    if subtract_background_first:
        Eid1 = np.where(np.round(data[:, 0], decimals=decimals) ==
               np.round(low_E, decimals=decimals))[0][0]
        Eid2 = np.where(np.round(data[:, 0], decimals=decimals) ==
               np.round(high_E, decimals=decimals))[0][0]
        if Eid1 > Eid2:
            Eid1, Eid2= Eid2, Eid1
        subtract_lin_background(data=data, Eid1=Eid1, Eid2=Eid2)

    peaks = []  # index of peaks for all cycles
    peak_info = []  # information about peaks (width etc.)

    cycle_peaks = find_peaks(data[:, 1], width=width, height=height)  # from scipy.signals
    peaks.append(cycle_peaks[0])
    peak_info.append(cycle_peaks[1])

    # PLOTTING FOR DEBUGGING
    if debug_plot:
        plt.figure()
        plt.plot(data[Eid1:Eid2, 0], data[Eid1:Eid2, 1])
        plt.show()
        # peak with removed background

    # peaks is a list of the peak positions for all cycles in cv.
    # Each element contains an array with the index of the found peak values (not the peak
    # current or voltage !)

    return peaks, peak_info


# given output form find_CV_peak you will be left with a number of peaks that is not useful
# This function will find the peak you are looking for in the given voltage range
# If no peak or more than one is found an error will be raised.

def find_real_peak_current(trace, peaks, E_low, E_high, remove_background = False):
    indices_in_voltage_range = []
    data = trace
    decimals = 1
    if remove_background:
        Eid1 = np.where(np.round(data[:, 0], decimals=decimals) ==
                        np.round(E_low, decimals=decimals))[0][0]
        Eid2 = np.where(np.round(data[:, 0], decimals=decimals) ==
                        np.round(E_high, decimals=decimals))[0][0]

        if (Eid2 < Eid1):
            Eid1, Eid2 = Eid2, Eid1
        trace, _ = subtract_lin_background(trace, Eid1, Eid2)

    for peak_index in peaks[0]:
        if ((trace[:, 0][peak_index] < E_high) and (trace[:, 0][peak_index] > E_low)):
            indices_in_voltage_range.append(peak_index)


    if len(indices_in_voltage_range) < 1:
        raise Exception('Not peak found in voltage range - check parameters')
    if len(indices_in_voltage_range) == 2 and indices_in_voltage_range[1] ==
       indices_in_voltage_range[0]+2:
        return trace[:, 1][indices_in_voltage_range[0]+1]
    if len(indices_in_voltage_range) > 2:
        return max(trace[:, 1][indices_in_voltage_range])

```

(a) File `analyze_CV.py` part 1.

Die approbierte gedruckte Originalversion dieser Diplomarbeit ist an der TU Wien Bibliothek verfügbar
The approved original version of this thesis is available in print at TU Wien Bibliothek.
TU Bibliothek Your knowledge hub WIEN

```
72      #return current at peak in µA
73      return trace[:, 1][indices_in_voltage_range[0]]
74
75
76  def get_anodic_trace(data): # only oxidation (in standard convention)
77      index_end_ox = np.argmax(data[:, 0])
78      index_begin_ox = np.argmin(data[:, 0])
79      if index_end_ox == 0:
80          index_end_ox = len(data[:, 0])
81      return data[index_begin_ox:index_end_ox,:].copy()  # deep copy!
82
83
84  def get_cathodic_trace(data): # only reduction (in standard convention)
85      index_begin_red = np.argmax(data[:, 0])
86      index_end_red = np.argmin(data[:,0])
87      if index_end_red == 0:
88          index_end_red = len(data[:, 0])
89      return data[index_begin_red:index_end_red, :].copy()  # deep copy!
90
91  ############### FUNCTIONS below require single data trace!!!!
92
93  # calculates peak area for an oxidation peak using a linear background subtraction
94  # scan rate in mV/s
95  def calc_peak_area(data, low_E, high_E, scan_rate, background_type = 1, smoothness = 0.03,
96                     decimals = 2):
97      data = data.copy() # avoids plotting the curve with substracted background!
98      if data == []:
99          raise ValueError('clac_peak_area() was passed empty data')
100
101     Eid1 = np.where(np.round(data[:, 0], decimals=decimals) ==
102                     np.round(low_E, decimals = decimals))[0][0]
103     Eid2 = np.where(np.round(data[:, 0], decimals=decimals) ==
104                     np.round(high_E, decimals = decimals))[0][0]
105
106     if (Eid2 < Eid1):
107         Eid1, Eid2 = Eid2, Eid1
108
109     # remove background type as set
110     if background_type == 0:
111         pass
112     elif background_type == 1:
113         data, background = subtract_lin_background(data, Eid1, Eid2)
114
115     peak = data[Eid1:Eid2,:]
116
117     #numerical integration with trapezoidals; factor 1000 to go from mV/s -> V/s (SI units)
118     area = np.trapz(peak[:,1], peak[:,0])/(scan_rate/1000)
119     return area
120
121
122 #removes linear background calculated from values at low_E and high_E
123 def subtract_lin_background(data, Eid1, Eid2):
124     lin_fit_params = np.polyfit([data[Eid1, 0], data[Eid2, 0]], [data[Eid1, 1],
125                                 data[Eid2, 1]], deg=1)
126     background = (data[Eid1:Eid2, 0] * lin_fit_params[0] + lin_fit_params[1])
127     data[Eid1:Eid2, 1] -= background
128     return data, background
129
130
131 # divides the measured current by a factor to normalize to current per area
132 def normalize_current_by_area(data,area):
133     for cv in data:
134         cv[:,1] /= area
135
136     return data
```

(b) File `analyze_CV.py` part 2.

Figure C.2.: File `analyze_CV.py`.

Die approbierte gedruckte Originalversion dieser Diplomarbeit ist an der TU Wien Bibliothek verfügbar
The approved original version of this thesis is available in print at TU Wien Bibliothek.
TU Bibliothek Your knowledge hub WIEN

```python
import matplotlib.pyplot as plt

'''This file provides some functionalities and presets to plot CVs that may be useful.
If you need anything more custom though, you may want to write your own script though.'''

# formats the plot information as is required for CV plotting
def format_plot_information(scan_nr = None, legend = None, legend_size=10, title="",
                            title_on=False, grid_on=False,
                            title_size=20, x_label="", x_label_size=15, y_label="",
                            y_label_size=15, figsize=(), x_lim=[], y_lim=[], x_ticks=0,
                            y_ticks=0, dpi=200, linewidth=None, linestyle=None,
                            colors=None, show_zero_line = True, ticks_inwards = True,
                            offset_in_y_axis = 0.0):
    ''' NOTE: setting x_ticks and y_ticks will no give the exact number of ticks set but
        rather roughly that many ticks at sensible position (i.e 0.1, 0.2, 0.3 etc.)'''

    if (scan_nr == None or legend == None):
        raise ValueError('required arguments missing')
    # liststyle and linewidth if set
    if linewidth == None:
        linewidth = []
        for i in range(len(scan_nr)):
            linewidth.append(2)
    if linestyle == None:
        linestyle = []
        for i in range(len(scan_nr)):
            linestyle.append('-')

    CV_plot_information = {'title': title, 'title_on': title_on, 'title_size': title_size,
                           'use_scan_nr': scan_nr,
                           'legend': legend,
                           'legend_size': legend_size,
                           'grid_on': grid_on,
                           'x_label': x_label,
                           'x_label_size': x_label_size,
                           'y_label': y_label,
                           'y_label_size': y_label_size,
                           'figsize': figsize,
                           'x_lim': x_lim,
                           'y_lim': y_lim,
                           'x_ticks': x_ticks,
                           'y_ticks': y_ticks,
                           'dpi': dpi,
                           'linestyle': linestyle,
                           'linewidth': linewidth,
                           'show_zero_line': show_zero_line,
                           'colors': colors,
                           'ticks_inwards': ticks_inwards,
                           'offset_in_y_axis': offset_in_y_axis}
    return CV_plot_information

def plot(CV_plot_information, data, plot_filename="default.png", save_plot=False, dpi=200):
    # clear figure
    plt.clf()
    plt.cla()

    # If no color is specified fall back to default colors
    if CV_plot_information['colors'] == None:
        defaults = plt.rcParams['axes.prop_cycle'].by_key()['color'] #default colors
        while len(data) > len(defaults): #make sure list is long enough for all cycles
            defaults.append(plt.rcParams['axes.prop_cycle'].by_key()['color'])
        colors = defaults
    else:
        colors = CV_plot_information['colors']

    # Offset in y axis is set
    for i in range(len(data)):
        use_scan_nr = CV_plot_information['use_scan_nr'][i]
        data[i][use_scan_nr][:, 1] += i*CV_plot_information['offset_in_y_axis']

    # Actually plot the data
```

(a) File `plot_CV.py` part 1.

Die approbierte gedruckte Originalversion dieser Diplomarbeit ist an der TU Wien Bibliothek verfügbar
The approved original version of this thesis is available in print at TU Wien Bibliothek.
TU Bibliothek Your knowledge hub WIEN

```
72      for i in range(len(data)):
73          use_scan_nr = CV_plot_information['use_scan_nr'][i]
74          plt.plot(data[i][use_scan_nr][ :, 0], data[i][use_scan_nr][:, 1],
75                   label=CV_plot_information['legend'][i],
76                   linewidth=CV_plot_information['linewidth'][i],
77                   linestyle=CV_plot_information['linestyle'][i], color=colors[i])
78
79      # set axis labels and title
80      plt.legend(fontsize=CV_plot_information['legend_size'])
81      plt.xlabel(CV_plot_information['x_label'], fontsize=CV_plot_information['x_label_size'])
82      plt.ylabel(CV_plot_information['y_label'], fontsize=CV_plot_information['y_label_size'])
83
84      # title, grid, figure size
85      if CV_plot_information['title_on']:
86          plt.title(CV_plot_information['title'], fontsize=CV_plot_information['title_size'])
87      if CV_plot_information['grid_on']:
88          plt.grid()
89      if CV_plot_information['figsize'] != ():
90          plt.figure(figsize=CV_plot_information['figsize'])
91
92      # Limits in x and y
93      if CV_plot_information['x_lim'] != []:
94          plt.xlim(CV_plot_information['x_lim'])
95      if CV_plot_information['y_lim'] != []:
96          plt.ylim(CV_plot_information['y_lim'])
97      if CV_plot_information['x_ticks'] > 0:
98          plt.locator_params(axis='x', nbins=CV_plot_information['x_ticks'])
99      if CV_plot_information['y_ticks'] > 0:
100         plt.locator_params(axis='x', nbins=CV_plot_information['y_ticks'])
101
102     # make ticks point inwards
103     if CV_plot_information['ticks_inwards']:
104         plt.axes().tick_params(direction ='in')
105
106     # Line at y = 0
107     if CV_plot_information['show_zero_line']:
108         plt.axhline(linewidth=0.3, color='grey')
109
110     # save plot or show it
111     if save_plot:
112         plt.savefig("plot/" + plot_filename, dpi=CV_plot_information['dpi'])
113     else:
114         plt.show()
```

(b) File `plot_CV.py` part 2.

Figure C.3.: File `plot_CV.py`.

Die approbierte gedruckte Originalversion dieser Diplomarbeit ist an der TU Wien Bibliothek verfügbar
The approved original version of this thesis is available in print at TU Wien Bibliothek.
TU Bibliothek Your knowledge hub WIEN

```
'''
Template for CV plotting from PSTrace in Python 3.8
by Alexander M. Imre
'''

import read_CV
import analyse_CV
import plot_CV
import numpy as np

'''
To plot Cyclic Voltammetry data you need to load the data and configure the settings for
plotting.
'''
########################
# SETTINGS
########################

title = "Example"  # Title displayed in plot
plot_filename = "CV_plot.png" # Name of file where the plot will be saved
save_plot = False # Set to True to save file

# Cosmetic settings
title_on = False # Show title?
x_label = "Potential vs. Ag/AgCl [V]" # Leave empty to remove
y_label = "Current [µA]" # Leave empty to remove

'''
Further settings are:
Linestyles (as a list)
Linewidths (as a list)
Grid
Size of labels
Size of legend
Figure size when saved
dpi (resolution of figure file)
x, y limits
Number of ticks on axis
Title size
Offset (in y) between CVs
Ticks inwards or outwards
...
'''

# Initialize lists - data will be read into these lists
data = []
scan_nr = []
legend = []

########################
# READ DATA FROM FILE(S)
########################

'''
For every cycle/dataset you want to plot append to the lists data, scan_nr and legend.
data holds the data array, scan_nr is the cycle index you want to plot and legend is the
label for that cycle.
This can either be used to plot data from one file or multiple files.
Just make sure to specify data and scan number for each entry. You can pass data from the
same file multiple times to show CV progression over time or you can pass many files to
show multiple scan rates.

Example 1 - CV over time
data_nr = (0, 0, 0, 0)
scan_nr = (0, 9, 19, 29)
legend = ('Cycle 1', 'Cycle 10', 'Cycle 20', 'Cycle 30')

Example 2 - scan rates
data_nr = (0, 1, 2, 3)
scan_nr = (0, 0, 0, 0)
legend = ('100 mV/s', '200 mV/s', '300 mV/s', '400 mV/s')
```

(a) File `analysis_script.py` part 1.

Die approbierte gedruckte Originalversion dieser Diplomarbeit ist an der TU Wien Bibliothek verfügbar
The approved original version of this thesis is available in print at TU Wien Bibliothek.
TU Bibliothek Your knowledge hub WIEN

```
72
73  '''
74  # Area and scan rate
75  area = 1 # geometric surface area
76  scanrate = 50 # scanrate in mV/s
77
78  # Filename
79  directory = '../data/Exp_XX'
80  filename = 'data_file_1.csv'
81
82  #read file(s)
83  file_data = read_CV.PSTrace_to_np(directory, filename)
84  file_data = analyse_CV.normalize_current_by_area(file_data, area)
85
86  #plot 10 cyles from that file
87  for i in range(10):
88      data.append(file_data)
89      scan_nr.append(i)
90      legend.append('cycle ' + str(i+1))
91
92
93  ########################
94  # PLOTTING
95  ########################
96
97  # Pass and format cosmetic setting and labels
98  CV_plot_settings = plot_CV.format_plot_information(scan_nr, legend, x_label=x_label,
99                                                     y_label=y_label, title=title,
100                                                    title_on=title_on)
101
102 # Plot data (and save)
103 plot_CV.plot(CV_plot_settings, data, save_plot=save_plot, plot_filename=plot_filename)
```

(b) File `analysis_script.py` part 2.

Figure C.4.: File `analysis_script.py`.

xxx

Die approbierte gedruckte Originalversion dieser Diplomarbeit ist an der TU Wien Bibliothek verfügbar
The approved original version of this thesis is available in print at TU Wien Bibliothek.
TU Bibliothek Your knowledge hub WIEN

C.2. Electrochemical Surface Force Apparatus

Analysis of (EC-)SFA data was performed in Jupyter Notebook using python 3.8. A directory tree with the relevant files is shown below:

```
data
    Exp_XX
        Distance
            FR1.txt
            ...
        Force
            FR1.csv
            ...
Exp_XX
    SFA support
        read_in.py
        data_manip.py
        widget_support.py
    Exp_XX_analysis.ipynb
    adh_force.csv
    jump_in_forces.csv
    Exp_XX_fits.json
    Exp_XX_info.csv
    make_dataframe.ipynb
    analysis.csv
```

Experiments consisted of a number of force runs. Each force run is analyzed individually by running it through the script `Exp_XX_analysis.ipynb`. This interactive Jupyter Notebook script accesses the modules `read_in.py`, `data_manip.py` and `widget_support.py`. Parameters for the force background subtraction and time delay between force and distance data are saved to `Exp_XX_fits.json`. Adhesion and jump-in forces are also calculated and stored in `adh_force.csv` and `jump_in_forces.csv` respectively. Additional information about each force run (e.g. the applied potential) is manually saved in `Exp_XX_info.csv`. When all force-runs are analyzed, `make_dataframe.ipynb` is used to collect information from `Exp_XX_info.csv`, `adh_force.csv`, `jump_in_forces.csv` and output all of it in `analysis.csv`.

Die approbierte gedruckte Originalversion dieser Diplomarbeit ist an der TU Wien Bibliothek verfügbar
The approved original version of this thesis is available in print at TU Wien Bibliothek.
TU Bibliothek Your knowledge hub WIEN

```python
import pandas as pd
import numpy as np
from datetime import datetime, timedelta
import json
import csv

# read in the text file containing the distance data produced by SFA explorer
def read_dist_file(FR_nr, dir_dist, dir_exp, rate):
    directory = dir_exp + dir_dist
    filename = 'FR' + str(FR_nr) + '.txt'
    read_in_dist = pd.read_csv(directory + filename, delimiter=' ', header=1)
    start_tiff_no = read_in_dist['#tifno'][0]
    distance_df = read_in_dist[['#tifno', 'Tliquid']].copy()
    distance_df['#tifno'] /= rate
    distance_df = distance_df.rename(columns={'#tifno': 'time', 'Tliquid': 'distance'})
    return distance_df

# convert strain gauge signal (mV/V) to force (mN) using calibration factor
def voltage_to_force(voltage, calibration):
    #using the new calibration method that converts directly from mV/V to mN
    force = calibration*voltage
    return force

# read in the csv file containing the force data
def read_force_file(FR_nr, dir_force, dir_exp, rate, calibration):
    directory = dir_exp + dir_force
    filename = 'FR' + str(FR_nr) + '.csv'
    data = pd.read_csv(directory+filename, header = 5)
    recording_date_str = data['Date        Time'][0][0:10]
    start_time_str = data['Date        Time'][0][11:]

    ## Clean up a bit
    # get date & time to proper format
    data['Time'] = data.apply(lambda row: (datetime.strptime(row['Date        Time']+'0',
                                                             '%d/%m/%Y %X,%f')), axis = 1)
    data = data.drop(['Date        Time'], axis=1)
    start_time = data['Time'][0]
    data['t [s]'] = data.apply(lambda row: (row['Time']-start_time).total_seconds(),
                               axis = 1)

    # clean up volatage
    data['U [mV]'] =  data.apply(lambda row: float((row['Y[Chan. 5_1]']).replace(',','.')),
                                 axis = 1)
    data = data.drop(['Y[Chan. 5_1]'], axis=1)

    data['F [mN]'] = data.apply(lambda row: voltage_to_force(row['U [mV]'], calibration),
                                axis = 1)
    data['F [mN]'] *= -1 # more force causes drop in voltage! => needs to be negative

    return data, recording_date_str, start_time_str



#######
# Saving and reading force fit and time shift parameters in a json file
# This way the fit can be loaded again later on

# save the parameters to the json file
def save_to_json(filename, Exp_data):
    filename += '.json'
    out_file = open(filename, 'w')
    json.dump(Exp_data, out_file)
    out_file.close()
    return

# read data back out of the json file
def read_from_json(filename):
    filename += '.json'
    with open(filename) as file:
        import_dict = json.load(file)
    Exp_data = {}
```

(a) File `read_in.py` part 1.

Die approbierte gedruckte Originalversion dieser Diplomarbeit ist an der TU Wien Bibliothek verfügbar
The approved original version of this thesis is available in print at TU Wien Bibliothek.
TU Bibliothek Your knowledge hub WIEN

```
72      for key in import_dict.keys():
73          Exp_data[int(key)] = import_dict[key]
74      return Exp_data
75
76  #######
77  # Saving and reading adhesion force values for experiment in a csv table
78
79  # read in existing table
80  def read_adh_forces_csv(filename):
81      adh_forces_list = []
82      try:
83          file = open(filename, 'r')
84          reader = csv.reader(file)
85          for row in reader:
86              adh_forces_list.append([int(row[0]), float(row[1])])
87
88          file.close()
89      except:
90          print('No previous Adhesion data found')
91
92      return adh_forces_list
93
94  # write new force values to file
95  def write_adh_forces_csv(filename, adh_forces_list):
96      adh_forces_list.sort()
97      file = open(filename, 'w')
98      writer = csv.writer(file)
99      writer.writerows(adh_forces_list)
100     file.close()
101
```

(b) File `read_in.py` part 2.

Figure C.5.: File `read_in.py`.

Die approbierte gedruckte Originalversion dieser Diplomarbeit ist an der TU Wien Bibliothek verfügbar
The approved original version of this thesis is available in print at TU Wien Bibliothek.
TU Bibliothek Your knowledge hub WIEN

```python
import pandas as pd

# read saved parameters back out of JSON
def extract_params_from_dict(Exp_data, FR_nr):
    if FR_nr in Exp_data.keys():
        in_lin_fit = Exp_data[FR_nr][0]
        out_lin_fit = Exp_data[FR_nr][1]
        offset = int(Exp_data[FR_nr][2])
        skip_fitting = True # change mode accordingly, so the values don't get overwritten
        print ('loaded from JSON')
    else:
        Exp_data[FR_nr]= []
        in_lin_fit = None
        out_lin_fit = None
        offset = None
        skip_fitting = False

    return in_lin_fit, out_lin_fit, offset, skip_fitting


# cleans up the force and distance data and puts it into one combined dataframe FR
def clean_FR(FR_force, FR_dist, radius):
    # 1) find first and last usable datapoint
    if min(FR_dist['time']) > min(FR_force['t [s]']):
        start_time = FR_dist['time'][0]
    else:
        start_time = FR_force['t [s]'][0]

    indeces_to_remove = FR_force[ (FR_force['t [s]'] < start_time)].index
    FR_force.drop(indeces_to_remove, inplace = True)

    indeces_to_remove = FR_dist[ (FR_dist['time'] < start_time)].index
    FR_dist.drop(indeces_to_remove, inplace = True)

    # 2) reset time
    # Using time from strain gauge as reference
    FR_dist['time'] = FR_dist['time'] - min(FR_force['t [s]'])
    FR_force['t [s]']  = FR_force['t [s]']- min(FR_force['t [s]'])

    # 3) put into proper array
    FR = pd.concat([FR_dist['distance'].reset_index(drop=True),
                    FR_force['F [mN]'].reset_index(drop=True)], axis = 1)

    FR = FR.dropna(axis = 0, how = 'any')
    FR = FR.rename(columns = {'distance':'D [nm]', 'F [mN]': 'F [mN/m]'})
    FR['F [mN/m]'] = FR['F [mN/m]']/radius

    max_force_index = FR['F [mN/m]'].idxmax() # index of max force for plotting

    return FR, max_force_index
```

Figure C.6.: File `data_manip.py`.

Die approbierte gedruckte Originalversion dieser Diplomarbeit ist an der TU Wien Bibliothek verfügbar
The approved original version of this thesis is available in print at TU Wien Bibliothek.
TU Bibliothek Your knowledge hub WIEN

```python
import matplotlib.pyplot as plt
import numpy as np
import pandas as pd
from numpy import linalg as LA

######################################################################
# Background fitting

# calculate the linear background to be subtracted from the force data
def fit_lin_background(FR_force ,index1, index2):
    return np.polyfit(FR_force.index[index1:index2], FR_force['F [mN]'][index1:index2],1)

# update plot after range change
def bckg_fit_update_diff(ax, FR_force, in_lin_fit, out_lin_fit, in_1, in_2, out_1, out_2):
    [l.remove() for l in ax.lines] # clears plot
    try:
        in_lin_fit = fit_lin_background(FR_force,int(in_1), int(in_2))
        out_lin_fit = fit_lin_background(FR_force,int(out_1), int(out_2))

        """Remove old lines from plot and plot new one"""
        [l.remove() for l in ax.lines]
        ax.plot(FR_force.index, FR_force['F [mN]'], color = 'C0', label = 'Force')
        ax.plot(FR_force.index, FR_force.index*in_lin_fit[0]+in_lin_fit[1],
                color = 'C1', label = 'In run fit')
        ax.plot(FR_force.index, FR_force.index*out_lin_fit[0]+out_lin_fit[1],
                color = 'C2', label = 'Out run fit')

        plt.legend(loc = 'lower left')
    except(TypeError):
        print('IN INDEX LOWER THAN OUT INDEX!!!')
    except(ValueError):
        print('FIELD EMPTY!!!')
    except(LA.LinAlgError):
        print('TRY OTHER INDICES - Fitting needs more datapoints!!!')
    return in_lin_fit, out_lin_fit

# dummy update function if skipped
def bckg_fit_update_skip(ax, FR_force, in_lin_fit, out_lin_fit):
    ax.plot(FR_force.index, FR_force['F [mN]'], color = 'C0', label = 'Force')
    ax.plot(FR_force.index, FR_force.index*in_lin_fit[0]+in_lin_fit[1],
            color = 'C1', label = 'In run fit')
    ax.plot(FR_force.index, FR_force.index*out_lin_fit[0]+out_lin_fit[1],
            color = 'C2', label = 'Out run fit')
    print('Fitting parameters loaded from file')
    return

######################################################################
# Offset estimation

# update plot when new value is entered
def update_offset(ax, FR_force, FR_dist, rate, offset = '0'):
    [l.remove() for l in ax.lines]
    [l.remove() for l in ax.lines] # do this again because of memory issues...
    ax.plot(FR_force['t [s]'], FR_force['F [mN]']/max(FR_force['F [mN]']),
            label = 'Force [mN]', color = 'C0', linestyle = '', marker = '.')
    ax.plot(FR_dist['time'] + int(offset)/rate,FR_dist['distance']/max(FR_dist['distance']),
            label = 'Distance [nm]', color = 'C1', linestyle = '', marker = 's')
    ax.legend()
    return offset


# dummy update function if skipped
def update_offset_skip(ax, FR_force, FR_dist, offset, rate):
    ax.plot(FR_force['t [s]'], FR_force['F [mN]']/max(FR_force['F [mN]']),
            label = 'Force [mN]', color = 'C0', linestyle = '', marker = '.')
    ax.plot(FR_dist['time'] + int(offset)/rate,FR_dist['distance']/max(FR_dist['distance']),
            label = 'Distance [nm]', color = 'C1', linestyle = '', marker = 's')
    ax.legend()
    print('Offset loaded from file')
    return

```

(a) File `widget_support.py` part 1.

Die approbierte gedruckte Originalversion dieser Diplomarbeit ist an der TU Wien Bibliothek verfügbar
The approved original version of this thesis is available in print at TU Wien Bibliothek.
TU Bibliothek Your knowledge hub WIEN

```
72
73  ######################################################################
74  # Final plot
75
76  # button to save force-run
77  def save_fig_button_clicked(plt, FR_nr):
78      plt.savefig('FR_plots/FR' + str(FR_nr) + '.png', dpi = 300)
79      return
80
81  # plot force-distance profile
82  def plot_FR_final(FR, max_force_index, FR_nr, xrange, yrange):
83      fig, ax = plt.subplots(figsize=(6, 4))
84      plt.title('Force-Distance, FR ' + str(FR_nr), fontsize = 13)
85      ax.grid(True)
86      ax.set_xlabel('Distance [nm]', fontsize = 11)
87      ax.set_ylabel('Force [mN/m]', fontsize = 11)
88      ax.set_xlim(xrange)
89      ax.set_ylim(yrange)
90
91      ax.plot(FR.loc[0:max_force_index-1]['D [nm]'], FR.loc[0:max_force_index-1]['F [mN/m]'],
92              color = 'C0', label = 'In run', linestyle = '', marker = '.', markersize = 3)
93      ax.plot(FR.loc[max_force_index:]['D [nm]'], FR.loc[max_force_index:]['F [mN/m]'],
94              color = 'C1', label = 'Out run', linestyle = '', marker = '.', markersize = 3)
95
96      ax.legend(loc = 'upper right', fontsize=12)
97
98
99      plt.xticks(fontsize=10)
100     plt.yticks(fontsize=10)
101     return
102
103
104 ######################################################################
105 # Adhesion calculation (can also be used for jump-in force)
106
107 def plot_adh_checker(FR_part, FR_nr, index_range):
108     if index_range:
109         adh_force = min(FR_part[index_range[0]:index_range[1]])
110         adh_force_idx = FR_part[index_range[0]:index_range[1]].idxmin()
111     else:
112         adh_force = min(FR_part)
113         adh_force_idx = FR_part.idxmin()
114
115     # plot to check - don't save force if it looks wrong...
116
117     fig, ax = plt.subplots(figsize=(6, 4))
118     plt.title('Adhesion Force, FR ' + str(FR_nr), fontsize = 13)
119     ax.grid(True)
120     ax.set_xlabel('Index', fontsize = 11)
121     ax.set_ylabel('Force [mN/m]', fontsize = 11)
122     ax.set_xlim([adh_force_idx-500, adh_force_idx+250])
123     ax.set_ylim([min([adh_force-1,1.5]),max([adh_force-1,1.5])])
124     ax.plot(FR_part, color = 'C0', label = 'In run', linestyle = '', marker = '.',
125             markersize = 3)
126     plt.arrow(adh_force_idx, 0, 0, adh_force, width = 3, length_includes_head = True,
127               head_length= -0.2*adh_force, color = 'red')
128
129     print('Force = ' + str(adh_force) + ' mN/m')
130
131     return adh_force
```

(b) File `widget_support.py` part 2.

Figure C.7.: File `widget_support.py`.

Die approbierte gedruckte Originalversion dieser Diplomarbeit ist an der TU Wien Bibliothek verfügbar
The approved original version of this thesis is available in print at TU Wien Bibliothek.
TU Bibliothek Your knowledge hub WIEN

In [1]:
```
# Imports
import matplotlib.pyplot as plt
from ipywidgets import interactive
import ipywidgets
import pandas as pd
import numpy as np
from SFA_support_library import read_in, data_manip, widget_support

# change to notebook or qt if necassary — This may break functionality though!
# inline will not work, gtk may work
%matplotlib notebook
```

In [2]:
```
## EDIT HERE
################################################################################
FR_nr = 10

# Directories
save_filename = 'Exp_28_fits'
dir_exp = '../data/Exp_28/'
dir_dist = 'Distance/'
dir_force = 'Force/'

# Fitting params
radius = 0.01 # Disc radius in m
calibration = 1.001 # Calibration factor mV/V to mN

# Paramters
rate = 10
vert_shift = 0.8

# DO NOT EDIT BELOW
################################################################################

# Check to see if offsets need to be estimated
try:
    Exp_data = read_in.read_from_json(save_filename)
except:
    Exp_data = {}
    print('error loding data')

in_lin_fit, out_lin_fit, offset, skip_fitting =  data_manip.extract_params_from_dict(Exp_data, FR_nr)

# Read in data — handled by external script
FR_force, recording_date_str, start_time_str = read_in.read_force_file(FR_nr, dir_force,
                                                                       dir_exp, rate, calibration)
FR_dist = read_in.read_dist_file(FR_nr, dir_dist, dir_exp, rate)

print('FR ' + str(FR_nr) + ' was recorded on ' + recording_date_str + ' at ' + start_time_str)
```

```
loaded from JSON
FR 10 was recorded on 15/12/2020 at 13:00:16,06543
```

In [3]:
```
# set up plot for Backgroudn estimation
fig, ax = plt.subplots(figsize=(6, 4))
ax.grid(True)
ax.set_xlabel('Index')
ax.set_ylabel('F [mN]')

in_1_default = '200'
in_2_default = '300'
out_1_default = str(max(FR_force.index)-100)
out_2_default = str(max(FR_force.index))

if not skip_fitting:
    interactive = ipywidgets.widgets.interactive(widget_support.bckg_fit_update_diff, in_1=in_1_default,
                                                 in_2=in_2_default, out_1 =out_1_default, out_2 =out_2_default,
                                                 ax = ipywidgets.fixed(ax), FR_force = ipywidgets.fixed(FR_force),
                                                 in_lin_fit = ipywidgets.fixed(in_lin_fit),
                                                 out_lin_fit = ipywidgets.fixed(out_lin_fit))
else:
    interactive = ipywidgets.widgets.interactive(widget_support.bckg_fit_update_skip, ax = ipywidgets.fixed(ax),
                                                 FR_force = ipywidgets.fixed(FR_force),
                                                 in_lin_fit = ipywidgets.fixed(in_lin_fit),
                                                 out_lin_fit = ipywidgets.fixed(out_lin_fit))

interactive
```

(a) File `Exp_XX_analysis.ipynb` part 1.

Die approbierte gedruckte Originalversion dieser Diplomarbeit ist an der TU Wien Bibliothek verfügbar
The approved original version of this thesis is available in print at TU Wien Bibliothek.
TU Bibliothek Your knowledge hub WIEN

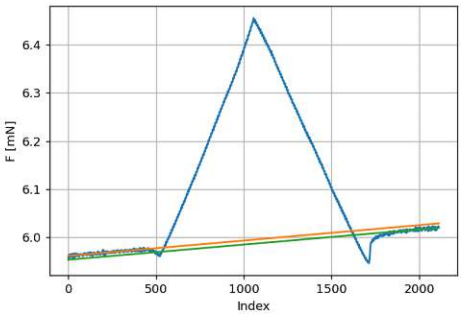

In [4]:

```
#Background substraction
plt.close('all')

if not skip_fitting:
    in_lin_fit, out_lin_fit = interactive.result
    in_lin_fit = in_lin_fit.tolist()
    out_lin_fit = out_lin_fit.tolist()

max_force_index = FR_force['F [mN]'].idxmax()

#In run
FR_force.loc[0:max_force_index-1, 'F [mN]'] = FR_force.loc[0:max_force_index-1,
                                                           'F [mN]']-(FR_force.index[0:max_force_index]*in_lin_fit[0]+
                                                                      in_lin_fit[1])
in_run_force = FR_force.loc[0:max_force_index-1, 'F [mN]'].copy()/radius # for calculating jump in later
in_run_force.reset_index(drop=True, inplace=True)
#Out run
FR_force.loc[max_force_index:, 'F [mN]'] = FR_force.loc[max_force_index:,
                                                        'F [mN]']-(FR_force.index[max_force_index:]*out_lin_fit[0]+
                                                                   out_lin_fit[1])
out_run_force = FR_force.loc[max_force_index:, 'F [mN]'].copy()/radius # for calculating the adhesion force later
out_run_force.reset_index(drop=True, inplace=True)
```

In [5]:

```
# Take care of time offset
fig, ax = plt.subplots(figsize=(6, 4))
ax.grid(True)
ax.set_xlabel('Time [s]')
plt.title('Offset assessment FR' + str(FR_nr))

if not skip_fitting:
    interactive_offset_assessment = ipywidgets.widgets.interactive(widget_support.update_offset, offset = '0',
                                                                   ax = ipywidgets.fixed(ax),
                                                                   FR_force = ipywidgets.fixed(FR_force),
                                                                   FR_dist = ipywidgets.fixed(FR_dist),
                                                                   rate = ipywidgets.fixed(rate))
else:
    interactive_offset_assessment = ipywidgets.widgets.interactive(widget_support.update_offset_skip,
                                                                   ax = ipywidgets.fixed(ax),
                                                                   FR_force = ipywidgets.fixed(FR_force),
                                                                   FR_dist = ipywidgets.fixed(FR_dist),
                                                                   offset = ipywidgets.fixed(offset),
                                                                   rate = ipywidgets.fixed(rate))


interactive_offset_assessment
```

(b) File `Exp_XX_analysis.ipynb` part 2.

Die approbierte gedruckte Originalversion dieser Diplomarbeit ist an der TU Wien Bibliothek verfügbar
The approved original version of this thesis is available in print at TU Wien Bibliothek.
TU Bibliothek Your knowledge hub WIEN

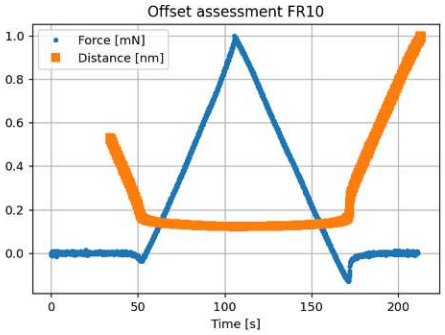

In [6]:
```
# use offset value to stick data together properly
if not skip_fitting:
    offset = interactive_offset_assessment.result

FR_dist['time'] = FR_dist['time'] + int(offset)/rate # shift to right place

# Rest is handled by external script
FR, max_force_index = data_manip.clean_FR(FR_force, FR_dist, radius)
```

In [7]:
```
#Plot FR
plt.close('all')
# Plotting range
xrange = [0, 40] # nm
yrange = [-10,12] # nN/m

# handled by external script
widget_support.plot_FR_final(FR, max_force_index, FR_nr, xrange, yrange)

# because the button widget can not be passed any arguments this def needs to be here to see FR_nr & plt
def save_fig_button_clicked(b):
    plt.savefig('FR_plots/FR' + str(FR_nr) + '.png', dpi = 300)
    return

save_fig_button = ipywidgets.Button(description="Save Figure")
save_fig_button.on_click(save_fig_button_clicked)
save_fig_button
```

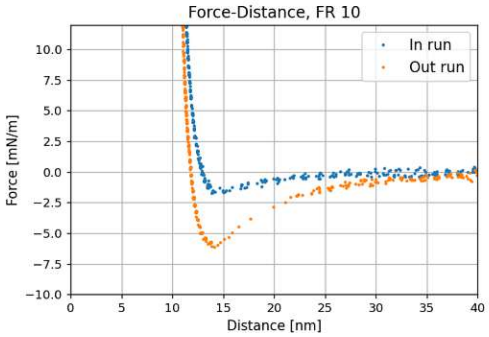

In [8]:
```
# Update fitting data and write new to file
# WILL OVERWRITE old file
Exp_data[FR_nr] = [in_lin_fit, out_lin_fit, offset]
```

(c) File `Exp_XX_analysis.ipynb` part 3.

Die approbierte gedruckte Originalversion dieser Diplomarbeit ist an der TU Wien Bibliothek verfügbar
The approved original version of this thesis is available in print at TU Wien Bibliothek.
TU Bibliothek Your knowledge hub WIEN

```
# Write to file
read_in.save_to_json(save_filename, Exp_data)
```

In [9]:
```
# Adhesion measurement
index_range = [0,1000]
adh_force = widget_support.plot_adh_checker(out_run_force, FR_nr, index_range)
```

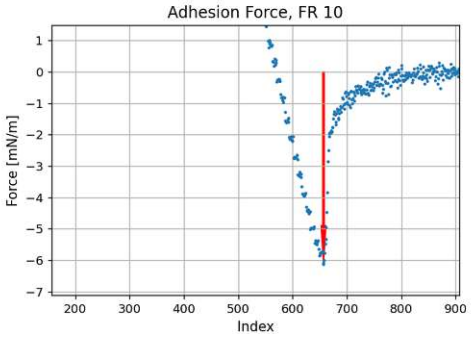


```
Force = -6.119427054037629 mN/m
```

In [10]:
```
# load file with adhesion forces and add new entry
filename = 'adh_forces.csv'
adh_forces_list = read_in.read_adh_forces_csv(filename)
adh_forces_list = [val for val in adh_forces_list if val[0] != FR_nr]
adh_forces_list.append([FR_nr, adh_force])

# write adhesion forces to file
read_in.write_adh_forces_csv(filename, adh_forces_list)
```

In [11]:
```
# Jump-in measurement
index_range = [0,1000]
j_in_force = widget_support.plot_adh_checker(in_run_force, FR_nr, index_range)
```

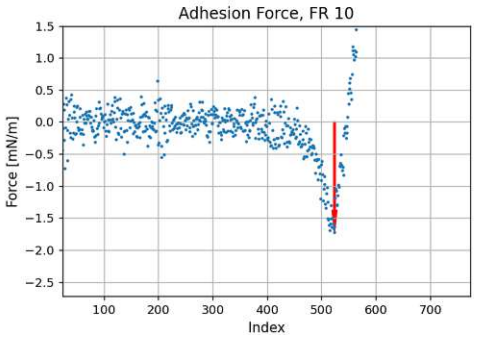


```
Force = -1.7244927079866912 mN/m
```

In [12]:
```
# load file with adhesion forces and add new entry
filename = 'jump_in_forces.csv'
j_in_forces_list = read_in.read_adh_forces_csv(filename)
j_in_forces_list = [val for val in j_in_forces_list if val[0] != FR_nr]
j_in_forces_list.append([FR_nr, j_in_force])

# write adhesion forces to file
read_in.write_adh_forces_csv(filename, j_in_forces_list)
```

(d) File `Exp_XX_analysis.ipynb` part 4.

Figure C.8.: File `Exp_XX_analysis.ipynb`.

xl

Die approbierte gedruckte Originalversion dieser Diplomarbeit ist an der TU Wien Bibliothek verfügbar
The approved original version of this thesis is available in print at TU Wien Bibliothek.
TU Bibliothek Your knowledge hub WIEN

In [1]:
```
# Imports
import matplotlib.pyplot as plt
from ipywidgets import interactive
import ipywidgets
import pandas as pd
import numpy as np
from datetime import datetime, timedelta
from SFA_support_library import read_in
```

In [2]:
```
FR = 28

filename = 'adh_forces.csv'
force_df = pd.read_csv(filename, header = None)
force_df.columns =['FR','F_adh']


filename = 'jump_in_forces.csv'
j_in_df = pd.read_csv(filename, header = None)
j_in_df.columns =['FR','F_j_in']

force_df['F_j_in'] = np.NaN


filename = 'Exp_' + str(FR) + '_info.csv'
info_df = pd.read_csv(filename, delimiter = ';')

force_df['E'] = np.NaN
force_df['Electrolyte'] = np.NaN
force_df['Comment'] = np.NaN
```

In [3]:
```
for index, row in force_df.iterrows():
    try:
        force_df.loc[index,'F_j_in'] = j_in_df.loc[np.isclose(j_in_df['FR'],
                                                              row['FR']))]['F_j_in'].values[0]
    except:
        continue

for index, row in force_df.iterrows():
    try:
        force_df.loc[index,'E'] = info_df.loc[np.isclose(info_df['FR'],
                                                         row['FR']))]['E'].values[0]
    except:
        continue
for index, row in force_df.iterrows():
    try:
        force_df.loc[index,'Electrolyte'] = info_df.loc[np.isclose(info_df['FR'],
                                                                   row['FR']))]['Electrolyte'].values[0]
    except:
        continue
for index, row in force_df.iterrows():
    try:
        force_df.loc[index,'Comment'] = info_df.loc[np.isclose(info_df['FR'],
                                                               row['FR']))]['Comment'].values[0]
    except:
        continue
```

In [4]:
```
lowest_FR_nr = int(force_df.min()['FR'])

directory = '../data/Exp_' + str(FR) + '/Force/'
_, date, time = read_in.read_force_file(lowest_FR_nr, directory, '', 10, 1)
starttime = datetime.strptime(date+time, '%d/%m/%Y%X,%f')
starttime

force_df['Sec'] = np.NaN

for index, row in force_df.iterrows():
    try:
        FR_nr = row['FR']
        directory = '../data/Exp_' + str(FR) + '/Force/'
        _, date, time = read_in.read_force_file(FR_nr, directory, '', 10, 1)
        FR_time = datetime.strptime(date+time, '%d/%m/%Y%X,%f')
        force_df.loc[index,'Sec'] = int((FR_time - starttime).total_seconds())
    except:
        continue
```

In [5]:
```
force_df.to_csv('analysis.csv', index = False)
```

Figure C.9.: File `make_dataframe.ipynb`.

Die approbierte gedruckte Originalversion dieser Diplomarbeit ist an der TU Wien Bibliothek verfügbar
The approved original version of this thesis is available in print at TU Wien Bibliothek.